MAY 2019

M.Sc. in Electrical and Electronics Engineering

MUSTAFA LATEEF HASAN

REPUBLIC OF TURKEY

GAZİANTEP UNIVERSITY

GRADUATE SCHOOL OF NATURAL & APPLIED SCIENCES

DEVELOPMENT OF DIGITAL CONTROLLER FOR PERMANENT MAGNET DC MOTORS WITH APPLICATIONS

M. Sc. THESIS

IN

ELECTRICAL AND ELECTRONICS ENGINEERING

BY

MUSTAFA LATEEF HASAN

MAY 2019

DEVELOPMENT OF DIGITAL CONTROLLER FOR PERMANENT MAGNET DC MOTORS WITH APPLICATIONS

M.Sc. Thesis

in

Electrical and Electronics Engineering

Gaziantep University

Supervisor

Prof. Dr. Ergun ERÇELEBİ

by

Mustafa Lateef HASAN

May 2019

REPUBLIC OF TURKEY
GAZİANTEP UNIVERSITY
GRADUATE SCHOOL OF NATURAL & APPLIED SCIENCES
ELECTRICAL-ELECTRONICS ENGINEERING

Name of the thesis: Development of Digital Controller for Permanent Magnet DC Motors with Applications

Name of the student: Mustafa Lateef HASAN

Exam date: 03.05.2019

Approval of the Graduate School of Natural and Applied Sciences

Prof. Dr. A. Necmeddin YAZICI

Director

I certify that this thesis satisfies all the requirements as a thesis for the degree of Master of Science.

Prof. Dr. Ergun ERÇELEBİ

Head of Department

This is to certify that we have read this thesis and that in our consensus opinion it is fully adequate, in scope and quality, as a thesis for the degree of Master of Science.

Prof. Dr. Ergun ERÇELEBİ

Supervisor

Examining Committee Members:	Signature
Prof. Dr. Ergun ERCELEBİ	…………………..
Prof. Dr. İlyas EKER	…………………..
Assoc. Prof. Dr. Mete VURAL	…………………..

I hereby declare that all information in this document has been obtained and presented in accordance with academic rules and ethical conduct. I also declare that, as required by these rules and conduct, I have fully cited and referenced all material and results that are not original to this work.

Mustafa Lateef HASAN

ABSTRACT

DEVELOPMENT OF DIGITAL CONTROLLER FOR PERMANENT MAGNET DC MOTORS WITH APPLICATIONS

Mustafa Lateef HASAN
M.Sc. in Electrical and Electronics Engineering
Supervisor: Prof. Dr. Ergun ERÇELEBİ
May 2019
81 pages

This work concerns with designing and implementing of a system which is competent enough to resist the disturbances on the DC motors, fed by a step-down DC-DC power converter. The electrical component values of the buck converter and its appendix (bootstrap circuit) have been opted minutely in strict range to guarantee the minimal dissipation losses during power conversion. Furthermore, this work involves using an optical speed sensor for feeding back the actual speed into Proportional Integral controller which is implemented on PIC18F4580. For the PI tuning, the fourth order transfer function that describes the whole system precisely has also been derived and converted from the continuous to the discrete domain. At the end, the data was sent via UART pin to an Arduino UNO which works here as a data acquisition with the help of PLX-DAQ software, forming a Microsoft Excel file. The simulation results have been presented in the time domain for checking the DC motor parameters estimation and the relationship between both of the duty cycle and the speed versus the time. In addition, the results have been presented in the frequency domain for testing the stability of the system via bode plot. To show the efficiency of the designed system, both the duty cycle and the output voltage of the buck converter have been presented and analyzed. Moreover; the actual, the desired speed of the DC motor and the error between them for two different speed cased are also presented and discussed.

Keywords: Step-down DC-DC converter, PI control, Permanent magnet DC motor, Optical speed sensor, Capture compare mode.

ÖZET

KALICI MIKNATISLI DC MOTORLAR İÇİN UYGULAMALARLA SAYISAL KONTROLCÜNÜN GELİŞTİRİLMESİ

Mustafa Lateef HASAN
Yüksek Lisans Tezi, Elektrik-Elektronik Mühendisliği
Tez Yöneticileri: Prof. Dr. Ergun ERÇELEBİ
May 2019
81 sayfa

Bu çalışma, DC-DC güç dönüştürücü tarafından beslenen, DC motorlardaki bozulmalara karşı dayanıklı bir sistemin tasarlanması ve uygulanmasıyla ilgilidir. Buck dönüştürücünün ve ekinin (önyükleme devresi) elektriksel bileşen değerleri, güç dönüşümü sırasındaki minimum tüketim kayıplarını garanti etmek için tamamen sınırlı bir aralıkta seçilmiştir. Ayrıca bu çalışma, gerçek hızı PIC18F4580'de uygulanan Orantılı İntegral kontrolöre geri beslemek için bir optik hız algılayıcısı kullanılmasını içermektedir. PI ayarlaması için, tüm sistemi kesin olarak tanımlayan dördüncü dereceden transfer fonksiyonu da türetilmiş ve sürekli alandan ayrık alana dönüştürülmüştür. Sonunda, veriler UART pin aracılığıyla, burada bir Microsoft Excel dosyası oluşturan PLX-DAQ yazılımı yardımıyla veri toplayıcı olarak çalışan bir Arduino UNO'ya gönderildi. Simülasyon sonuçları, DC motor parametreleri tahminini hem görev döngüsü hem de hız ve zaman arasındaki ilişkiyi kontrol etmek için zaman alanında sunulmuştur. Ayrıca, sonuçlar sistemin kararlılığını bode grafiği aracılığıyla test etmek için frekans alanında da sunulmuştur. Geliştirilen sistemin verimliliğini göstermek için, hem görev çevrimi hem de buck dönüştürücünün çıkış gerilimi sunulmuş ve analiz edilmiştir. İlaveten, DC motorun gerçek, istenen hızları ve aralarındaki hata iki farklı hız için de sunulmuş ve tartışılmıştır.

Anahtar Kelimeler: Aşağıya doğru DC-DC dönüştürücü, PI kontrolü, kalıcı mıknatıslı DC motor, optik hız sensörü, yakalama karşılaştırma modu.

To My Parents

ACKNOWLEDGEMENTS

I would like to express my deep gratitude to Prof. Dr. Ergun ERÇELEBİ, my research supervisor, for his patient guidance, enthusiastic encouragement and useful critiques of this research work. His willingness to give his time so generously has been very much appreciated.

I am very grateful to my parents, my sisters and brother who encouraged me and prayed for me throughout the time of my research.

Finally, I would like to express my gratitude to all the people who helped me by providing their valuable assistance and time for this thesis.

TABLE OF CONTENTS

LIST OF TABLES

page

LIST OF FIGURES

page

LIST OF SYMBOLS

$\mathbf{I_a}$	Armature Current
$\boldsymbol{\omega}$	Motor Speed
Φ	Electrical Magnetic Flux
$\mathbf{k}$	Motor Constant
$\mathbf{F}$	Lorentz Electromagnetic Force
$\mathbf{B}$	Magnetic Field
$\mathbf{Q}$	Electrical Charge
$\mathbf{L}$	Conductor Length
$\mathbf{k_e}$	Back EMF Constant of The Motor
$\mathbf{E_b}$	Voltage Back EMF of The DC Motor
$\boldsymbol{\omega}$	DC Motor Speed
$\mathbf{K_t}$	Torque Constant of The DC Motor
$\mathbf{T_m(t)}$	Torque of The DC Motor
$\mathbf{R_M}$	Armature Resistance
$\mathbf{L_M}$	Inductance of The Armature
$\mathbf{J}$	Moment of Inertia
$\mathbf{B}$	Damping Coefficient
$\mathbf{T_{stalling}}$	Stalling Torque
$\mathbf{I_{stalling}}$	Stalling Current
$\boldsymbol{\omega_{no\_load}}$	No Load Speeds
$\mathbf{\frac{rad}{sec}}$	Radians Per Second
$\mathbf{D}$	Duty Cycle
$\mathbf{T}$	Chopping Period
$\mathbf{f}$	Chopping Frequency
$\mathbf{R_{effective}}$	Effective Resistance
$\mathbf{I_{average}}$	Average Current

$\mathbf{L}$	The Inductance of The Buck Converter
$\mathbf{C}$	The Capacitor of The Buck Converter
$\mathbf{P_{in}}$	Input Power
$\mathbf{P_{out}}$	Output Power
$\mathbf{V_{in}}$	Input Voltage
$\mathbf{i_s}$	Current through The Switch
$\mathbf{L_{Critical}}$	Critical Inductance Value
$\mathbf{C_{Critical}}$	Critical Capacitance Value
$\mathbf{T_{ON}}$	On Period of The Switch
$\mathbf{T_{OFF}}$	OFF Period of The Switch
$\mathbf{V_T}$	Thresholding Voltage
$\mathbf{V_{PIV}}$	Peak Inverse Voltage across The Diode
$\mathbf{V_{GS}}$	Gain to Source Voltage on the MOSFET
$\mathbf{i_f}$	Forward Current across The Diode.
$\mathbf{V_{DC}}$	Drain to Source Voltage on the MOSFET
$\mathbf{i_{DS}}$	Drain to Source Current through The MOSFET
$\mathbf{P_{gate}}$	Gate Drive Losses of The MOSFET
$\mathbf{r_d}$	The Dynamic Resistance
$\mathbf{P_{reverse\_loss}}$	Reverse Static Losses in The Diode
$\mathbf{P_{forward\_loss}}$	Forward Static Losses in The Diode
$\mathbf{P_L}$	Copper Power Loss
$\mathbf{P_{ESR}}$	Losses Power in The Equivalent Series Resistance
$\mathbf{Q_g}$	High-Side Gate Charge of the FET
$\mathbf{I_{Cbs(leak)}}$	Leakage Current in The Bootstrap Capacitor
$\mathbf{I_{qbs(max)}}$	Maximum Quiescent Current for The High Side Driver Circuit
$\mathbf{I_{QBS}}$	Quiescent Current for The Circuit That Driven in A High-Side
$\mathbf{V_f}$	Forward Voltage Descent Through External Bootstrap Diode
$\mathbf{V_{cc}}$	Logic Signal of Voltage Supply
$\mathbf{V_{LS}}$	Voltage Descent through Low-Side for Load Or FET
$\mathbf{V_{min}}$	Minimal Voltage Between V_S And V_B Pins
$\mathbf{Q_{ls}}$	The Required Level Shifting Charge in One Cycle
$\mathbf{k_p}$	Proportional Constant
$\mathbf{k_i}$	Integral Constant

LIST OF ABBREVIATIONS

EMF	Back Electromotive Force
RPM	Resolution Per Minute
RMS	Root Mean Square
PWM	Pulse Width Modulation
DMPS	Discontinuous Mode Power Supply
CMPS	Continuous Mode Power Supply
SISO	Single Input Single Output
MOSFET	Metal-Oxide-Semiconductor Field-Effect Transistor
FET	Field-Effect Transistor
ESR	Equivalent Series Resistance
MGT	MOS Gated Transistor.
PI	Proportional Integral Controller
TMR0	Timer Zero
TMR1	Timer One
T1CON	TIMER1 Control Register
TMR1IF	TIMER1 Interrupt Flag Bit
TMR1IE	TIMER1 Interrupt Enable Flag Bit
TMR1L	The Low Byte of Timer1
TMR1H	The High Byte of Timer1
CCP1	Capture/Compare/PWM(CCP) Modules
CCP1IE	Interrupt Enable Bit Of CCP
CCP1IF	CCP Interrupt Flag Bit
CCP1L	The Low Byte Of CCP
CCP1H	The High Byte Of CCP
CCP1CON	Capture/Compare/PWM Control Register
GIE	The Global Interrupt Enable Bit
PEIE	Peripheral Interrupt Enable Flag
UART	A Universal Asynchronous Receiver-Transmitter
IC	Integrated Circuit

CHAPTER 1

INTRODUCTION

1.1 Organization of the Thesis

In this study, five chapters have been organized for involving the whole of the subject an as the following: Chapter one concerns with presenting a brief introduction on the DC motors, the step-down converters, PI control and on PIC18F45880. Chapter two contains historical literature review related to the thesis, furthermore the previous studies in related works besides the purposes and the contributions of this study. Chapter three illustrates the deriving of the DC motor transfer function, the principal operations of the step-down converter, the estimation of the DC motor parameters, the combined modeling of the step-down power converter with the permanent DC motor and deriving the transfer function that precisely describes the whole of the system, and the principal concepts of the bootstrap circuit. Moreover, discussing the PI controller design and inferred its transfer function in the discrete domain, illustrate the Principle work of the timers that related directly to the capture mode for measuring the frequency of a digital signal. While chapter four describes the experimental implementation besides the procedures of building the capture mode and PI algorithms on PIC18F4580 microcontroller for measuring the Revolution Per Minute and adjusting that speed as a desiring. Furthermore, checking the DC motor parameters estimation, besides testing the stability of the system before and after implement the PI algorithm and present the simulation and experimental results and discuss them in details. In the end, chapter five presents the conclusion of the works and give suggestions related to this thesis for any similar future works.

1.2 Background

Freshly, DC motors have been intensively utilized in various fields of industrial control applications because they are generally inexpensive and have simple control structure with a broad scope of speed and torque, although the handling with the AC motors seeming as more straightforward, the improvement in the innovations field of a high-efficiency AC-DC and DC-DC power converters have made the dealing with the DC motors are more feasible and even most cost-effective. DC drives are commonly using in applications requiring frequent starting, braking, reversing, and proper speed regulation. Generally, DC motors appear in a large variety of shapes and sizes according to the requirements of its specific characteristics: Huge-motors, typically used in the industry like hoists, electric trains, elevators, and mills. Small motor applications include motors used in food blenders, robots, hand power tools, and automobiles. Tiny machines are electric machines with parts the size of red blood cells that used in many medical applications. Kirchhoff's law led up to:

$$\omega = k(V - I_a R_a)/\Phi \tag{1.1}$$

Where, I_a- is the armature current, ω- motor speed, Φ- electrical magnetic flux, k-is constant and R_a- the resistance of the armature. So, there are three facts inferred from the above formula: The DC motor Speed is proportional to the applied voltage and inversely related to each of the voltage drops in the armature ($I_a R_a$) and the electrical flux which arises from the coil windings. Because of the inherent obstacles in both of the armature resistance control method (due to the dissipated power in the series resistance) and the field flux control method (due to its failure in the handling with an accurate speed ranges), Pulse-width modulation (PWM) method sounds like the best options for driving the DC motors and surmount these problems. Nonetheless, this strategy leads to inadmissible dynamic actions by setting up very noisy shaped paths which result in subsequently vast forces applying on the DC machine, which will inevitably lead to consuming much more current by the motor, the final outcome is a mischievous effect on both of the power supply and the electronic components [1]. So, the needing for voltage regulation appears.

To overcome this problem, DC-DC power converters "Boost", 'Buck" or "Buck-Boost" can be used as an appropriate driver “starter” for any types of DC motor. A combination connected between the DC machines with the DC-DC power converters is proposed by [2]. In specifically, the composition of a DC motor driven via a step-down (buck converter) was mentioned by [3,4].

Pursuant to the preexisting of two storing energy elements (capacitor and coil) in the step-down DC-DC (buck converter), smooth with tiny ripple output waveform (voltage and current) is obtained via some manipulation in the circuit parameters to get access to the optimum power transmission rate fed to the DC motor at any time in speed control tracking systems. These days all power converters are using semiconductor equipment like MOSFET which is utilized for high-pace switching in the output voltage and to supply high current with minimum dissipated power (in heating), they are comparatively small in size, economical and operate with minimum losses power, providing efficient and feasible control ways for the DC machines.

In the high side switching mode, the high voltage rail power supply connected to the drain terminal of the MOSFET and its source terminal is connecting to the load, while in the low side switching mode, the load is located in the middle between the voltage source and drain terminal of the MOSFET. One of the most important things for driving a power MOSFET as a high side switching mode with full enhancement (in the minimum range of the voltage drop at its terminals) can be illustrating in a crucial essential phrase " the source voltage must be 15 V to 10 V lower than the Gate voltage". In this regard, several techniques developed to drive the MOSFET gate in a high side switching mode such as an isolated DC-DC converter, an optocoupler, and PNP/NPN driver circuit, but the bootstrap circuit is the most efficient method which is using to provide gate-source voltage higher than the thresholding voltage ($V_{GS} > V_T$). Noteworthy that there is no such complexity in handling with the low side switching mode because the source terminal of the MOSFET is connecting with the ground; so, the gate-source voltage will be bigger than the thresholding of the MOSFET with any 5V apply on the gate.

In general, control systems are categorizing as modern control and classical control systems. The contemporary controller uses state-space representation, fuzzy logic, neural networks, and digital computers [5], while the conventional control systems depend on transfer function, besides its operation, and feedback. PI controller is categorizing as a classic controller but since it implemented as a code in a control loop, so became a modern controller. Modern high-speed microcontrollers and microcomputers are commonly used in digital control systems because its reasonable cost, speed, efficiency, and, compactness [6].

The output value from the PI-driven equation (PI-driven equation$= K_p + \frac{K_i}{s}$) is entering a mapping process for converting this analog output (from a PI plant) to a PWM signal with frequency predetermined according to the designer. PI wittingly controls the steady-state and transient response of the closed-loop control system, the efficacy of PI relates to the PI parameters (K_p and K_i) tuning, the correct tuning lead to an efficient and robust performance for most of the control problems [7]. Generally, in the closed-loop control system designing, the Proportional- Integral control (PI) considered as one of the most popular control techniques to gain the smallest allowable tolerance between the reference setpoint (desired speed) and the actual pace of the DC motor (actual speed). This process is implementing by taking advantage of P-part features in minimizing the percent of the offset between the (desired and actual speed) right off the bat, the other term (I-part) is playing a pivotal role in reducing this gap over the time, this process is going on until achieving the desirable pre-requirements. In this work, the PI algorithm has been implemented on the PIC18F4580 MCU to control the speed of a DC motor under different external load torque.

Measuring rotational speed is an essential operation in automation and industry applications essentially in electrical drive system [8], nowadays the high resolution of the speed encoder is crucially important in applications that deal with the high precision. The most traditional unit in measuring the angular velocity of a DC motor is Revolutions Per Minute (RPM), it stands for how many times the DC motor's shaft will rotate during one minute. The conventional RPM for most of DC motors is typically from 3000 RPM up to 8000 RPM, although this range may seem as bizarre since the higher RPM is may be much more advantageous, but it is not always considered to be desirable. For robotic applications that handling with high responding in the unnormal speeds (high speed), may cause a malfunction in the responses because of the discordance with the CPU respond, for instance, robotic arms are accomplishing an accurate process with speeds below 50 RPM, on the other hand, ventilating fans usually have RPM scope from 3000 up to 6500, which is deemed quick.

One of the old techniques for getting a rough DC motor speed estimation was done by connected a colored disc on the engine shaft and attach a bit of strip on it then the user computes the number of rotations per minute (RPM) manually. This technique depends on the ability to focus on the moving object, so it seems like a useless since the accuracy declines with increasing the RPM. A more convention technique for measuring the RPM is the tachometer, which can precisely measure the angular velocity of DC motor up to thousands of RPM, the tachometer devices are classifying according to its contacting with the rotor shaft to a non-contact and a contact tachometer. In the contact tachometer, there is a physical connection with the engine shaft, but the weakness in this technique is the speed diminishing which appears at exposure the system to an external force on the attaching point, so in this case, the tachometer provides an incorrect speed perusal. The second kind is a non-contact tachometer uses optocouplers light or a brightness sensor that can detect the rotation. For example, when put brightness sensor in front of a white- black disc on the motor shaft and the engine starts its turns, the tachometer blinks and forming a square wave via sensing the changing in the reflected light from the dark to the light on the rotational disc. Another technique implements by infrared light transmitter-receiver fixed in one package between a perforated disc then using a microcontroller chip to count the number of the received signals through the slots in one a minute.

For angular velocity, the internationally accepted metric units in the electronics technology fields are rad/s (radian per second) and RPM (Revolution per minute) both of them are using for measuring the same thing. To convert from radian per second (rad/s) to Revolution Per Minute (RPM), divide the rad/s by ($\frac{\pi}{30} = 0.10472$), while to convert back RPM to rad/s, divide the RPM by ($\frac{30}{\pi} = 9.54929$). The revolutions per minutes are directly proportional to the frequency (in Hz) which can be measured by utilizing microcontroller to count the number of received signals through perforated disc during one second. Which represent the frequency (Hz) then multiply it by the resolution (the number of slots in the disk) divided by 60 to convert it to revolutions per minutes instead of revolutions per second ($\mathrm{RPM} = \mathrm{Hz} * \frac{\mathrm{resolution/sec}}{60}$).

Over the years, the driving circuits which depending on the microcontroller are getting widish attraction in implementing a robust and cheaper controller via its integrated peripherals (such as Pulse Width Modulation (PWM) generator and Analog to Digital Converters (ADC), etc.,) and its enhanced features over the other techniques(using analog electronics). Such as improved reliability, less need of components, more adaptability to the latest control technique, increased flexibility of design and fast speed operation [9].

PIC18F4580 microcontroller is an 8-bit core size, within comparison to PIC16 microcontrollers family, it offers the benefits of all PIC16 MCU–i.e., high computational efficiency at a low price and minimal absorbing power during the operations – in addition to the high-stamina, Enhanced, 32 Kbytes Flash program memory, furthermore, the PIC18F4580 introduces enhanced designing that makes these microcontrollers as a logical choice for numerous of high-performance applications. The PIC18F4580 has four timers are referred to as Timers 0, 1, 2 and 3, which can be used either as timers (to generate a precise time delay, turn on an activity after or before a Predefined time, and used to measure the period that elapsed between two successive events), or as counters (to count external events which are happening outside the PIC microcontroller). The timer inside the PIC microcontroller is a free running binary counter, which increments synchronously with the applied pulse continuously from 0 to (2^{n})-1, where n-represents the number of bits in the timer register. In PIC18F4580, there are 8-bit (e.g., TIMER2**)** and 16-bit timers register (e.g., TIMER1 and TIMER3), So, the TIMER2 will count up to 255 while up to 65535 in TIMER1 and TIMER3, while TIMER0 can be triggered to work either as 8-bit or as 16-bit according to the user requirements [10]. The timer takes the internal clock source as a reference for ticking (in this case quarter of the crystal oscillator frequency which connecting between the OSC1 and OSC2 pins), while the counter counts external events feed through one port of the PIC18F4580 pins. So substantially, the timer can be considered as a counter with an internal clock pulse.

PIC18F4580 has one Capture Compare Pulse width modulation (CCP) module inside it (CCP1 in pin RC2), and Enhanced CCP module, each one consists of a 16-bit register associated with it, besides one-timer, for capture mode in PIC18F4580 timer1 or timer3 are initialized to count the number of pulses or the period between two consecutive rising or falling edges [10]. In PIC18F4580 microcontroller there are two ways to measure the feedback frequency: The first ones (the Casual way) is triggered the TMR1 to operate in time mode to give as one second in this duration, TMR0 operating as a counter to count the number of the rising or falling edges. The second way is using the capture mode to measure the period elapsed between two successive rising or falling edges (time duration) hence calculate the frequency of the wave (frequency = $\frac{1}{T}$), where T-is the time duration.

CHAPTER 2

LITERATURE REVIEW

2.1 Historical View

The experiments performed within the early nineteenth century in the physics field resulted in discovery the electromagnetic phenomena which paved the way for the invention DC Motor, those prototype versions came with a significant failing in dealing with the high-power applications, hence came up the need to invent much more powerful motors. The first real step in upgrading series of DC motors came in 1839 AD by Moritz Hermann Jacobi with Jacobi's motor construction with 1kW of a rated power [11]. The first invention model of the traditional brushed DC motor was carried out by Werner Von Siemens in 1856 AD [12].

DC motors are constructing on the principle of Lorentz Force's Law, the whole electromagnetic force (F) on the molecule charged is called the Lorentz force, which stipulates on: the force applied on a molecule has charge (q) moving with velocity (v) through a magnetic field (B) and electric field (E). Is given as:

$$F = q\, v \times B + q\, E \tag{2.1}$$

With the beginning of the industrial renaissance, emerged the demand for more powerful motors with an accurate controlling range. The earliest techniques for controlling the speed of DC motor was done manually, which is needing for much additional hardware resulted in unpractical and inefficient in many critical loads [13]. To overcome on the dilemma of that manual speed controlling, Ward Leonard in 1891 AD created a smart invention in the DC motor's world kept being used from 1900 up to 1960 by combining between several of rotating electrical machines for changing the motor speed [14].

After that, in 1947 with the invention of semiconductor chips, a huge turn happened in the speed control of the DC motors [15]. Specifically, in 1958 the world witnessed invented of the first thyristor to handle with the low power applications, after that date in 1961, Japan after significant efforts in this field has succeeded in upgrading thyristor devices to deal with 400V 80A [16]. Since then, Progress had created a further upgrading in the thyristor until it reached 750V and 1200V in 1976 [16]. After that, the voltage-current ratings and operation frequency of the semiconductor switches have increased rapidly, which paved the way for designing different driver circuits for the DC motor. Another significant imprint was added in the modern electronics between the duration from 1975 up to 1995 by invented the Gate Turn-off Thyristor (GTOs), Insulated Gate Bipolar Transistors (IGBTs) and Metal-Oxide-Semiconductor Field Effects Transistors (MOSFETs) [17].

All of these electronics preceding is either voltage or current controlled devices, so it is crucially important for looking for the tools or types of equipment that could give rise switching signal to control these devices. At the end of 1990 scientific types of research had already yielded the development of integrated PWM generating circuits, digital signal processors and a microprocessor which provided much simpler control techniques [18].

2.2 Related Studies

The related studies with the DC motor driven by step-down (buck converter) as follows:

Fourth order mathematical models proposed in 1999 by Lyshevski [19] for combining between the DC motor and its driver circuit (DC-DC power converters), in addition to that, the researcher was succeeded in designing a conventional analytical PI (proportional-integral) controller for the whole of the system to regulate the angular velocity of the DC motor.

After that, in 2004, Sira-Ramírez and Linares Flores presented a design to control the angular velocity of the dc motor driven by step-down (buck converter) within flat trajectory [3,4,20], wherein the smooth angular velocity path and the entire control system were confirmed only by numerical simulations.

In [4], discussed the regulation for the angular velocity of the dc motor driven by step-down (buck converter) based on the smooth differential approach, for achieving a smooth starter path for the angular velocity. That was done by proposed the second-order mathematical models for the entire system by taking into account neglecting the effect of both the capacitor on the step-down converter and the armature inductance on the DC motor.

Likewise, in [20], depending on implementation through a Σ-Δ modulator, they proposed an average General-Purpose Interface (GPI) control law, for the task of speed path chasing, for achieving this, they exploited both of the mathematical model and the flatness of the combined system (DC motor driven by buck converter) that derived in [4]. Similarly, for the same task and same system in [3], they presented a design for the dynamic output feedback controller based on the 4^{th}-order model extracted in [19], executed by utilizing the damping injection and the energy shaping method [21].

Furthermore, [22] (section published in [23]), and [1], depending on the fourth-order model and the differential flatness of the DC motor driven by a step-down converter, they presented a control technique for task of speed path chasing, the experimental implementation for the controller was done by utilizing the Pulse Width Modulation (PWM) technique via data acquisition cards. Nevertheless, in both of these works no including for the experimental verification when parametric suspicions exported in the system.

Furthermore, El Fadil and Giri in 2006[24], with regard toward the issue of speed control of DC motor driven by step-down (buck converter), they designed a voltage regulator based on the 4th order model of the global system and the backstepping technique, furthermore they designed both of the adaptive and the nonadaptive versions. They proved that the adaptive version transacts deals better with the changing in the load torque, they confirmed that through numerical simulations, where the Pulse Width Modulation (PWM) technique had utilized. Notwithstanding, neither parametric suspicions nor smooth references were tacked into the account.

Other work, by Ahmad et al. [25], in the late of in 2010, they implemented evaluation comparison through the numerical simulations for the performance between LQR controllers, traditional PI, and PI of a fuzzy logic type for the task of speed path chasing of a DC motor driven by a step-down (buck converter). Similarly, Ganeshkumar and Sureshkumar, in 2011 [26], they implemented a numerical simulations comparison for the similar system to check the performance of the backstepping and PI controllers that related with the regulation of the speed.

Unlike any previous works Bingöl and Paçaçi in 2012 [27], offered a virtual laboratory for the task of speed chasing, through the neural network controllers training selected for DC motor driven by step-down (buck converter), and it had constructed with a technique that allows the changing process in the controller and the DC motor parameters. Also, the feature of the GUI had added for monitoring the whole system's reaction under different operational circumstances.

Mohd Tumari et al. in 2012 [28], they proposed a numerical simulation for H-infinity control scheme with cluster pole premised on the linear matrix disparity styles for tracking the angular velocity of DC motor driven by step-down (buck converter), their proposed design warranties the higher angular velocity chasing concurrently with the minimum level of the duty cycle.

More recently, Oliver-Salazar and Sira-Ramírez in 2013[29], they proposed a robust control law premise on flatness-based control and external disturbance rejection control, taking into consideration unbeknown time-varying load for DC motor fed by a DC-DC step-down converter, it can be noted that they confirmed their proposal only by numerical simulations without experimental results.

Finally, Silva-Ortigoza et al. in 2013[30], they offered described in two phases a control system premise on differential flatness for the speed management without considering to measuring the revolution per minutes for the DC motor driven by DC-DC step-down converter. Basing on the numerical simulations involved a Σ - Δ modulator they proved that their design successfully provides more robustness for the task of DC motor speed chasing when parametric suspicions exported in the system.

As well as there are remarkable contributions associated with the combining of DC motor with DC-DC step-down converter were presented in [31, 32-39].

Depth audits in the literature review which related to the DC motor driven by DC-DC step down (buck converter) found the issue of controlling the former system (DC motor and buck converter) summarized in two main headlines:

I) With employing a 2nd order mathematical model. Which is awkward for medium- and low power applications, since they neglect some states or parameters from the consideration [26].

II) By using a 4^{th} order model which leads to a complex system.

Furthermore, in spite of the authors' knowledge concerning the action of the controllers designed, the speed trajectory tracking tasks and the angular velocity regulation just numerical simulation yet. No experimental verification published in a paper for answering on the many parametric suspicions or other issues that were put forward, for each of the motor and the DC-DC power converter, nor even when the system parameters' nominal values are undergoing in a wide range of the differences.

Motivated by the hierarchical control approaches that utilized in artificial intelligence and by those mentioned above, Ramón Silva et al., [(see [40– 44]) published their paper. They accomplished experimental validation of a hierarchical controller that performs the task of speed chasing for DC motor driven by DC-DC step-down (buck converter). The work had done by designing two independent controllers: The first one for the Buck converter (through SMC and the PI control) and the another via differential flatness (for the dc motor), these controllers were combined performing one controller for the whole system.

It is important to mention, for the voltage regulation job of Cuk converter, Buck-Boost, noninverting Buck-Boost, and the Boost converters was presented in [45-48] using cascade controller for the analyzing and designing processes, while they didn't take any consideration to the chasing mission of the voltage path in the DC-DC step down (buck converter) by the cascade controller.

Supported by somewhat of admissibility in the results beforehand discussed when appears a sudden changed on the system parameters and motivated by all contributions aforementioned. In this work robustness designing to control the DC motor driven by step-down (buck converter) basing on a 4^{th} order mathematical modeling is presented beside the experimental implementation results. The stability of the whole system is testing by the bode-plots before and after the including of the proportional-Integral (PI) controller which will be implementing on PIC18F4580.

So, the main headlines for this contribution are: implementing a bootstrap circuit to drive the MOSFET in the high-side mode, designing a buck converter to regulate the voltage that supposed to feed into the DC motor (for preventing the unacceptable dynamic behavior in the DC motor), and designing a tachometer for feeding back the angular velocity to the microcontroller. Besides implementing the PI controller algorithm in PIC18F4580 and tuning its parameters.

2.3 Purpose and Contributions of the Thesis

Due to the inverse relationship between the DC motor speed and the torque, all DC motors are elevating speed when they are unloaded, while to declining in speed as they are loaded, according to their torque /speed gradient linearly. For the purposes wherein, particular speed is in demand: Either with the obscure load (so a final angular velocity cannot be elaborated mathematically), or an oscillated load (grinding tools, pump, reel/converter, Cam, and conveyor belt). For those cases, the necessity of using the controller become mandatory for the motor.

In the camshaft application especially, wheresoever the motor acts as a “generator,” for half cycle and a “motor” for the next half, as the fluctuation load thrusts the DC motor, utilizing a four-quadrant driver become compulsory in the system. By this way the system gives dynamic stopping control, to guarantee that the angular velocity of the engine remains in beneath control. It is impossible to achieve that with a single quadrant controller or a simple power supply, besides that the controller must also handle with the fluctuated load, yet keep remaining the motor at a constant angular velocity by changing the applied voltage on it simultaneously with the load variant to compensate the speed fluctuations.

In pump and ventilating fan applications the power curve works according to the “square law,” i.e., the power increase doubling as gradually increase of the speed occurring. Using an angular velocity controller to descend the speed of the motor for achieving the requirement of a system, instead of inhibiting the flow from the ventilating fan or pump whereas operating the engine at full angular velocity will reduce the consumption of the power.

In industrial applications, there are many situations needed to drive any load at a specific speed for example, in sawmilling, high-speeds are requirable for cutting purposes, or in some cases like in paper mills, the low-speeds are in demand. In traction systems, wherein the motile between two locations, we need to slow down the engine speed on approaching the required station. Otherwise, high speed is required.

In the electric cars, motor controllers are done either manual or automatic for the stopping/starting the motor, choosing reverse/forward rotation, selecting, modifying or limiting the torque, and controlling the speed when the driver drives on a hill or a steep precipice.

In robotics world, the motile of robotic arms needs to accurate speed controller for maintaining the speed at a constant limited range for the cases of raise or lower objects.

CHAPTER 3

THEORETICAL METHODS

3.1 Transfer Function Model of Dc Motor

The general construction of the brushed DC motor divided into three main parts and as the following:

- Stationary part (the stator): is composed of permanent magnets which fixed on the inner shield of the motor.
- The rotor (armature): that carries the armature coils.
- The brushes and commutator: are providing electrical contact between the armature and the power supply while the motor is rotating.

According to Maxwell's equation in the electromagnetic field, a current ($I_a(t)$) flowing in a conductor with length (L) will produce an interaction with the magnetic field (B) so that the armature will experience a force f(t) impact on it.

$$f(t) = B.L.i_a(t) \tag{3.1}$$

This force will cause the armature to move (rotate), which will lead to arising an induce back EMF ($E_b(t)$) in the armature due to the variation in the magnetic field with the time which has emerged from that rotation:

$$E_b(t) = k_e \frac{d\theta_{(t)}}{dt} = k_e \omega(t) \tag{3.2}$$

Where k_e refers to the back EMF constant of the motor.

$$k_e = \frac{E_b}{\omega} \quad \text{with units } V.s.rad^{-1} \tag{3.2a}$$

The torque generated by the motor is proportional to the amount of current flowing across the motor (armature current).

$$T_m(t) = K_t I_a(t) \tag{3.3}$$

Where K_t refers to the torque constant, and $T_m(t)$ is the Torque in Nm unit.

$$K_t = \frac{T_m(t)}{I_a(t)} \text{ with units } Nm.A^{-1} \tag{3.3a}$$

The value of both these constants (voltage constant and torque constant) are related to the physical and geometrical properties of the brushed DC motor, such as the physical dimensions, numbers of turns in the coil, numbers of series conductors per coil, Cross-sectional area of wire, the metal of the wires, and the magnetic flux density.

Interestingly, based on the energy conservation law, we can infer the fact that the back EMF constant (k_b) and the torque constant(K_t) both of them are equals. The electrical input power must be equal to the summation of the mechanical output power plus the overall losses (electrical and mechanical losses), if we ignored the mechanical and the electrical losses (neglecting friction, the effects eddy currents, resistive and the alternative losses) that inherently associated with the motor operation, this will lead to

$$\text{Electrical power = Mechanical power.} \tag{3.4}$$

Where the mechanical power = (Torque * angular displacement)/time= (Torque* rotational speed).

$$P_m = T_m \boldsymbol{\omega} \quad \text{With W unit.} \tag{3.5}$$

And The electrical power= (output voltage * output current)

$$P_e = E_b i_a \quad \text{With W unit.} \tag{3.6}$$

So that:

$$T_m \boldsymbol{\omega} = E_b i_a \qquad \text{with the rearranging, } \frac{T_m}{i_a} = \frac{E_b}{\omega}$$

$$\text{This means that } K_t = k_e \tag{3.7}$$

Equation (3.7) is valid as long as k_b and K_t are measuring with a consistent unit, this is reasonable because all factors are the same (physical and geometrical) and related to each other. For simplification, we will define K as a new constant (the motor constant) which is the same as torque constant and the same as speed constant.

$$k = k_e = k_t \tag{3.8}$$

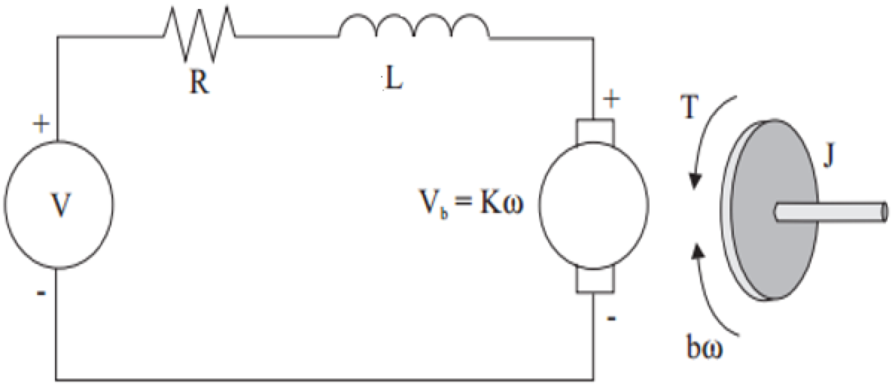

Figure 3.1 Schematic representation of the considered DC motor [49].

From figure 3.1 we can infer the following equations which have been basing on Newton's law combined with the Kirchhoff's law:

$$J\frac{d^2\theta}{dt^2} + b\frac{d\theta}{dt} = ki \tag{3.9}$$

$$Ri + L\frac{di}{dt} = V - K\frac{d\theta}{dt} \tag{3.10}$$

After taking the Laplace transform for the previous equations:

$$Js^2\theta(s) + bs\theta(s) = kI(s) \tag{3.9a}$$

$$LsI(s) + RI(s) = V(s) - ks\theta(s) \tag{3.10a}$$

Where S denotes to the Laplace operator. From equation (3.10a) we can express on $I_{(s)}$ as:

$$I_{(s)} = \frac{V(s) - Ks\theta(s)}{R + Ls} \tag{3.10b}$$

And substitute it in equation (3.9a) for obtaining:

$$Js^2\theta(s) + bs\theta(s) = k\frac{V(s) - Ks\theta(s)}{R + Ls} \tag{3.11}$$

This equation is the synopsis of the brushed DC motor modeling which is present in the below figure 3.2.

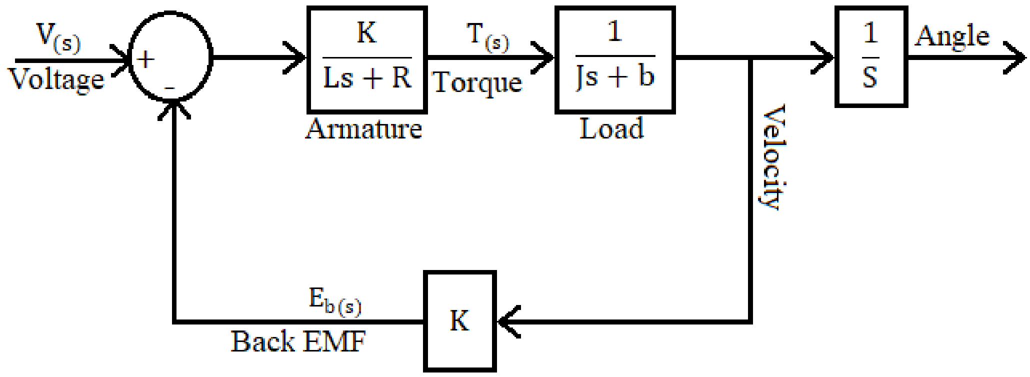

Figure 3.2 A block diagram represents the modelling of the DC motor.

From equation (3.10), the transfer function of the input voltage ($V_{(s)}$) to the output angular displacement (θ) is:

$$G_a(s) = \frac{\theta_{(s)}}{V_{(s)}} = \frac{k}{s[(R+Ls)(js+b)+k^2]} \tag{3.12}$$

From the block diagram in figure 3.2, it is easy to see that the transfer function of the input voltage ($V_{(s)}$) to the angular velocity ($\omega_{(s)}$) is:

$$G_v(s) = \frac{\omega_{(s)}}{V_{(s)}} = \frac{k}{[(R+Ls)(js+b)+k^2]} \tag{3.13}$$

3.2 Parameters Estimation of The DC Motor

From equation (3.12), we can realize some parameters that must be found depending on the empirical measurement. These parameters are the armature inductance, the armature resistance, the motor constant, and the motor inertia.

3.2.1 Measuring the Armature Resistance (R_M)

It is representing the resistance across the motor terminals by taking into consideration the influence of the fluctuating between the brushes and the commutator which is caused by the back EMF. So, the best technique for measuring the armature resistance by preventing the motor from rotating and measuring the current at that moment in a particular applied voltage.

From equation 3.10, at stalling case (the angular velocity is zero, and there is no changing in the amount of current with the time) so, both of $\frac{di}{dt}$ and ω are zero.

$$R = \frac{V}{I_{stall}} \text{ in ohm.} \tag{3.14}$$

In this work, with applying 7.2V nominal voltage, the value of stalling current was found as 0.52A.

$$R_M = \frac{7.2}{0.52} = 13.846 \text{ ohm.} \tag{3.14a}$$

3.2.2 Measuring the Armature Inductance (L_M)

Experimentally there are two ways for measuring the inductance of the armature, one of the ways is done by applying step input voltage and preventing the motor from the rotating (stalling case) and measuring the time constant of the electrical subsystem (RL circuit) [54]. The second technique involves using the LC meter to estimate the inductance value of the motor.

To calculate the current consumed by the motor an external resistance ought to be connected in a series with the motor terminals to measure the voltage drop across it, and so measuring the current.

$$I = \frac{V}{(R_S + R_M)} \tag{3.15}$$

By using this technique, the value of the motor inductance was found as 0.719 mH.

$$L_M = 0.719 \text{ mH.} \tag{3.16}$$

3.2.3 Measuring the Motor Constant (k)

There are two techniques for measuring the motor constant either from the voltage-current relationship $K_e = \frac{v - IR}{\omega}$, where ω measures either by tachometer or speed encoder, or from the torque-current relationship at stalling case $K_t = \frac{T_{stall}}{I_{stall}}$.

With applying 7.2 V as the nominal voltage, the current consumed by the motor at no-load was 14mA, and from the tachometer measurement, the speed was 6130 rpm (641.93209815 rad/sec). So, after rearranging equation 3.10 with $\frac{di}{dt} = 0$.

$$K_e = \frac{7.2 - (13.8 * 14 * 0.001)}{641.93209815} = 10.914 \text{ mV-sec/rad}$$

From equation 3.8 we proved that $K_e = K_t$ so:

$$K = K_e = K_t = 10.914\ m\frac{V}{rad/_{sec}} \tag{3.17}$$

Equation 3.17 can be used to infer the value of stalling torque as the following:

Experimentally, at the stalling case, the amount of the consumed current was about 0.52 A. So, based on the equation 3.3

$$K{=}10.914{=}\frac{T_{stall}}{I_{stall}} \Rightarrow T_{stall} = 0.52 * 10.914 = 5.675m\ Nm. \tag{3.18}$$

3.2.4 Measuring the Moment of Inertia (J)

Based on the mechanical time constant we can measure the moment of inertia, which is done by turning off the motor and measuring the time that the angular velocity takes it to decay. As in the below formula [54].

$$\text{Time decay after turning off the motor} = \frac{\text{motor inertia}}{\text{damping coefficient}} \tag{3.19}$$

The damping of the motor was measured based on the combination of equation 3.9 and the torque-current relationship at steady state (equation 3.3) to yield the below equation:

$$J\frac{d\omega}{dt} + b\omega = T \tag{3.20}$$

At steady state condition $\frac{d\omega}{dt} = 0.$

$$b\omega = T \Rightarrow \text{ damping of the motor(b)} = \frac{T}{\omega}$$

$$T_{no\_load} = k * I_{no-load} \ \Rightarrow \text{which is arising from the friction.}$$

$$T_{no-load} = 10.914\ m * 14m = 152.796\ \mu Nm \tag{3.21}$$

$$b = \frac{152.796\ \mu}{641.93209815} = 2.3771928 * 10^{-7}\ Nms/rad \tag{3.22}$$

The decay time was found empirically as 0.87s. Substituted the value of the damping coefficient and the decay time in equation 3.19 to yield:

$$\text{Motor inertia}{=}2.3771928 * 10^{-7} * 0.8791{=}2.09{*}10^{-7}\ \text{kg-m}^2. \tag{3.23}$$

3.3 The Relationship Between Torque and DC Motor Output Speed

Grasping the equation of torque in addition to the relevance between torque and speed are significant portions in the operating and selecting the proper DC motor.

Generally, from equation 3.3, we inferred that the torque is a function of current not speed, however, for a given supply voltage (V) the torque will inversely drop off with speed in a nearly linear fashion. As long as the back EMF rises (that happens when increasing rotational speed) more resistance will be added on the motor (from the decreasing of the current), when the back EMF reaches its maximum (equalize to the applied voltage) no torque is available for output because the current dropped to zero according to equation 3.10b. Now, rearranging equation 3.10b to yield:

$$\omega_{(s)} = \frac{V(s) - I(s)(R + Ls)}{K} \tag{3.24}$$

In the case of applying a fixed external load on the motor shaft, the angular velocity will be directly proportional with the applied voltage on the DC motor terminals. In the other side, the using of a fixed voltage causes the angular velocity to be in inverse relation with the with the applying load (the consuming current) as depicted in the speed-torque curve see figure 3.3.

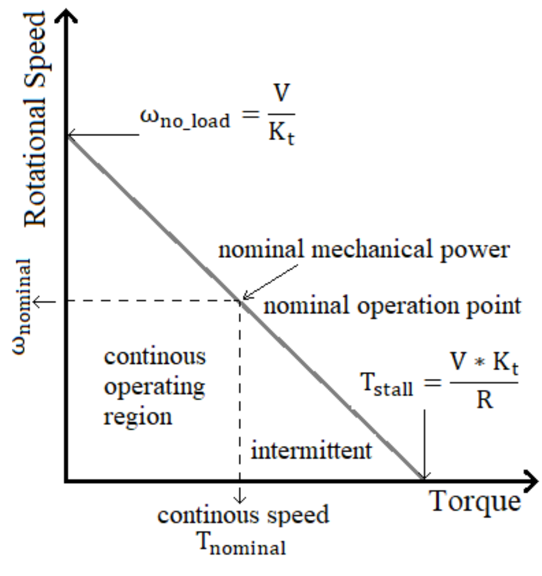

Figure 3.3 Operating points of the DC motor.

The inverse relevance between torque and speed denotes that the increase of the applied torque (that lead to increasing the consuming current) will cause a speed descending, that was according to the below formula which also inferred from equation 3.10b.

$$T(s) = \left(\frac{V_{(s)} - Ks\theta_{(s)}}{R+Ls}\right) * K \quad (3.25)$$

In figure 3.3 we see two significant points:

1-The $T_{stalling}$ (stalling torque): It is the point in which the applied load (external torque) becomes higher than the ability of DC motor to maintain the rotate of its rotator shaft (the angular velocity reaches zero ω=0) causing the engine to persist stalemate until burning from overheating, which caused from consuming much more current than the nominal case. It's not desirable to operate the DC motor close to this point for a long time. So, to protect the DC motor from melting it is preferable operates it at the nominal torque as shown in figure 3.3.

At steady state, the current is not changing. So, we can ignore the term $L\frac{di}{dt}$ from the accounts in equation 3.10 to yield:

$$K\omega + Ri = V \quad (3.26)$$

Now, rearranging the above equation according to the definition of torque constant (T=KI) we can get

$$\omega = \frac{V}{K_t} - \frac{R}{K_t^2}T \quad (3.27)$$

In case of stalling current ω=0. So

$$T_{stall} = \frac{V * K_t}{R} = \frac{7.2 * 10.9m}{13.8} = 5.686 \text{ in Nm.} \quad (3.28)$$

Which is the maximum delivered torque from the DC motor.

In general, the stalling torque occurs when the motor shaft torque is equals or minimums than the load torque (i.e., break down torque condition). In this case, in spite of pulling maximums of current by the motor but the angular velocity is rapid fall down to the zero, so it is lead to detrimental effects on the whole of the system.

2- The ω_{no_load}(no-load speed): It is the engine angular velocity in case of zero an external torque applied on the motor. So, in this case, the minimum current will be consumed due to the maximum back EMF occurred as demonstrated in equation 3.10b. Now with substituting ($I_{min} = \frac{T_{min}}{K}$) in equation 3.27 with dropping out the external torque from the consideration.

$$\omega_{no\_load} = \frac{V-IR}{K_t} = \frac{7.2-(14m*13.8)}{10.9m} \quad (3.29)$$

$$\omega_{no\_load} = 641.932 \text{ in rad/sec or 6130 rpm.} \quad (3.29a)$$

That represents the maximum speed of the motor on a specific applied voltage, with neglecting the friction torque and the other losses.

3.4 The General Concepts of the Step-Down Converter

A general concept of a step-down DC-DC converter was explained by the depicting in Figure 3.4. The applied voltage (V_{in}) appears on the load for the time duration t_1 (the closed period of the switch) while for the other period t_2 (switch opening period) zero volt appears on the load side and so on in a consecutive manner.

The average voltage that appears on the load is:

$$V_{out\_average)} = \frac{1}{T}\int_0^{t_1} V_{in}\ dt + \frac{1}{T}\int_{t_1}^{t2} V_{in}\ dt = \frac{t_1}{T}V_{in} + 0 = f * t_1 V_{in}$$

$$V_{out\_(average)} = DV_{in} \quad (3.30)$$

Where D represents the duty cycle, T is the chopping period which is ($t_1 + t_2$), and f represents the chopping frequency which is equal to $\frac{1}{T}$.

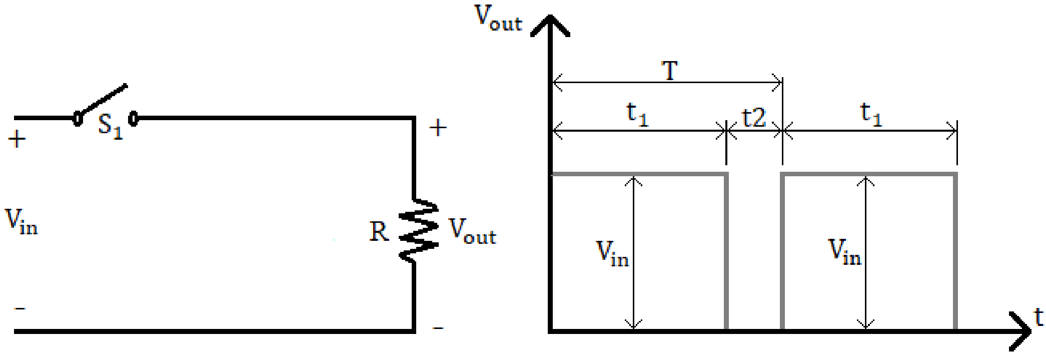

Figure 3.4 Step-down operation and the applied voltage on the load.

The average current consumed by the load is:

$$I_{out\_(average)} = \frac{V_{out\_(average)}}{R} = \frac{DV_{in}}{R} \quad (3.31)$$

The Root Mean Square (RMS) that appears on the load is:

$$V_{out\_(RMS)} = \sqrt[2]{\frac{1}{T}\int_0^T V_{out}^2\,dt} = \sqrt{D}V_{in} \tag{3.32}$$

If we assumed that the power converter to be lossless, the output power of the step-down converter is equalizing to the input power. So, the input power of the chopping is:

$$P_{in} = \frac{1}{T}\int_0^{DT}(I_{out} * V_{out})dt = \frac{1}{T}\int_0^{DT}\frac{V_{out}^2}{R}dt = D\frac{V_{in}^2}{R} \tag{3.33}$$

The source sees the effective resistance as:

$$R_{effective} = \frac{V_{in}}{I_{average}} = \frac{R_{load}}{D} \tag{3.34}$$

3.5 RLE Load Fed by the Step-Down Converter

The step-down converter is a current step-up and voltage step-down conversation. In the methodology of a step-down converter, The MOSFET switch will turn on and off in succession so it will form two operation modes. as depicted in figure 3.5.

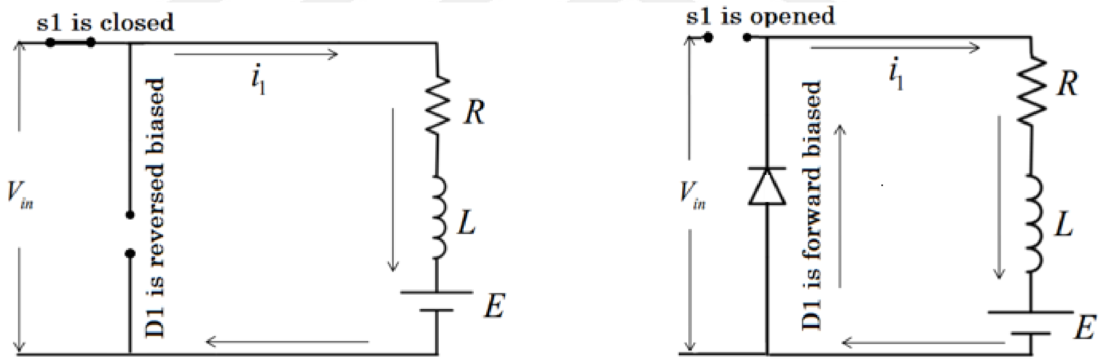

Figure 3.5 The two operation modes of the step-down converter.

The first mode when S_1 is closing, so the diode (D1) is reverse biased. The current across the load infer by applying Kirchhoff's voltage law:

$$Ri_1 + L\frac{di_1}{dt} + E = V_{in} \tag{3.35}$$

By taking the Laplace transforms for both sides:

$$RI_{1(s)} + LsI_{1(s)} - LI_{01} + \frac{E}{s} = \frac{V_{in}}{s} \tag{3.35a}$$

Wherein the initial current value is $I_{01} = I_1$.

$$I_{1(s)} = \frac{V_{in} - E}{(R+Ls)s} + \frac{I_1\, L}{(R+Ls)} \tag{3.35b}$$

After taking the Laplace inverse for the above equation:

$$i_{1(t)} = I_1 e^{-t\frac{R}{L}} + \frac{V_{in} - E}{R}\left(1 - e^{-t\frac{R}{L}}\right) \tag{3.36}$$

The above equation is valid for the period from $0 \le t \le t_1$, since t_1 =DT, so $0 \le t \le DT$. At the terminus of this period, the load current becomes $i_1(T_1 = t = DT) = I_2$, where I_2 is the initial current value for the second mode.

Now for the second operation mode, S1 is opening, so the diode (D1) is forward biased. The current across the load infer by applying Kirchhoff's voltage law:

$$Ri_2 + L\frac{di_2}{dt} + E = 0 \tag{3.37}$$

By taking the Laplace transforms for the above equation:

$$RI_{2(s)} + LsI_{2(s)} - LI_{02} + \frac{E}{s} = 0 \tag{3.37a}$$

Substituting $I_{02} = I_2$, where I_{02} is the initial current value for this mode.

After taking the Laplace inverse:

$$i_{2(t)} = I_2 e^{-t\frac{R}{L}} + \frac{0 - E}{R}\left(1 - e^{-t\frac{R}{L}}\right) \tag{3.38}$$

Now, the initial current of the third mode will be:

$$I_3 = i_2(T_2 = t = (1 - D)T)$$

$I_3 = I_1$ because it is a repetitive process.

By the substituting instead of (t) in equation 3.36 by (D), and instead of (t) in equation 3.38 by (1-D) to yield:

$$I_2 = I_1 e^{-DT\frac{R}{L}} + \frac{V_{in} - E}{R}\left(1 - e^{-DT\frac{R}{L}}\right) \tag{3.39}$$

$$I_1 = I_2 e^{-(1-D)T\frac{R}{L}} - \frac{E}{R}\left(1 - e^{-(1-D)T\frac{R}{L}}\right) \tag{3.40}$$

By solving equations (3.39) and (3.40).

$$I_1 = \frac{V_{in}}{R}\left(\frac{e^{DT\frac{R}{L}-1}}{e^{D}-1}\right) - \frac{E}{R} = \left[\frac{V_{in}}{R}\left(\frac{e^{\left(D\frac{R}{fL}\right)-1}}{e^{D}-1}\right)\right] - \frac{E}{R} \tag{3.41}$$

$$I_2 = \frac{V_{in}}{R}\left(\frac{e^{-DT\frac{R}{L}-1}}{e^{-D}-1}\right) - \frac{E}{R} = \left[\frac{V_{in}}{R}\left(\frac{e^{-\left(D\frac{R}{fL}\right)-1}}{e^{-D}-1}\right)\right] - \frac{E}{R} \tag{3.42}$$

3.5.1 The Ripple Current for RLE Load Fed From The Step-Down Converter

The electrical current from peak to peak is giving as depicted in the below formula:

$$\Delta I = I_2 - I_1 \tag{3.43}$$

With compensating the equation 3.41 and the equation 3.42 in the equation 3.43:

$$\Delta I = \frac{V_{in}(1-e^{D\frac{R}{fL}+e^{-\frac{R}{fL}}-e^{(1-D)\frac{-R}{fL}}}}{R\left(1-e^{-\frac{R}{fL}}\right)} \tag{3.44}$$

If R≪ Lf, this leads to $\frac{R}{fL}\approx 0$. After taking the limit equation 3.44 with $\frac{R}{fL} \to 0$:

$$\Delta I = \frac{V_{in}D(1-D)}{fL} \tag{3.44a}$$

The maximum value of equation 3.44 is obtaining by deriving the equation with respect to D, then equivalent it with the zero.

$$\Delta I_{maximum} = \frac{V_{in}}{R}\tanh\frac{R}{4fL} \tag{3.44b}$$

For the case $R \ll 4fL$

$$\tanh\frac{R}{4fL} \approx \frac{R}{4fL}$$

$$\text{So, } \Delta I_{maximum} = \frac{V_{in}R}{4fL} \tag{3.44c}$$

Which gives the same result of the equation 3.44a.

3.5.2 Continuous and Discontinuous Conduction Modes

Sometimes the current consumed by the load may be discontinuous (large off time) especially when the switching frequency is low, i.e., $i_2(T_2 = t = (1 - D)T)$ might be zero. The compulsory stipulation to guarantee the continuous conduction is I_1 always must be higher than zero. Applying this condition on the equation 3.41 yielded:

$$I_1 > 0 \Rightarrow \frac{V_{in}}{R}\left(\frac{e^{\left(D\frac{R}{fL}\right)}-1}{e^{D}-1}\right)-\frac{E}{R} \geq 0$$

$$\text{So, } \frac{E}{V_{in}} \leq \left(\frac{e^{\left(D\frac{R}{fL}\right)}-1}{e^{D}-1}\right). \tag{3.45}$$

3.6 The Buck Converter with R Load and Filter

The buck regulator operates by varying the duration of time in which the source granted energy to the inductor. Buck converter (see Figure 3.6) is a DC to DC converter in which the duty cycle is manipulated to achieve a flat output voltage waveform (V_{out}) with a range from 0V up to the input voltage (V_{in}), since it used SMPS, so the efficiency here is much higher than the voltage regulator.

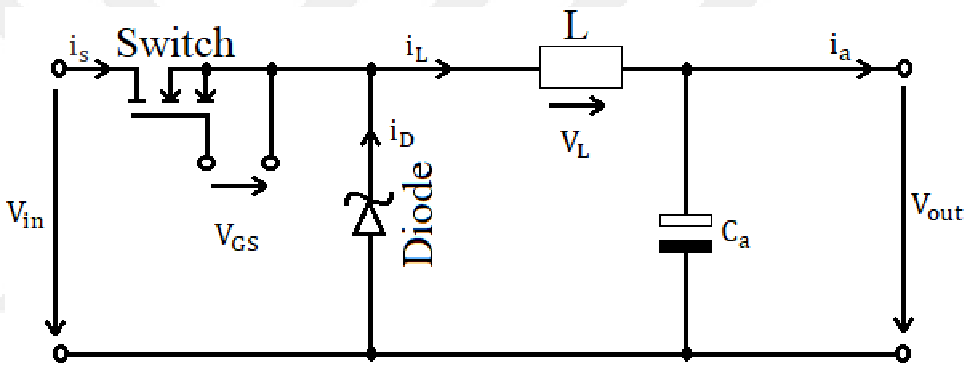

Figure 3.6 Buck converter topology.

In switching operation, there are two modes, a discontinuous mode (DMPS) and a continuous mode (CMPS). In DMPS there is a zero-inductor current period between the switch on and off, while in CMPS the inductor current flow continuously, which turn on and off consecutively in the same of the switching frequency, as depicted in figure 3.7.

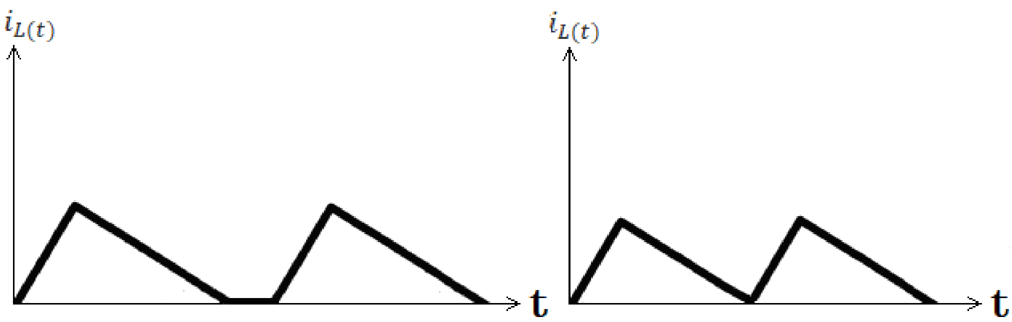

Figure 3.7 Discontinuous and Continuous modes in the buck converter.

Generally, the DMPS is using in the small loads in spite of it has less switch power loss (more efficient) than CMPS but it has a large pinnacle current than CMPS so, it is not preferred to use it with the large loads.

To decrease the 12 V applied from the voltage source, the N-channel MOSFET will be used as a Switch to drive the buck converter by a PWM signal feeds by a microcontroller with 5V amplitude. So, to initialize the MOSFET to work as a switch we need a bootstrap circuit to provide gain -source voltage larger than (12+V_T) when the switch is closing, and 0 V when the switch is opening.

3.7 Ideal Buck Converter

To remove the harmonics in the output waveform (current and voltage) that emerged from switching actions, a low pass filter (LC) has been used.

In the first mode when the MOSFET switch is on (closed), see figure 3.8. According to Kirchhoff's law, the voltage across the inductor is equal to the voltage source that appears when the switch is closing minus the output voltage (capacitance-voltage).

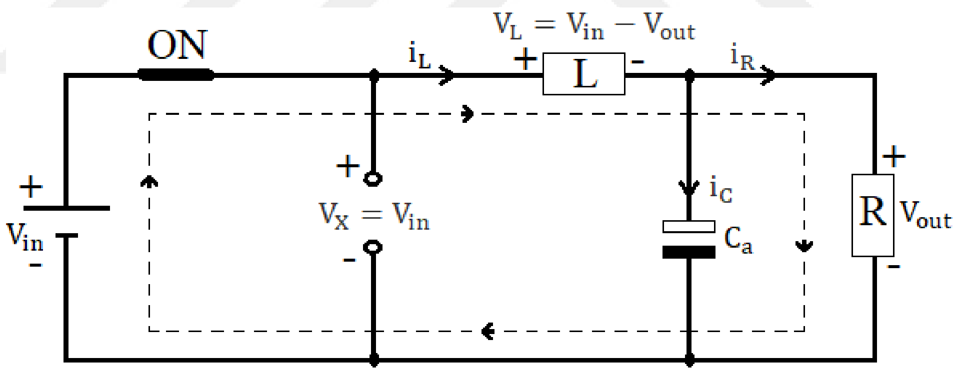

Figure 3.8 Equivalent buck converter circuit when the switch is on.

$$V_L = V_{in} - V_{out} \tag{3.46}$$

$$\text{Since } V_L = L\frac{di}{dt}\ , \ \Rightarrow \text{so} \quad L\frac{di_L}{dt} = V_{in} - V_{out} \ \text{ and } i_L = i_s$$

Where i_s represents the current flowing in the switch, and i_L represents the current flowing in the inductor.

$$\text{this led to } \frac{di_L}{dt} = \frac{V_{in}-V_{out}}{L}\ . \tag{3.47}$$

$\frac{V_{in}-V_{out}}{L}$ represents the rate of rising current across the inductor.

we know that $D = \frac{\Delta t_{ON}}{\Delta t_{ON} + \Delta t_{OFF}} = \frac{\Delta t_{ON}}{T}$

$$\Delta t_{ON} = DT \quad (3.48)$$

$$\Delta t_{OFF} = T - \Delta t_{ON} \Rightarrow \Delta t_{OFF} = T - DT$$

$$\text{So, } \Delta t_{OFF} = (1 - D)T. \quad (3.49)$$

Where Δt_{ON} represents the closing period of the switch, while Δt_{OFF} describes the opening period, and T represents the period for whole switching time (the closed duration plus the open duration). According to equation 3.47:

$\frac{\Delta i_L}{\Delta t_{LON}} = \frac{V_{in} - V_{out}}{L}$ this led to $\Delta i_L = \frac{V_{in} - V_{out}}{L} * \Delta t_{LON}$

$$\Delta i_{L\_ON} = \frac{V_{in} - V_{out}}{L} * DT \Rightarrow \Delta i_{LON} = \frac{V_{in} - DV_{in}}{L} * DT \Rightarrow \Delta i_L = V_{in} \frac{(1-D)}{L} * DT$$

$$\Delta i_{L\_ON} = V_{out} \frac{(1-D)}{L} * T \quad (3.50)$$

Where Δi_L represents the ripple of current and D represents the duty cycle.

So, reducing ΔI is done, either by a rising the inductance or by an elevating the switching frequency. At this period the diode is a reverse biased since the cathode (at Positive of Input) more positive than the anode (at 0 volts), so the diode does not conduct.

In the second mode see figure 3.9, when the MOSFET switch is off (open), the inductor will lose its charge rapidly which causing in reversing the voltage polarity of the inductor and descending its current in a slope equal to $\frac{-V_{out}}{L}$.

With compensating Δt_{LOFF} from equation 3.49 in equation 3.47 with zero V_{in} to yield:

$$\Delta i_{L\_OFF} = \frac{-V_{out}}{L} * (1 - D)T \quad (3.51)$$

The diode is forward biased since the anode (0 volts) is more positive than the cathode (at some negative voltage), this will make the diode looks like a closed switch, so the diode will form the return path for flowing the load current($i_{LOFF} = i_D$), where i_D represents the current flowing in the diode.

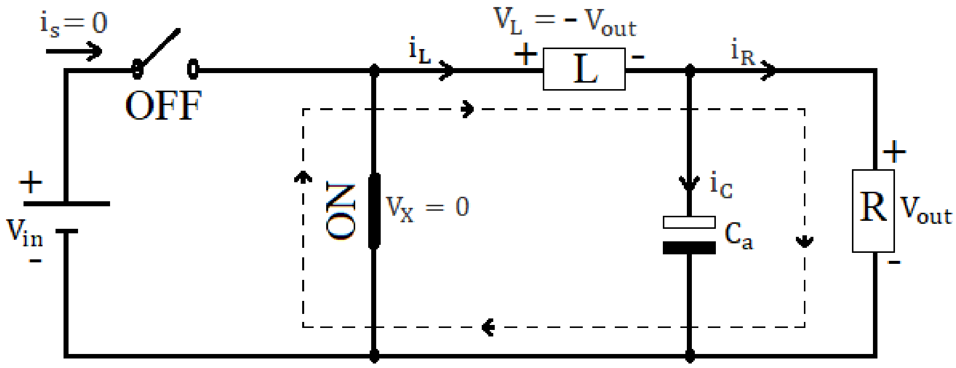

Figure 3.9 Equivalent buck converter circuit when the switch is off.

In the steady state case, the average voltage across the inductor is zero (with neglecting the tiny current in the capacitor i_c), so the inductor looks like a short to a DC.

$$V_L = V_{L\_ON} t_{ON} + V_{L\_OFF} t_{OFF} = 0$$

$$\text{So } (V_{in} - V_{out}) * D * T + (-V_{out})(1 - D)T = 0$$

$$V_{out} = D * V_{in} \tag{3.52}$$

So, the average voltage across the load is less than the source voltage source.

In the ideal case, the output power of the buck converter is equal to the input power (zero losses in the system).

$$\text{So, } P_{in} = P_{out} \Rightarrow V_{in} i_s = V_{out} i_{out} \Rightarrow V_{in} i_s = D V_{in} i_{out}$$

$$i_s = D i_{out} \tag{3.53}$$

3.7.1 The Critical Value of the Inductor

The maximum and minimum current flow through the inductor were founding as:

$$I_{L\_min} = I_L - \frac{|\Delta I_L|}{2} = \frac{V_{out}}{R} - \frac{1}{2}\left[\frac{V_{out}}{L}(1 - D)T\right] = V_{out}\left[\frac{1}{R} - \frac{(1-D)}{2Lf}\right] \tag{3.54}$$

$$I_{L\_max} = I_L + \frac{|\Delta I_L|}{2} = \frac{V_{out}}{R} + \frac{1}{2}\left[\frac{V_{out}}{L}(1 - D)T\right] = V_{out}\left[\frac{1}{R} + \frac{(1-D)}{2Lf}\right] \tag{3.55}$$

In general, the critical inductance is the minimums inductance value that below it the system falls in the DCM. The stipulations to find the critical inductance are either by the prior estimation of the maximum ΔI_L by the designer or by setting of the minimum load current in which the buck converter still maintains CCM.

The procedure to detect the critical inductance value is done by setting $I_{L_{min}=0}$, then solving the equation for $L_c = L$. After that, choosing $L > 1.4 * L_c$. Equalizing equation (3.54) with zero to get $I_{L\_min} = 0 = V_{out}\left[\frac{1}{R} - \frac{(1-D)}{2Lf}\right]$.

$$L_{Critical} = \frac{(1-D)R_{max}}{2f} \tag{3.56}$$

Where R_{max} calculating at minimum output current.

$$R_{max} = \frac{V_{out}}{I_{out,min}} \tag{3. 57}$$

For the DC motor the minimum current is occurring at the no-load case, in our empirical, it was 14mA, and the nominal voltage of the DC motor is 7.2V.

$$\text{So } R_{max} = \frac{0.6}{2m} = 300 \text{ ohm.} \tag{3.58}$$

From equation 3.52 and with a 12V input voltage, the value of the duty cycle is

$$D = \frac{V_{out}}{V_{in}} = \frac{0.6}{12} = 0.05 \tag{3.59}$$

Now, with substituting equation 3.58, 3.59 and the switching frequency which was selected to be 100KHz in equation 3.56 to yield $L_{Critical}$.

$$L_{Critical} = \frac{(1 - 0.05) * 300}{2 * 100K} = 1.425mH$$

So, this is the minimum inductance value in which the system maintains the CMPS mode. For guarantee, the buck converter work in CMPS mode, the inductance value will be multiplied by factor 1.4 to yield abound of safety to maintain the CMPS mode.

$$L = 1.4 * L_{Critical} = 2mH \tag{3.60}$$

From 3.54 and 3.55 we can find the minimum and maximum current across the inductance.

$$I_{L\_max} = 7.2\left[\frac{1}{13.8} + \frac{1-0.05}{2*2m*100k}\right] = 0.538A \tag{3.61}$$

$$I_{L\_min} = 7.2\left[\frac{1}{514.2857} - \frac{1-0.6}{2*2m*100k}\right] = 6.8mA \tag{3.62}$$

It is preferable to mention that these are the extreme pinnacle values for the current across the inductance. I_{Lmax} is the maximum value of the ripple at stalling case (when

$I_L = 0.52A$), while I_{Lmin} is the minimum value of the ripple at no load case (when $I_L = 14mA$).

3.7.2 The Critical Value of The Capacitor

The capacitor must endure the pinnacle value of the output voltage, for the ideal case Kirchhoff's law lead to:

$$V_{c\_max} = V_{out} + \frac{\Delta V_{out}}{2} \tag{3.63}$$

For more realistic, there is an Equivalent Series Resistance (ESR) in the capacitor which worsens ΔV_{out}. Using a parallel capacitor can help us in reducing the Equivalent Series Resistance.

After using Kirchhoff's law

$$i_L = i_c + i_{output} \tag{3.64}$$

The AC component (the ripple) of the capacitor current is equal to the current that flows through the inductor, leaving from it the average current through the load (which had neglected since it is very tiny), the resulting capacitor current waveform is showing in figure 3.10.

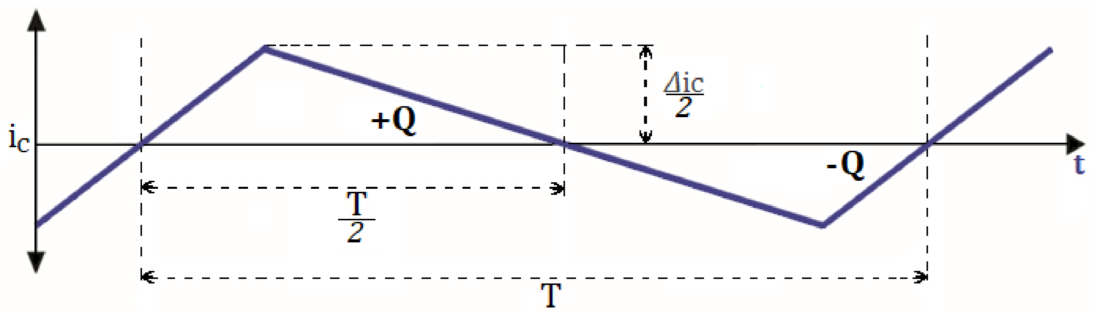

Figure 3.10 Capacitor current waveform in the buck converter.

The area under the triangle current waveform represents the amount of charge in the capacitor.

$$q = \frac{1}{2}\left(\frac{T}{2}\right)\left(\frac{\Delta i_L}{2}\right) = \frac{\Delta i_L}{8f} = \frac{\frac{Vout}{L}(1-D)T}{8f} = \frac{(1-D)V_{out}}{8Lf^2} \quad (3.65)$$

$$\text{Since } q = C * \Delta V_{out}\,. \quad (3.66)$$

$$\text{so,} \quad C = \frac{q}{\Delta V_{out}} = \frac{(1-D)V_{out}}{8Lf^2 \Delta V_{out}}$$

$$C = \frac{(1-D_{min})V_{out}}{8Lf^2 \Delta V_{out}} \quad (3.67)$$

With $\Delta V_{out} = 1\%$ V, the critical capacitor will be $C = \frac{(1-0.6)*7.2}{8*2m(100k)^2*0.01} = 1.8\mu F$

$$\text{For safety purposes it will be } C = 3\mu F \quad (3.68)$$

According to equation 3.63 to find the maximum voltage at the capacitor:

$$V_{c\_max} = 7.2 + \frac{0.001}{2} = 7.2005 \text{ V}. \quad (3.69)$$

Now to find the RMS value for current rating:

$$i_{c\_RMS} = \frac{\frac{\Delta i_L}{2}}{\sqrt{3}} = \frac{V_{out}(1-D)}{2\sqrt{3}Lf} \quad (3.70)$$

$$i_{c\_RMS} = \frac{I_{Lmax} - I_{Lmin}}{2\sqrt{3}} = \frac{0.0144}{2\sqrt{3}} = 0.00415A \quad (3.71)$$

3.7.3 Sizing for the Switch (MOSFET) and the Diode

It is so crucial to calculating the maximum and minimum voltage and current that the MOSFET and the diode must endure it:

Maximum voltage for the ideal case is:

$$V_{in\_max} = V_{DS-max} \qquad \text{for the MOSFET.} \quad (3.72)$$

$$V_{DS\_max} = 12V \quad (3.73)$$

$$V_{in\_max} = V_{PIV} \qquad \text{for the diode}$$

$$V_{PIV} = 12V$$

Where V_{PIV} represents the Peak Inverse Voltage across the diode

Maximum voltage for the non-ideal case is:

For safety purpose always, there are 20% safety factor must be taking on the account.

$$V_{in\_max} = V_{DS-max} - V_F \quad \text{for the MOSFET.} \tag{3.74}$$

$$V_{DS\_max} = 12 + (0.077 * 0.538) = 12.041 + (0.2 * 12.041)$$

$$V_{DS\_max} = 14.45\ \text{V} \tag{3.75}$$

$$V_{in\_max} = V_{PIV} - V_F \quad \text{for the Diode.} \tag{3.76}$$

$$V_{PIV} = 12 + (0.55) = 12.55 + (12.5 * 0.2) = 15.06\ \text{V} \tag{3.77}$$

At the maximum value of the load current, V_F represent the maximum forward voltage drops through the semiconductor at that moment.

Maximum current across the MOSFET:

From the Kirchhoff's current law, the inductor current equals the summation of the diode current and the switch current. During switch on, both of the switch current and the inductor current are equal, while During switch off, both of the diode current and the inductor current are equal. Now from the figure 3.11

$$i_{switch} = \frac{(i_{L\_min} + i_{L\_max}) * t_{on}}{2 * T} \tag{3.78}$$

$$i_{switch} = \frac{([i_{L\_max} - \Delta i_L] + i_{L\_max}) * DT}{2 * T} = \frac{(2i_{L\_max} - \Delta i_L) * D}{2}$$

$$i_{switch} = \left(i_{L\_max} - \frac{\Delta i_L}{2}\right) * D = i_L D = i_{out} * D \tag{3.79}$$

$$\text{So } i_{DS\_max} > i_{out\_max} * D_{max}. \tag{3.80}$$

$$i_{DS\_max} > 0.52 * 0.6 \Rightarrow \quad i_{DS\_max} > 0.312\text{A} \tag{3.81}$$

So, the MOSFET that we have to choose it must have the ability to handle with 12 V (drain-source) voltage, and 0.312 A (drain-source) current.

Maximum current across the diode:

$$i_f = \frac{(i_{L\_min} + i_{L\_max}) * t_{off}}{2 * T} \tag{3.82}$$

Where i_f represents the forward current across the diode.

$$i_f = \frac{([i_{L\_max} - \Delta i_L] + i_{L\_max}) * (1-D)T}{2*T} \tag{3.83}$$

$$i_f = \frac{(2i_{L\_max} - \Delta i_L) * (1-D)}{2}$$

$$i_f = I_L * (1-D) = i_{out} * (1-D) \tag{3.84}$$

$$\text{So } i_F > i_{out\_max} * (1 - D_{min})$$

$$i_F > 0.52 \text{ A} \tag{3.85}$$

So, the Diode that we have to choose it must have the ability to handle with 12 V Peak Inverse Voltage, and 0.52 A forward current.

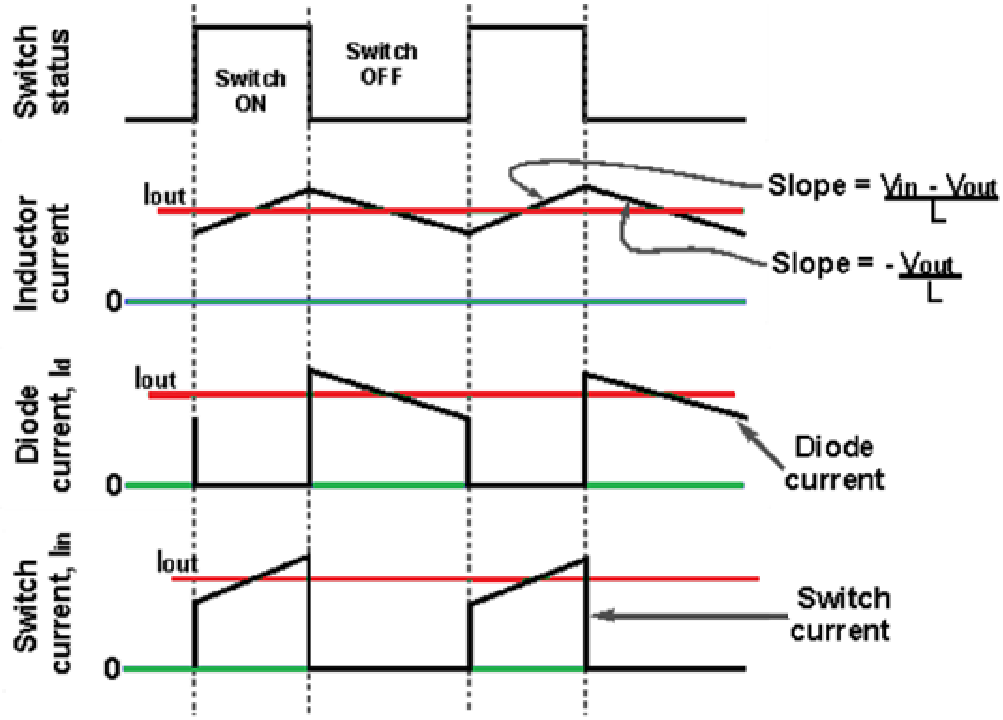

Figure 3.11 Currents in buck converter continuous mode [50].

So, MOSFET IRF540 and Schottky Diode 1N5818 are sufficient for our requirement. To summarize all of the previous critical values, (see Figure 3.12).

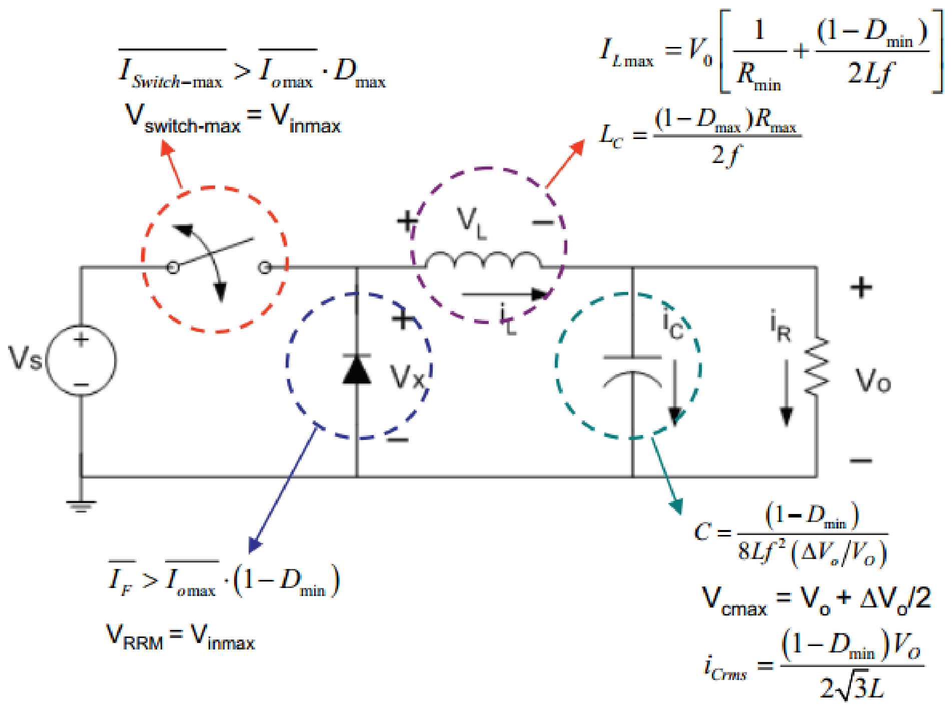

Figure 3.12 The summarize of all critical values in the buck converter.

3.8: Loss Considerations in Non-ideal Buck Converter

There are several losses in the step-down (buck) converter that needs to be taken into consideration when we have the desire to count the system efficiency:

- MOSFET Static losses.
- MOSFET Switching losses.
- Gate drive losses of the MOSFET.
- Diode static losses.
- Diode switching losses.
- Copper loss in the inductor.
- Equivalent Series Resistance (ESR) losses in the capacitor.

3.8.1 MOSFET Static Losses

In MOSFET the R_{DS_on} (drain to source resistance) depends on the junction temperature and on V_{GS} which both of them directly impacts on the MOSFET Static losses. As a result, the R_{DS_on} should be taken from the MOSFET datasheet because there is a specific value of the $R_{DS(on)}$ for each applied V_{GS}, as well as, there is a different value of $R_{DS(on)}$ for each ambient temperature [55].

The Static power losses for specific $R_{DS(on)}$ is

$$P_{static\ losses} = R_{DS\_on} * i^2_{switch\_RMS} \tag{3.86}$$

$$P_{static\ losses} = R_{DS\_on} * \left(i_{out} D \sqrt{1 + \frac{\Delta i_L}{2 i_{out}}}\right)^2 \tag{3.87}$$

From equations 3.50 and 3.51 To calculate Δi_L at nominal case (0.332 A).

$$|\Delta I_L| = \frac{7.2*(1-0.6)}{2m*100k} = 0.0144A \tag{3.88}$$

$$P_{static\ losses} = 0.077 * \left(0.332 * 0.6 \sqrt{1 + \frac{0.0144}{2*0.332}}\right)^2 = 0.003121W \tag{3.89}$$

3.8.2 MOSFET Switching Losses (Thermal Losses)

MOSFET Switching losses rely on how the overlaps occur between the current and the voltage waveforms, leading to (V*I) power losses from those overlaps. Current and voltage reaches their endpoints simultaneously and returns moving again in a consecutive manner as shown in the below figure 3.13.

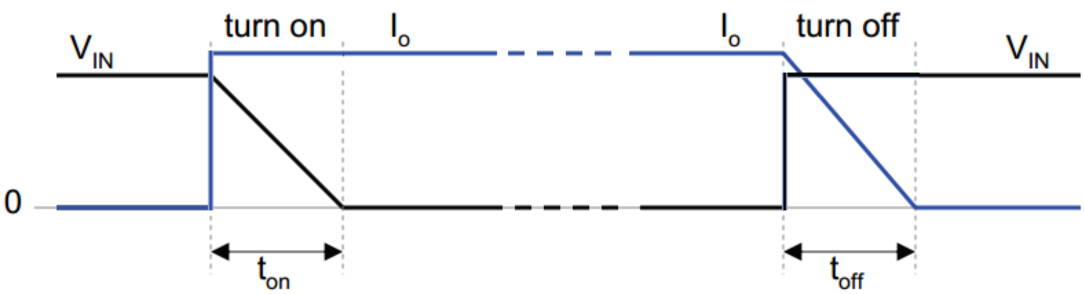

Figure 3.13 Voltage and current overlaps at MOSFET turning-off and turning-on.

In the hard loading, the switching losses occur in the periods between the turning-off and turning-on.

$$P_{sw(instantaneous)} = V_{sw(instantaneous)} * I_{sw(instantaneous)} \tag{3.90}$$

The slopes in the overlap periods are:

$$\text{For the current} \Rightarrow \quad I_{sw(instantaneous)} = I_{max} \tag{3.91}$$

$$\text{For the voltage} \Rightarrow V_{sw(instantaneous)} = \left(1 - \frac{t}{t_{ON}}\right) * V_{max} \tag{3.92}$$

Substitute equations 3.91 and 3.92 in equation 3.90 to yield the instantaneous power losses in the switch.

$$P_{sw(instantaneous)} = I_{max} * \left(\left(1 - \frac{t}{t_{ON}}\right) * V_{max}\right) \tag{3.93}$$

To calculate the amount of the energy that dissipates in the switch:

$$E_{(\text{for each cycle})} = \int_0^{t_{ON}} \left(I_{max} * \left(\left(1 - \frac{t}{t_{ON}}\right) * V_{max}\right)\right) dt \tag{3.94}$$

$$E_{(\text{for each cycle})} = (I_{max} * V_{max}) \left[\left(t - \frac{t^2}{2*t_{ON}}\right)\right]_0^{t_{ON}} \tag{3.95}$$

$$E_{(\text{for each cycle})} = (I_{max} * V_{max}) \left(\frac{t_{ON}}{2}\right) \quad \text{in joules per cycle} \tag{3.96}$$

So, the power losses for the whole of cycles is

$$P_{sw(ON)} = (I_{max} * V_{max}) \left(\frac{t_{ON}}{2}\right) * f \quad \text{in } \frac{\text{joules}}{sec} \text{ unit} \tag{3.97}$$

The same procedure can be repeated to find the power losses for the off period to yield.

$$P_{sw(OFF)} = (I_{max} * V_{max}) \left(\frac{t_{OFF}}{2}\right) * f \tag{3.98}$$

$$P_{switching\_losses} = P_{sw(ON)} + P_{sw(OFF)} \tag{3.99}$$

$$P_{switching\_losses} = (I_{max} * V_{max}) \left(\frac{t_{ON}}{2}\right) * f \quad + (I_{max} * V_{max}) \left(\frac{t_{OFF}}{2}\right) * f \tag{3.100}$$

$$P_{switching\_losses} = \frac{(I_{max}*V_{max})}{2} (t_{on} + t_{off}) * f \tag{3.101}$$

t_{on} and t_{off} are related with overlap period and found from the datasheet. For the nominal operation mode:

$$P_{switching\_losses} = \frac{7.2*0.332}{2} (12n + 50n) * 100k = 0.00741024 \text{ W} \tag{3.102}$$

3.8.3 Gate Drive Losses Of The MOSFET

It is coming from the applied voltage on the gate (V_{gate}) and the total gate charge (Q_{gate}).

$$P_{gate} = \frac{1}{2} V_{gate} Q_{gate} f \tag{3.103}$$

$$P_{gate} = \frac{1}{2} * 18 * 9n * 100K = 0.0081 \text{ W} \tag{3.104}$$

There is also another loss in the MOSFET come from the output capacitor (C_{oss}) which is charging when the MOSFET is turned off [55].

$$P_{C\_oss} = \frac{1}{2} {V_{in}}^2 C_{oss} f \tag{3.105}$$

$$P_{C\_oss} = \frac{1}{2} 12^2 * 390p * 100K = 2.808 \text{ µW} \tag{3.106}$$

3.8.4 Diode Static Losses

The static losses in the diode are coming from two prime reasons: The first one is from the forward biasing and the second one from the reverse loss.

• Forward loss

$$P_{forward-loss} = V_f * I_f + {I_f}^{\sim} * r_d \tag{3.107}$$

Where r_d is the dynamic resistance of the semiconductor device, V_f is taking from the diode datasheet, I_f from equation 3.84, which is $I_f = i_{out} * (1 - D)$, and ${I_f}^{\sim}$ as:

$${I_f}^{\sim} = \sqrt{\frac{(1-D)}{3} [I_{max}^2 + I_{min}^2 + I_{max} * I_{min}]} \tag{3.108}$$

$${I_f}^{\sim} = \sqrt{\frac{(1-0.6)}{3} [(0.332 + 0.014)^2 + (0.332 - 0.014)^2 + (0.332 + 0.014) * (0.332 - 0.014)]}$$

$${I_f}^{\sim} = 0.21 \text{ A} \tag{3.109}$$

$$I_f = 0.21 * (1 - 0.6) = 0.084 \text{ A} \tag{3.110}$$

$$P_{forward-loss} = 0.55 * 0.1328 + 0.21 * \frac{26m}{0.084} = 0.13804 \text{ W} \tag{3.111}$$

• Reverse loss

Which is represents the loss that occurs when the diode is in the non-conducting condition [55].

$$P_{reverse\_loss} = V_r * I_r(1 - D) \tag{3.112}$$

$$P_{reverse\_loss} = 12 * 1m(1 - 0.6) = 0.0048\ W \tag{3.113}$$

3.8.5 Diode Switching Losses

Because in this work we used Schottky diode so, the losses from switching are so tiny which can be neglect.

3.8.6 Copper Loss in the Inductor

Since the Inductor winding had constructed from the copper, so inherently there is a power loss arise from that internal resistance.

$$P_L = I_{\tilde{L}}^{2} R_L \tag{3.114}$$

P_L represents the power copper loss.

$$\text{Where, } I_{\tilde{L}} = I_{rms}\sqrt{1 + \frac{1}{3}\left(\frac{\Delta I_L}{2I_{rms}}\right)^2} \tag{3.115}$$

$$I_{\tilde{L}} = 0.332\sqrt{1 + \frac{1}{3}\left(\frac{0.0144}{2*0.332}\right)^2} = 0.332\ A \tag{3.116}$$

$$P_L = 0.332^2 * 3 = 0.33072\ W \tag{3.117}$$

There is also core loss emerging from the relation $P_{core\ loss} = K_1 * B^{k2} * F^{k3}$

Where B is the flux swing and F is the switching frequency and K_1, K_2, and K_3 are constant associated with the ambient temperature and provided by the manufacturer [55].

3.8.7 Equivalent Series Resistance (ESR) Losses in the Capacitor

In the real world, every capacitor has an Equivalent Series Resistance inherently associated with it leading to dissipation power.

$$P_{ESR} = I_c^{\sim 2} * ESR \quad (3.118)$$

$$\text{Where } I^{\sim}{}_{c} = \frac{\Delta I_L}{2\sqrt{3}} \quad (3.119)$$

$$I^{\sim}{}_{c} = \frac{0.0144}{2\sqrt{3}} = 0.0041569 \text{ A} \quad (3.120)$$

From the datasheet ESR = 4.33 m ohm

$$P_{ESR} = 0.0041569^{\ 2} * 4.33\text{m} = 0.07482\ \mu\text{W} \quad (3.121)$$

The total power losses are the summation of all of those losses, which found about 0.496351 W.

$$P_{\text{total losses}}\text{=0.496351 W} \quad (3.122)$$

3.9 Efficiency Improvement of the Buck Converter

There are several ways which can be utilized to reduce these losses:

- MOSFET: Utilize the MOSFET that has the following features:
    - ✓ At the High Duty Cycle have Low $R_{ds(on)}$.
    - ✓ At Low Duty Cycle have Low Gate Charge.
    - ✓ Using a bootstrap circuit: To drive N-channel MOSFET.
- Schottky Diode: using Schottky Diode that has these features:
    - ✓ Minimal forward voltage drops.
    - ✓ Short recovery time.
- Inductor:
    - ✓ Using Multiple parallel winding like three windings (Trifiliar), or two windings (Bifiliar).
- Capacitors:
    - ✓ Using the capacitor that has a low value of ESR.

- ✓ Using Paralleling capacitor (in parallel for reducing ESRs while increasing capacitance).

- Reduce the inductor current ripple:
  - ✓ Reduce the Root mean square losses (for output values of the capacitor and the inductor).
  - ✓ Increase the inductance or the switching frequency.
- Reduce the gate drive voltage as possible.
- Using Synchronous MOSFET as a switch (instead of the diode) on the low side.

3.10 Modeling of the DC Motor with a Step-Down (Buck-Converter) System

Due to the facts that associated with the MOSFET functionality (in the switching operation of turning on and off), the step-down (buck) converter is inherently a non-linear system. Manipulated the duty cycle of the Pulse Width Modulation (PWM) signal in a fixed frequency leads to regulating the DC input voltage by providing an output voltage in scale from zero volts up to the main entering voltage (source voltage) as has been shown in equation 3.30. The simplified model of the entire system (Permanente brushed DC motor fed by a DC-DC step-down power converter) is showing in figure 3.14.

The modeling of the switching-mode power supply part (MOSFET) has done by multiplying the main entering voltage source with a variable number (u) $\in \{0,1\}$. So, the switch considering as always closed with a main voltage source $u * V_{in}$. In this schema, the internal resistance for both of the step-down converter and DC motor coils winding had taken into consideration. The brushed DC motor modeled by $K_E\omega$ (electromagnetic voltage supply) and R_M (ohmic resistance) with L_M (inductance). In synopsis: the dynamic system consistency (Permanente brushed DC motor fed by a step-down DC-DC power converter) were taken into account and modeled in the state space and transfer function forms. As depicted in Figure3.14:

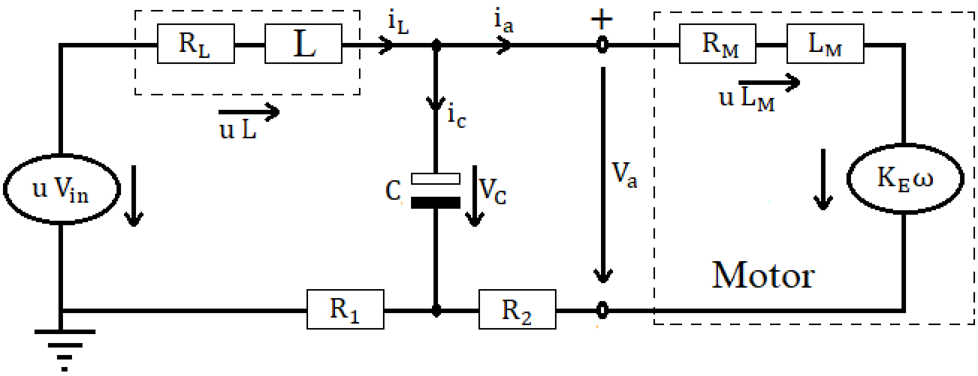

Figure 3.14 Scheme for the Permanente DC motor fed by buck converter.

$$u\,V_{in} = V_c + L\frac{di_L}{dt} + R_L i_L \tag{3.123}$$

$$V_C = K_E\omega + L_M\frac{di_a}{dt} + R_M i_a \tag{3.124}$$

$$i_L = i_a + C\frac{dV_C}{dt} \tag{3.125}$$

$$J\frac{d\omega}{dt} = T = K_M I_a \tag{3.126}$$

Where J considered as the inertia of the DC motor while K_M is the tacho generator gain of that motor. For simplifying purpose, in equations (3.123) and (3.124), the inherent resistances (R_1 and R_2) were discarded from the modeling because of their small measurements. The shaft dynamism of the brushed DC motor (the mechanical equation completed with the model of the state space) had described through equations (3.123) to (3.125), a fourth order linear system was represented by:

$$\dot{X} = Ax + Bu \tag{3.127}$$

$$Y = Cx + Du$$

With u is the input, Y is the output, the vector $x = [i_L \quad V_C \quad i_a \quad \omega]^T$ and the matrices A, B, and C are given by:

$$A = \begin{bmatrix} \frac{-R_L}{L} & \frac{-1}{L} & 0 & 0 \\ \frac{1}{C} & 0 & \frac{-1}{C} & 0 \\ 0 & \frac{1}{L_M} & \frac{-R_M}{L_M} & \frac{K_E}{L_M} \\ 0 & 0 & \frac{K_M}{J} & 0 \end{bmatrix} \tag{3.128}$$

$$B = \begin{bmatrix} \frac{V_{in}}{L} & 0 & 0 & 0 \end{bmatrix}^T, \quad C = [\,0 \quad 0 \quad 0 \quad 1\,] \text{ and } D=0$$

According to [21], the input discrete switching variable $u \in \{0,1\}$ is superseding by $\delta \in [0,1]$ where δ is the duty ratio.

An analog input signal can produce a duty cycle by using PWM-strategy, the outcome from that process may refer to an averaged dynamic model shown through

$$\dot{X} = Ax + B\delta \tag{3.129}$$

It should be mention at this point that the validity of the linear system characterization exists only in the case where there is no saturation impact in the inductor, otherwise, a non-linear relation occurs between the i_L (inductor current) and the L (inductance).

In this work, the values of the parameters had found as the following: from equation 3.14a R_M= 13.8 ohms, from equation 3.16 L_M= 0.719 mH, from equation 3.17 $K_M = 10.9 \text{ m } \frac{\text{Nm}}{\text{A}}$, from equation 3.8 we inferred that the speed constant is approximately identical to the torque constant $K_E = K_M = 10.9 \text{ m } \frac{\text{V-Sec}}{\text{rad}}$, from equation 3.23 the motor inertia found as J = 2.07×10^{-7}kg-m^2, V_{in}= 12 V, R_L= 3 ohms, from the designing equation (3.60) the inductance of the buck converter was selected to be L = 2 mH, and from equation (3.68) the capacitance is C = 3 μF and 100 kHz switching frequency has been used for the triggering the buck converter.

Since we are dealing with the SISO system (single-input single-output) and described in state space form through the equations:

$$\dot{X} = Ax + B\delta \tag{3.130}$$

$$Y = Cx$$

So, it possible to infer a relationship between the state-space and the transfer function equations, by assuming:

$$G(s) = \frac{\text{output}}{\text{input}} = \frac{\omega_{(s)}}{\delta_{(s)}} \tag{3.131}$$

After taking the Laplace transform for equation (3.130)

$$\mathrm{SX_{(s)}} - \mathrm{x_{(0)}} = \mathrm{AX_{(s)}} + \mathrm{B\delta}_{\ (s)} \tag{3.132}$$

$$\omega_{(S)} = \mathrm{CX_{(s)}} \tag{3.133}$$

Assuming zero initial condition $(x_{(0)} = 0)$,So

$$\mathrm{SX_{(s)}} - \mathrm{AX_{(s)}} = \mathrm{B\delta}_{\ (s)} \tag{3.134}$$

$$(\mathrm{SI} - \mathrm{A})\mathrm{X_{(s)}} = \mathrm{B\delta}_{\ (s)}$$

After multiplying both sides of the previous equation by $(\mathrm{sI} - \mathrm{A})^{-1}$ we obtain:

$$\mathrm{X_{(s)}} = (\mathrm{SI} - \mathrm{A})^{-1}\mathrm{B}\ \delta_{\ (s)} \tag{3.135}$$

Where (I) here is the identity matrix, by substituting equation (3.133) with equation (3.135), we obtain

$$\frac{\omega_{(S)}}{\mathrm{C}} = (\mathrm{SI} - \mathrm{A})^{-1}\mathrm{B}\ \delta_{\ (s)} \tag{3.136}$$

so

$$\mathrm{G_{(s)}} = \frac{\omega_{(S)}}{\delta_{\ (s)}} = \mathrm{C}(\mathrm{SI} - \mathrm{A})^{-1}\mathrm{B} \tag{3.137}$$

$$\mathrm{G_{(s)}} = ([0 \quad 0 \quad 0 \quad 1])\left(\begin{bmatrix} s & 0 & 0 & 0 \\ 0 & s & 0 & 0 \\ 0 & 0 & s & 0 \\ 0 & 0 & 0 & s \end{bmatrix} - \begin{bmatrix} -\frac{R_L}{L} & -\frac{1}{L} & 0 & 0 \\ \frac{1}{C} & 0 & -\frac{1}{C} & 0 \\ 0 & \frac{1}{L_M} & -\frac{R_M}{L_M} & \frac{K_E}{L_M} \\ 0 & 0 & \frac{K_M}{J} & 0 \end{bmatrix}\right)^{-1} * \begin{bmatrix} \frac{U_e}{L} \\ 0 \\ 0 \\ 0 \end{bmatrix}^{T} \tag{3.138}$$

$$\mathrm{G_{(s)}} = \frac{\omega_{(S)}}{\delta_{\ (s)}} = \frac{\mathrm{k}}{\mathrm{s^4 + a_3 s^3 + a_2 s^2 + a_1 s + a_0}} \tag{3.139}$$

Solving equation (3.138), $\mathrm{k} = \frac{K_M V_{in}}{J L L_M C} = 1.464 * 10^{17}$

$$a_3 = \frac{R_L}{L} + \frac{R_M}{L_M} = 20693.32406$$

$$a_2 = \frac{R_L R_M}{L L_M} + \frac{1}{LC} + \frac{1}{L_M C} + \frac{K_E K_M}{J L_M} = 659.861 * 10^6$$

$$a_1 = \frac{R_L + R_M}{L L_M C} + \frac{R_L K_E K_M}{J L L_M} = 3.8955 * 10^{12}$$

$$a_0 = \frac{K_E K_M}{J L L_M C} = 1.33 * 10^{14}$$

$$\frac{\omega_{(S)}}{\delta_{(s)}} = \frac{1.464*10^{17}}{s^4+(20693.32406)s^3+(659.861*10^6)s^2+(3.8955*10^{12})s+(1.33*10^{14})} \qquad (3.140)$$

This transfer function describes precisely the relation between the duty cycle and the output speed of the DC motor. After converting the transfer function from the continuous domain to a discrete one with 0.1 sampling time which obtained from our code algorithm and the designing requirements, we get:

$$\frac{\omega_{(z)}}{\delta_{(z)}} = \frac{(1065\,)Z^3+(0.2085)Z^2-(4.953*10^{-23})Z+(5.287*10^{-45})}{Z^4-(0.03225)Z^3-(2.289*10^{-19})Z^2-(3.894*10^{-38})Z-(2.298*10^{-56})} \qquad (3.141)$$

3.11 Bootstrap

As shown in figure 3.15 the bootstrap diode and capacitor are the only exterior ingredients that ought to be opting minutely with strictly values in the applications that handling with a PWM criterion.

The decoupling capacitors on the low side fixed voltage supply (V_{cc}), and the logic supply voltage (V_{DD}) are so helpful in practice to recompense the undulation that inherently existed in the supply lines.

The value of the bootstrap capacitor which sees only the voltage from VCC supply is limited by the following restrictive:

1. The desired gate voltage to trigger the MGT (MOS Gated Transistor).
2. The quiescent current (I_{QBS}) for the circuit which driven in the high-side.
3. The currents with the level shifting that associated with the IC designing.
4. Forward leakage current from the gate to source in the MGT.
5. Leakage current in the Bootstrap capacitor.

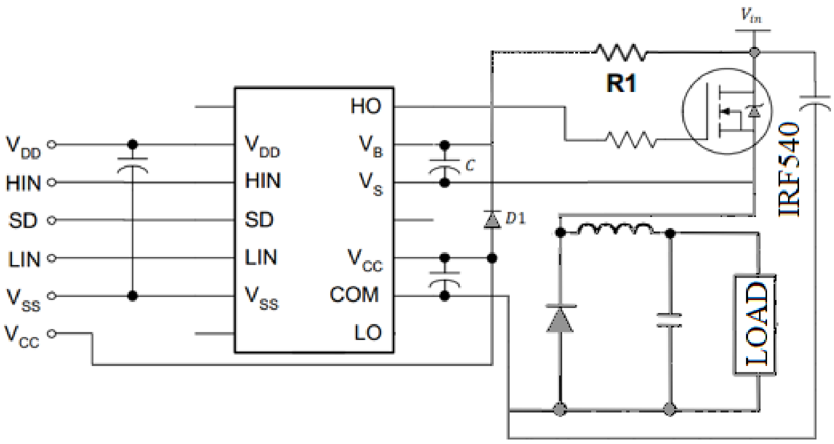

Figure 3.15 Typical connection of a bootstrap circuit with the buck converter [51].

The fifth factor is only relevant if the bootstrap capacitor is an electrolytic capacitor, and it ignored if other types of capacitor are using. Therefore, it is always better to use a non-electrolytic capacitor if possible. From the following equation, we can calculate the minimum value of the bootstrap capacitor [52].

$$C \geq \frac{2\left[2Q_g + \frac{I_{qbs(max)}}{f} + Q_{ls} + \frac{I_{Cbs(leak)}}{f}\right]}{V_{cc} - V_f - V_{LS} - V_{min}} \tag{3.142}$$

Where Q_g is the high-side Gate charge of the FET, f is the operation frequency, $I_{Cbs(leak)}$ represents the leakage current in the bootstrap capacitor, $I_{qbs(max)}$ is the quiescent current in maximum V_{BS}, V_{cc} is the logic part voltage supply, V_f represents the forward voltage descent through the external bootstrap diode, $V_{LS}$is the voltage descent through the low-side operation for load or FET, V_{min} is the minimal voltage between V_S and V_B, Q_{ls} represents the required level shifting charge in one cycle.

It is recommended for the bootstrap capacitor to be at least 0.47μF. The bootstrap diode which has been selecting must be able to prohibit the entire voltage seen in the specified electrical circuit, according to figure 3.15, this happens when the top appliance voltage equal to the power rail voltage. The diode rating current is equaling to the switching frequency times the gate charge. It is about 12 mA for the MOSFET IRF450 that operates at 100 kHz. Since the output voltage of the DC-DC step-down converter is always smaller than the voltage source, so, there is leakage current flowing through R_1 (to maintain the consistency of the Bootstrap capacitor charging by providing another charging trajectory for the bootstrap capacitor), the worst-case leakage current must be smaller than the average current across the resistance R_1 [51].

3.12 Controller Design

Generally, Proportional Integral (PI) controller is a consistent system founding by closed feedback loop as it had depicted in Figure 3.16.

It works on adjusting the error to preserve the angular speed of the Permanent brushed DC motor (in the time-domain) with a fixed control demeanor of duty cycle with concentrating on prohibiting the detriment behavior of the transient period that occurs at the starting moment and with every raising up or down of the PWM signal.

From the below figure

$$\delta_{(s)} = [\omega_{r(s)} - \omega_{(s)}]G_{c(s)} \tag{3.143}$$

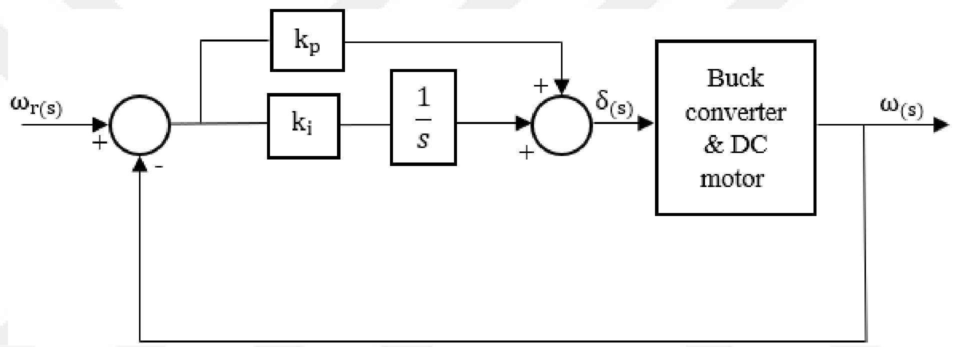

Figure 3.16 PI controller with permanent brushed DC motor fed by buck converter.

The transfer function for the whole system obtained as:

$$\frac{\omega_{(s)}}{\omega_{r(s)}} = \frac{G_{(s)}G_{c(s)}}{G_{(s)}G_{c(s)}+1} \tag{3.144}$$

The mathematical representation of the Proportional Integral control in the s- domain is:

$$G_{c(s)} = k_p + \frac{k_i}{s} \tag{3.145}$$

Where k_p represents the proportional gain constant, and k_i is the integral gain constant. The Proportional term (k_p) obtains the proportion reaction to current angular velocity error. Due to the limitations that pre-existed in the proportional controller (always exists an offset between the desired and actual speed), the integral term ($\frac{k_i}{s}$) has been added for obtaining reaction to the summation of the previous errors (the errors will be integrated for some time until the error reaches to a zero value). The effect of elevating Proportional Integral constant is showing in Table3.1.

Table 3.1 The effect of elevating Proportional Integral constant [53].

variable	**Rising time**	**The overshoot**	**The settling time**	**The steady-state error**	**The stability**
k_p	Dwindle	Rise	Small effect	Dwindle	Degrade
k_i	Dwindle	Rise	Rise	Eliminate	Degrade

The resulting signal from the parallel connection of the proportional and the integral controller is using as a driver for the buck converter. Which in turn, used to drive the permanent brushed DC motor by sending variant values of the duty cycle depending on the outcome of the DC motor (with taking into account the mapping operation to convert the PI results from an analog value to PWM signal with a fixed frequency). As a synopsis, the speed of the motor measured via a tachometer and fed again to the microcontroller for subtracting it from the reference speed and push it to PI controller multiply it by the PI parameters to make the manipulation and then the mapping operation is responsible for converting the outcomes to a PWM signal to drive the system.

3.12.1 Implementation of Proportional Integral Algorithm With The Discrete Time

The PI control algorithm had designed by taking into consideration that the microcontroller is dealing with a discrete signal, so the PI equation needs to be converted from analog to digital.

As is known, the integral part represents the area under the curve multiplied by the factor K_i, in Figure 3.17 it is clear that the area from (aT-T) up to (aT) can be approximated to be as a trapezoid.

$$y_{(t)} = K_i \int_0^t e_{(t)} * dt = \left[K_i \int_0^{aT-T} e_{(t)} dt\right] + \left[K_i \int_{aT-T}^{aT} e_{(t)} dt\right] \tag{3.146}$$

$$y_{(aT)} = y_{(aT-T)} + \Delta y_{(aT,aT-T)} \tag{3.147}$$

Where $y_{(aT-T)}$ represents the area up to $(aT - T)$, and $\Delta y_{(aT,aT-T)}$ represents the incremental area for T period.

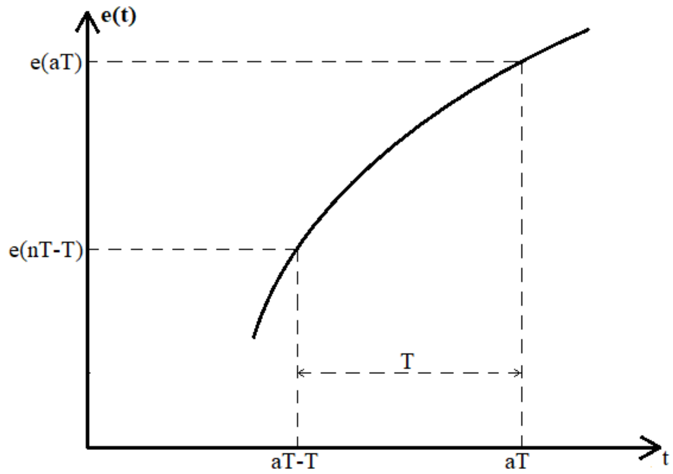

Figure 3.17 Illustrating the derivation of an integral part in PI control.

The area of the trapezoid can be separating to a rectangle and triangle part as it explains in the equation below.

$$\Delta y_{(aT,aT-T)} = K_i * T * e_{(aT-T)} + K_i * \frac{1}{2} * T\left[e_{(aT)} - e_{(aT-T)}\right] \quad (3.148)$$

$$\Delta y_{(aT,aT-T)} = \frac{K_i T}{2}\left[e_{(aT)} + e_{(aT-T)}\right] \quad (3.148a)$$

Now, substitute equation 3.147 in the previous equation yielded

$$y_{(aT)} = y_{(aT-T)} + \frac{K_i T}{2}\left[e_{(aT)} + e_{(aT-T)}\right] \quad (3.149)$$

After taking the Z-transform for the previous equation

$$Y_{(z)} = Z^{-1}Y_{(z)} + \frac{K_i T}{2}\left[E_{(z)} + Z^{-1}E_{(z)}\right] \quad (3.150)$$

So, the transfer function for an integral part in the Z-domain is

$$\frac{Y_{(z)}}{E_{(z)}} = \frac{K_i T}{2}\left[\frac{1+Z^{-1}}{1-Z^{-1}}\right] = K_i \frac{T}{2}\left[\frac{Z+1}{Z-1}\right] \quad (3.151)$$

Now, after combining the proportional and integral parts

$$\frac{Y_{(z)}}{E_{(z)}} = K_p + K_i\left[\frac{Z+1}{Z-1}\right]\frac{T}{2} \quad (3.152)$$

$$\frac{Y_{(z)}}{E_{(z)}} = \frac{K_p(Z-1) + (Z+1) * K_i\frac{T}{2}}{-1+Z} = \frac{Z(K_p + K_i\frac{T}{2}) + (-K_p + K_i\frac{T}{2})}{-1+Z} \quad (3.153)$$

$$\frac{Y_{(z)}}{E_{(z)}} = \frac{(K_p + K_i\frac{T}{2}) + Z^{-1}(-K_p + K_i\frac{T}{2})}{1 - Z^{-1}} \tag{3.154}$$

$$Y_{(z)} = Z^{-1}Y_{(z)} + (K_p + K_i\frac{T}{2})E_{(z)} + (-K_p + K_i\frac{T}{2})Z^{-1}E_{(z)} \tag{3.155}$$

$$y_{(n)} = y_{(n-1)} + (K_p + K_i\frac{T}{2})e_{(n)} + (-K_p + K_i\frac{T}{2})e_{(n-1)} \tag{3.156}$$

Where n-represents the number of steps. In our work, equation 3.156 is using as the base for building the PI algorithm via the microcontroller. We used the capture mode for measuring the frequency (by taking the inverse of the time duration) with 0.1s sampling time (which represented in our code the execution cycle which is the same as the time that the microcontroller takes it to execute both of capture and PI loops). So, the minimum sensible frequency is $0.1^{-1} = 10$ HZ which lead to (10*$\frac{60}{18}$=33.333 rpm), where 18 represents the number of slots in the optical encoder, and 60 the ratio of converting from the second to the minute.

3.13 Measuring the Frequency

In the field of electrical and electronic engineering, measuring the frequency is a crucially important issue. Electric power and electronic circuit system had become more complex over the last years.

The use of external disturbance like exhibits DC motor to external torque will cause rotor speed variations and hence frequency fluctuations. So, measuring the DC motor speed is based on measuring the frequency (number of turns per second).

Generally, there are two ways for measuring the digital frequency a PIC microcontroller: The first one is triggered TMR1 to operate in time mode to give as one second in this one second TMR0 operate as a counter to count the number of raising edge so with each TMR1interrupt the microcontroller triggered for latching the value of TMER0 and present it on LCD. The second way is using the capture mode to get the time duration (T) hence calculate the frequency of the wave (frequency = $\frac{1}{T}$).

To implement these ways, we need to illustrate some of the basic concepts that related to the capture mode operation.

3.13.1 Overflow:

Overflow means the timer reached its maximum value and rolling over back to zero. For TIMER1, the PIC18F4580 has an overflow flag bit (TMR1IF) to generate interrupts after each overflowing, this operation is executing via setting TMR1IE which is using to enable the interrupt flag in TMR1, besides setting both of GIE and PEIE registers for enabling all unmasked and peripheral Interrupts such as serial port and Timers. The most exciting thing in the overflow is the possibility of extending the counter range by counting the number of overflowing occurs. For example, for counting up to 131070 with TMR1 in PIC18F4580, we can use the overflow flag. So, it is axiomatic after two overflows; the count will be 131070 (65535+65535).

3.13.2 Timer1

Timer1is consist of a 16-bits, that means for a single cycle it can count up to 65535 pulses, the 16-bits access either as low byte register called TMR1L or high byte register called TMR1H, these registers can be readable or writable at any moment, the 8-bit mode is not supporting in timer1 with PIC18F4580. Timer1 has a control register T1CON used for setting various operation modes, T1CON consist of 8-bits each one support a specific feature by filling it with either 1 or 0.

3.13.3 Capture Compare Pulse Width Modulation (CCP) Mode

Whenever a flag bit (CCP1IF) is detected (which occurs at every rising or falling edge), Timer1 register (which is consisting of TMR1L and TMR1H) is loading into the CCP1 register (which is consisting of CCPR1L and CCPR1H). To enable that flag bit, we must set CCP1IE after initializing the CCP pin as an input. The external events in the capture mode are defining as: either each rising or falling edges, or even each 4th or 16th rising edge depending on the designer and the requirements. One way of reducing the overhead associated with the program is to select the rising edge every 4^{th} or 16^{th} from the CCP1CON register.

For more information about the registers that related to the Timers and capture mode, look at [10].

CHAPTER 4

CIRCUIT IMPLEMENTATION AND EXPERIMENTAL RESULTS

In this chapter, the suggested circuit diagram (DC_DC step down converter with DC motor) was implemented and tested by the simulation and the experimental implementation in the laboratory.

4.1 Checking the DC Motor Parameters Estimation

The accentuated comparison between the Simulation and the empirical results confirmed the validity of the analytical DC motor parameter identifications by comparing the no-load speed and the no-load current in both of the two tests (empirical and simulation). The simulation has accomplished by entering the values of R_M, L_M, J, and K which were previously extracted in the DC motor analytical part, as depicted in Figure 4.1. From Figure 4.2 we can observe the no-load simulating results as follows: the speed is 6130 RPM and the consumed current is 14m A, so if we compare these values with the empirical results (ω_{no_load}=6000 RPM, I_{no_load}=16m A) we infer the validity of our identification. In our case, it was acceptable and valid.

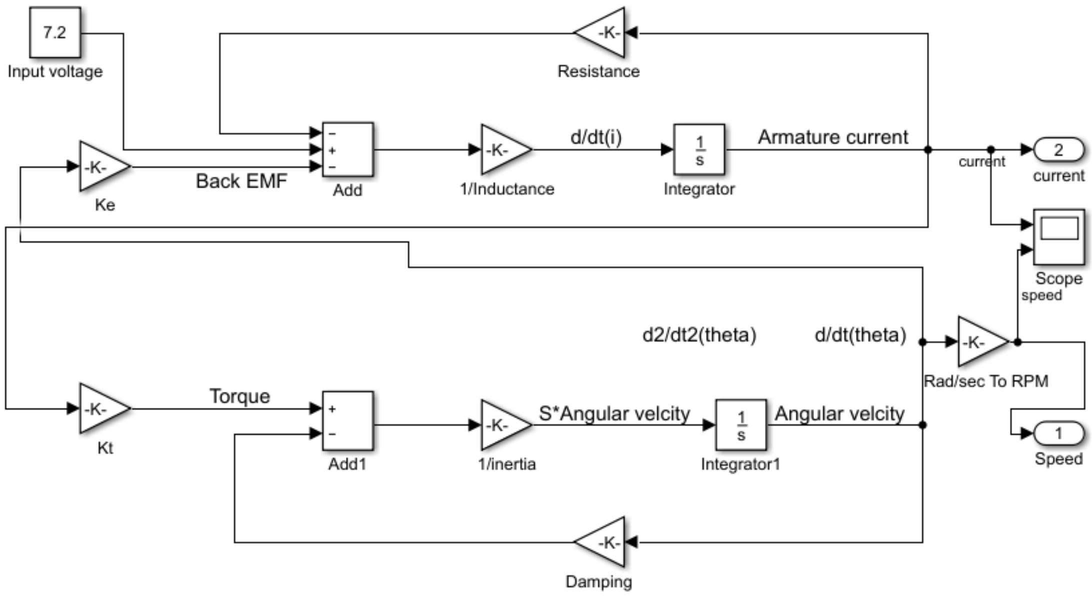

Figure 4.1 Simulink for the brushed DC motor model.

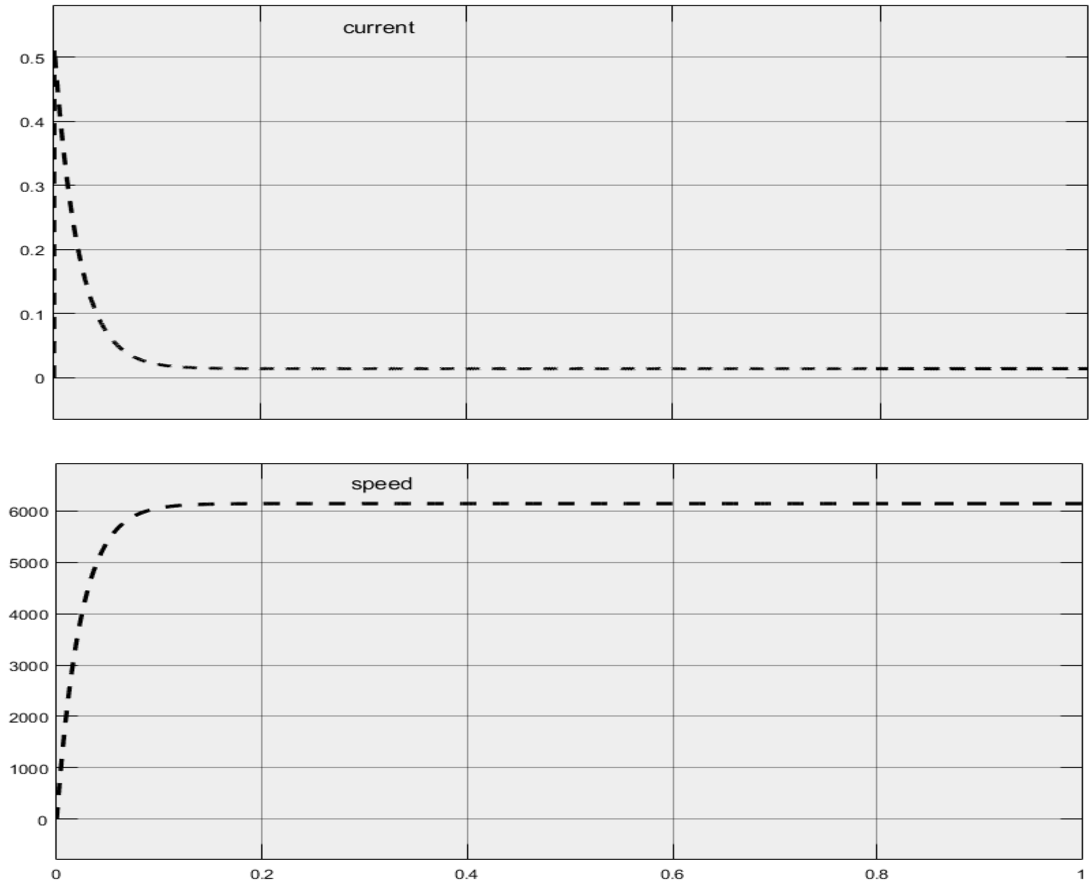

Figure 4.2 The speed and the consumed current at the no-load case.

4.2 The speed sensor

The schematic in figures 4.3 and figures 4.4 are illustrating the general circuit diagram for the optical speed sensor.

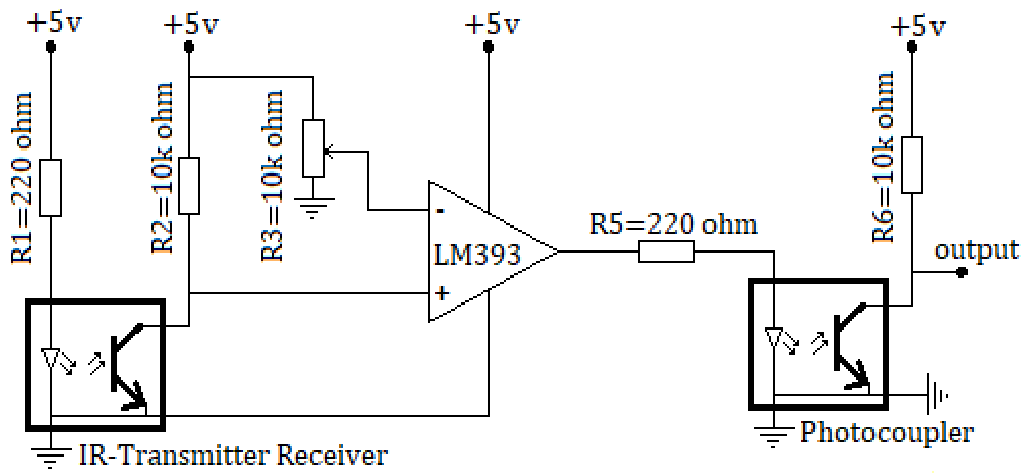

Figure 4.3 Schematic diagram for the optical speed sensor.

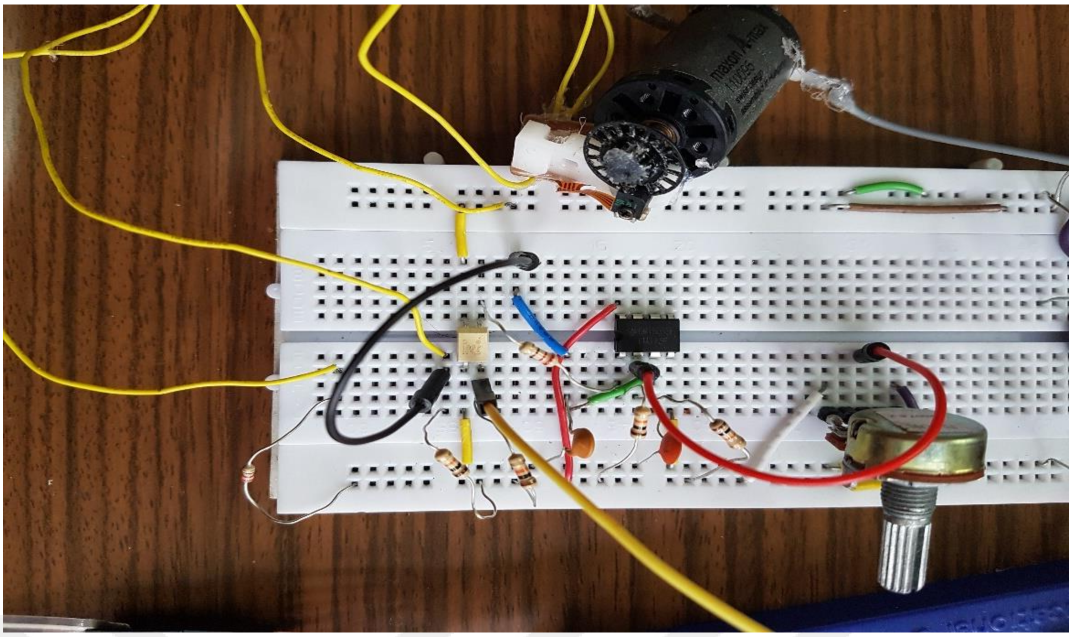

Figure 4.4 The experimental implementation in the laboratory for the optical speed sensor.

It is crucial to mention that the optical sensor disc which has used consists of 18 slots with equal dimensions between each of two successive slots.

The previous scheme consists of a 220-ohm resistance connected in a series manner with an infrared transmitter light to protect the diode from the excessive currents, on the other side, a 10k ohm was connecting with the infrared receiving part to prevent occurring the short-circuiting case when there is infrared light detecting by the infrared receiver part. The output of the infrared receiving part is present in Figure 4.5, for this case it was 1.12K Hz, and hence the revolution per minute is (1.12K*60)/18=3733.33 RPM.

LM393 is a Comprator IC used to convert the shapeless signal to a square waveform that can be sensed via the microcontroller as shown in Figure 4.6. The photocoupler here has been using to add more protection to the system, while $R_3$is using to specify the reference voltage that will be compared with the input wave.

It is accentuated that comparator IC adjusted the shape and the pinnacle signal values without any effecting on the signal frequency value.

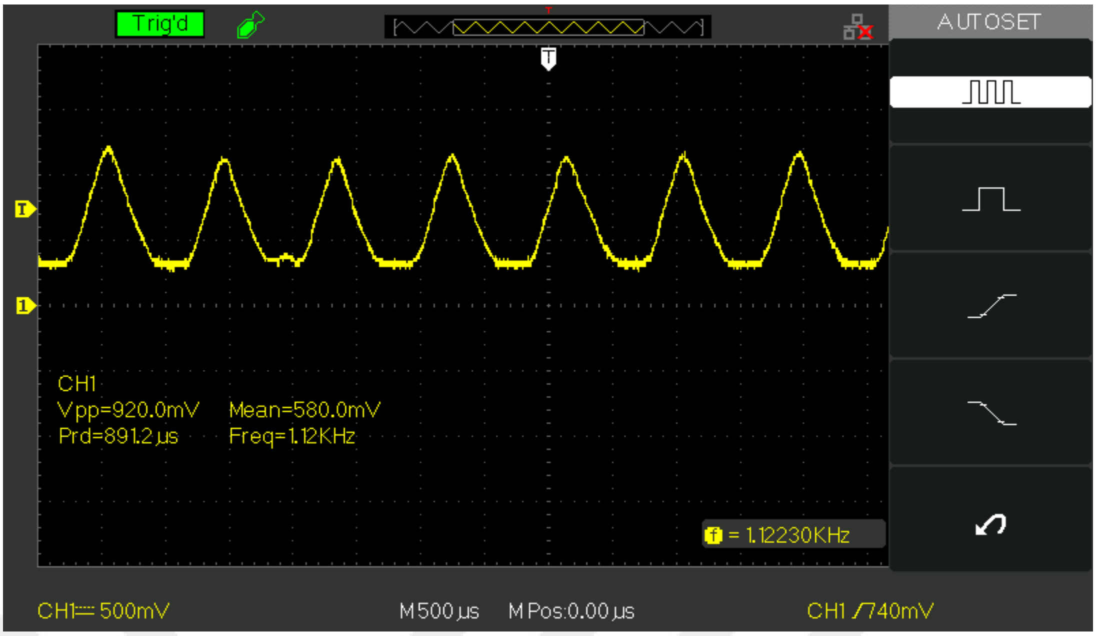

Figure 4.5 The output signal before entering the comparator IC on the oscilloscope.

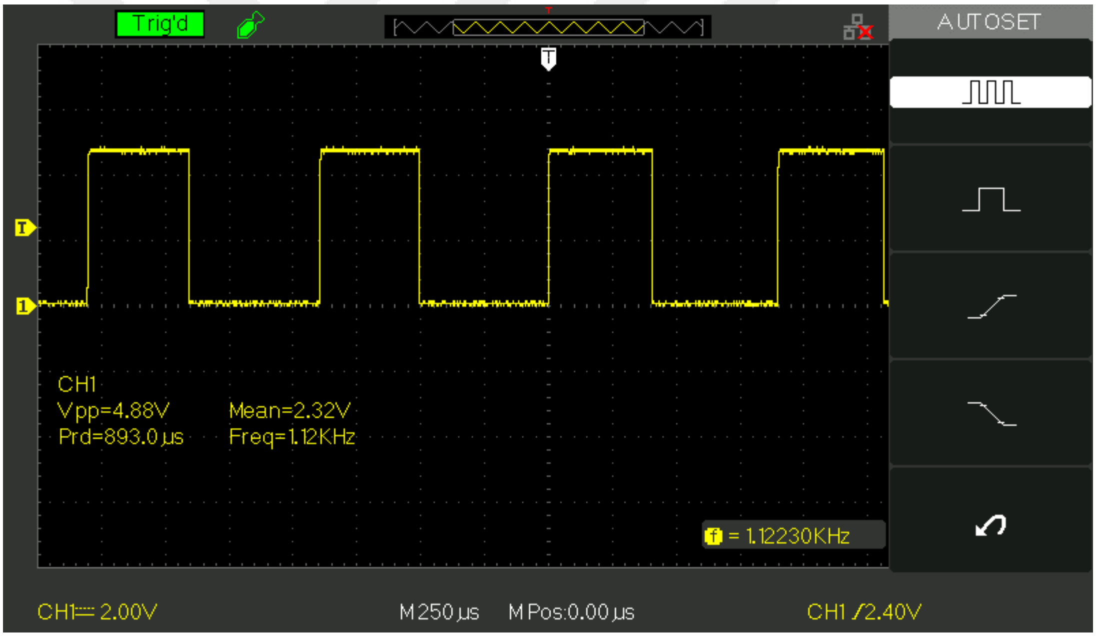

Figure 4.6 The final output signal from the optical speed sensor on the oscilloscope.

4.3 The Bootstrap Circuit

The schematic diagram in Figure 4.7 and its experimental implementation in Figure 4.8 are using to rising the 5 V output signal from the microcontroller (PWM signal) that supposed to feed the buck converter to be more than the V_{GS} for the turning ON switching period, pursuant to the stipulations of operating the N- channel MOSFET on the high side ($V_{GS} > V_T$).

The experimental results had presented on the oscilloscope instrument in figure 4.9. Channel 1 fed via the microcontroller, while the port of channel 2 was feed via the connection node between the buck converter and the bootstrap circuit (MOSFET source gate).

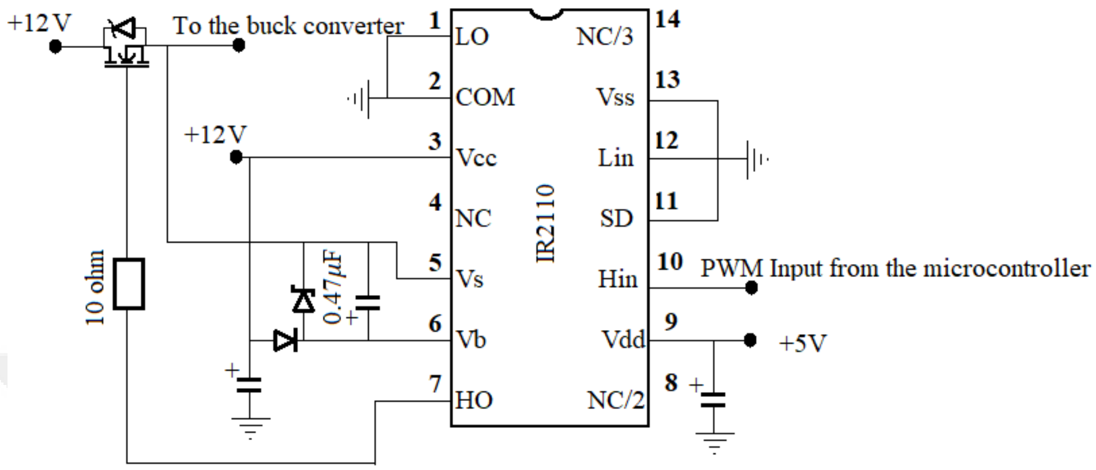

Figure 4.7 Schematic diagram for the high side N-channel MOSFET driver.

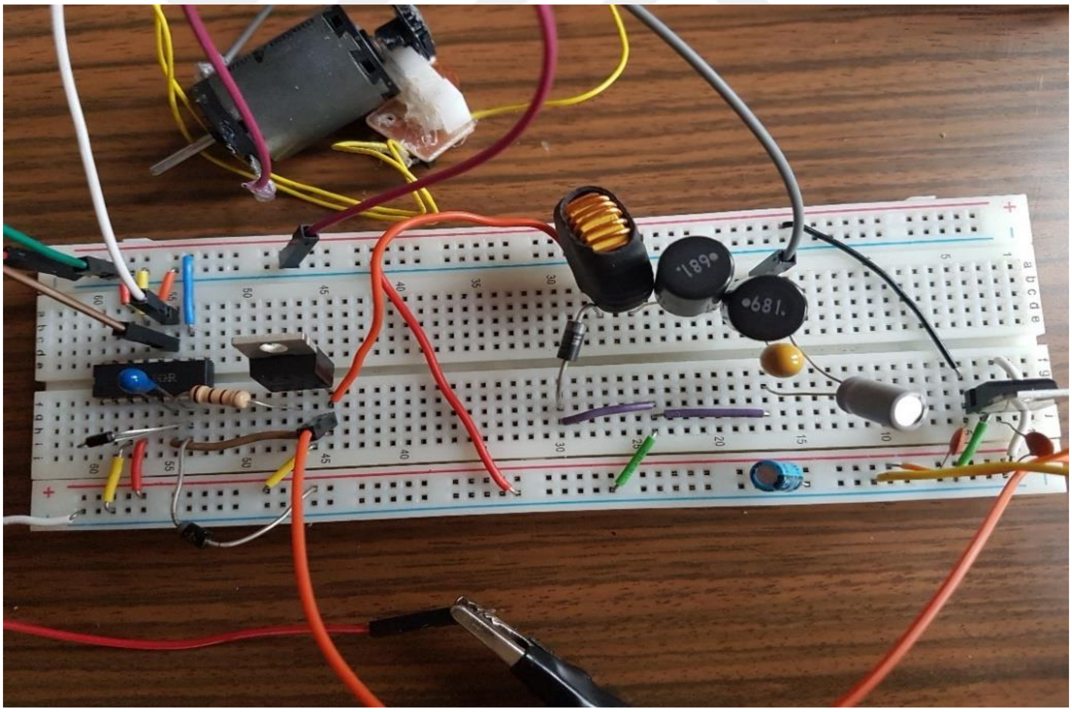

Figure 4.8 The experimental implementation in the laboratory for the IR2110 as a high side N-channel MOSFET driver for the buck converter.

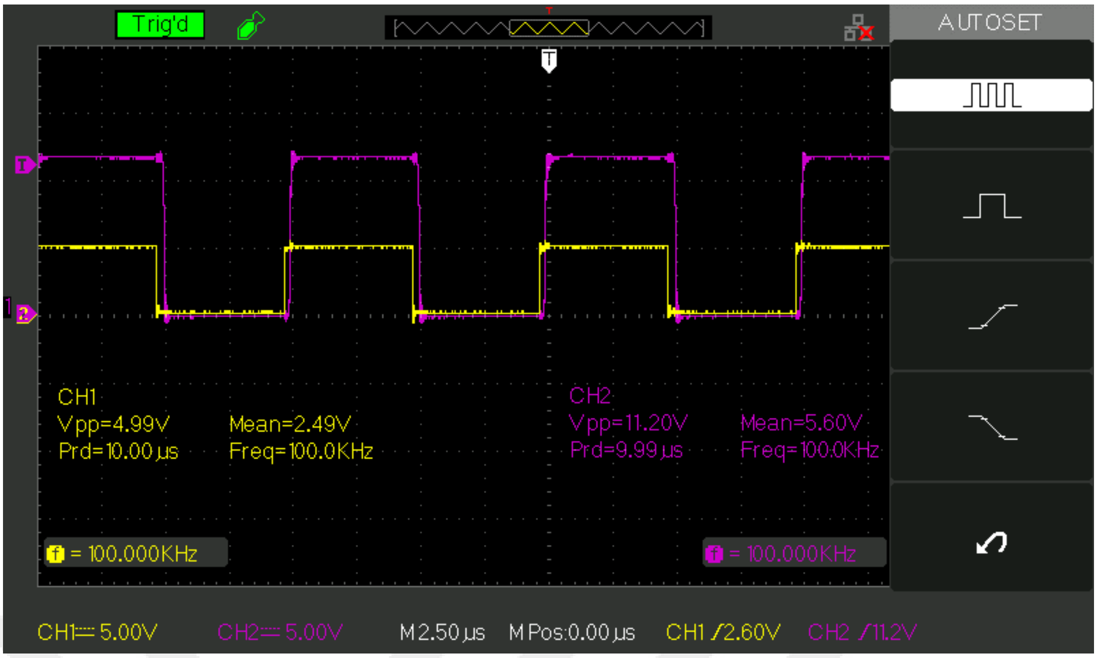

Figure 4.9 The output signal from the microcontroller and the bootstrap circuit on the oscilloscope.

4.4 Proportional Integral (PI) Tuning:

The most crucial thing in the proportional Integral control designing is the parameters tuning to acquire the best performance (minimum rise time, more robust, minimum overshoot, etc.) in both of transient and steady-state periods. After analyzing and plotting the bode plot, it is obviously from Figure 4.10 the system has a gain margin (-60.3 dB) at a frequency (31.4 rad/sec). So as overall the system is unstable.

After entering both of our transfer function that describes the whole system and the PI Simulink block in the simulation software with closing the loop, the optimum PI parameters values had found as the follows, $K_p = 0.00021706$ and $K_i = 0.0055$.

So, according to the bode diagram in Figure 4.11. With entering K_p and K_i values, the system had been stimulated to move from the unstable region to the stable one, with upgrading both of the gain margin (8.72 dB) and the phase margin to (51.7 dB).

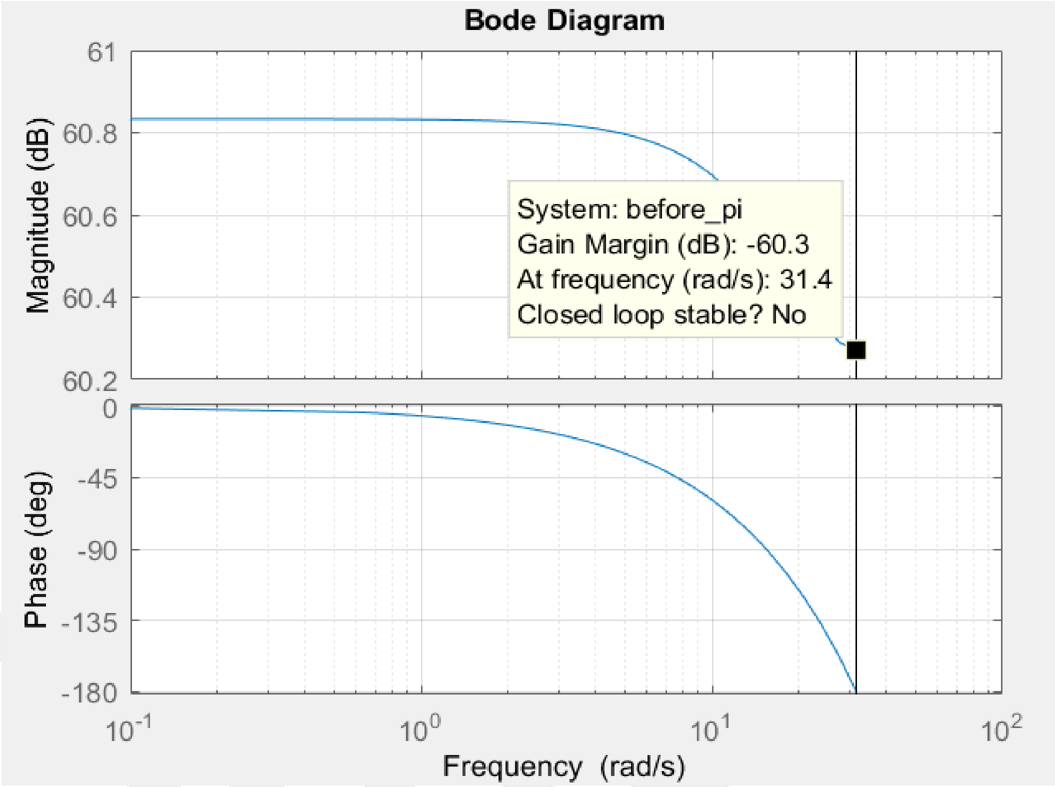

Figure 4.10 Bode plot before using the PI controller.

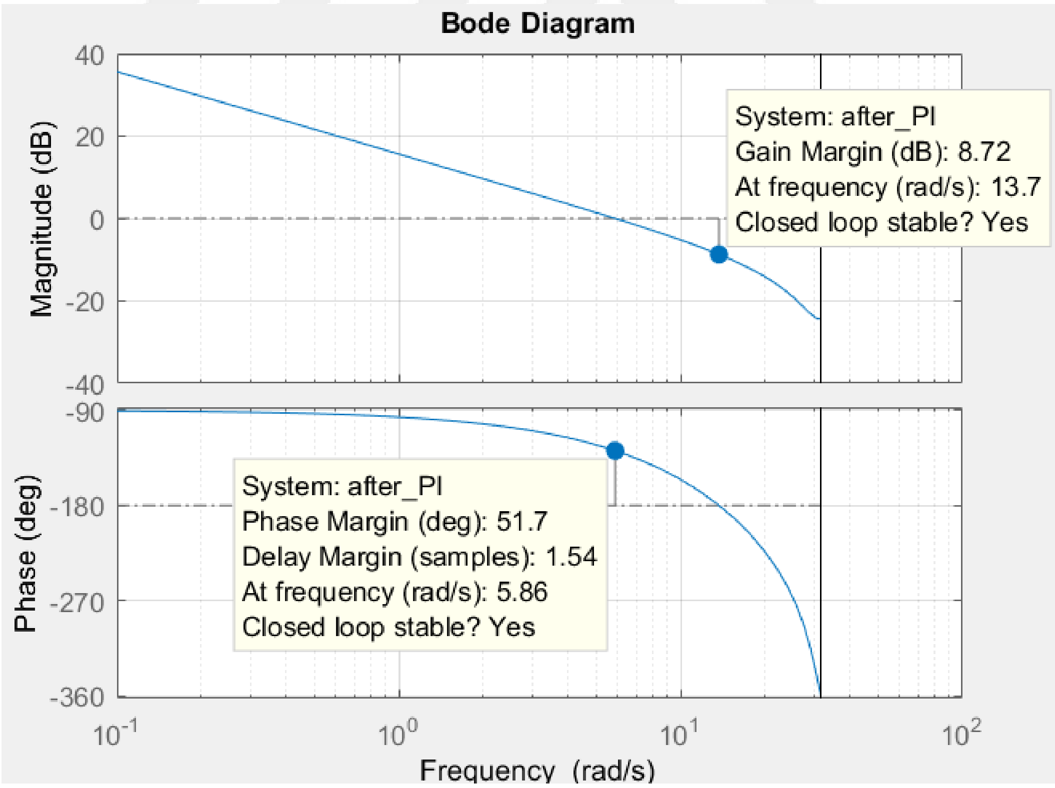

Figure 4.11 Bode plot after using the PI controller.

4.5 Code Algorithm and The Final Circuit Implementation

Figure 4.12 represents the algorithm for driving the DC motor that fed by a step-down DC-DC power converter at a specific speed under different external torque with taking into account that algorithm has been implemented using mikroC PRO for PIC software.

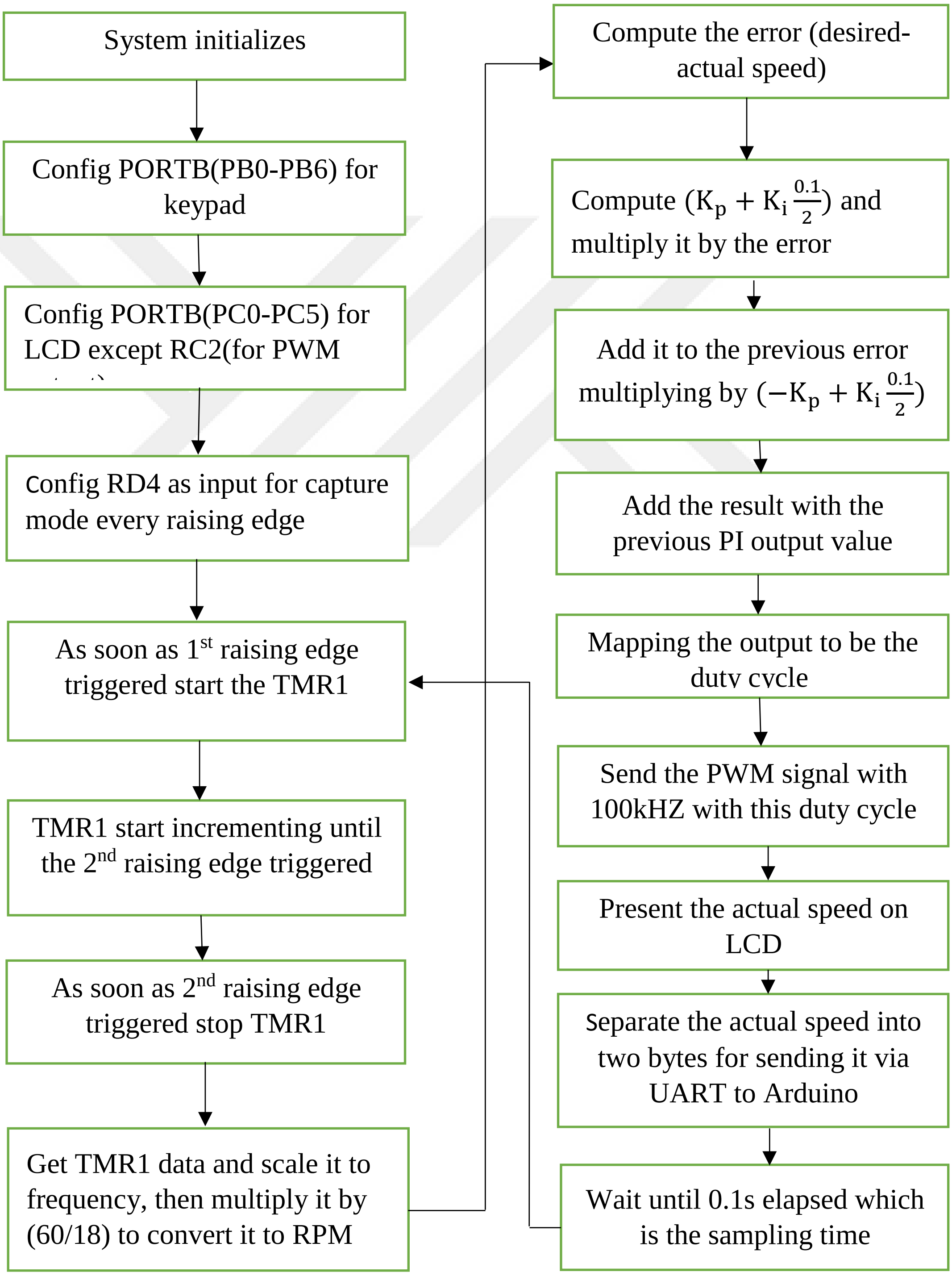

Figure 4.12 The algorithm for the whole of the system.

The schematic diagram for the whole of the circuit and the real implementation have been illustrating in figures 4.13 and figure 4.14 respectively.

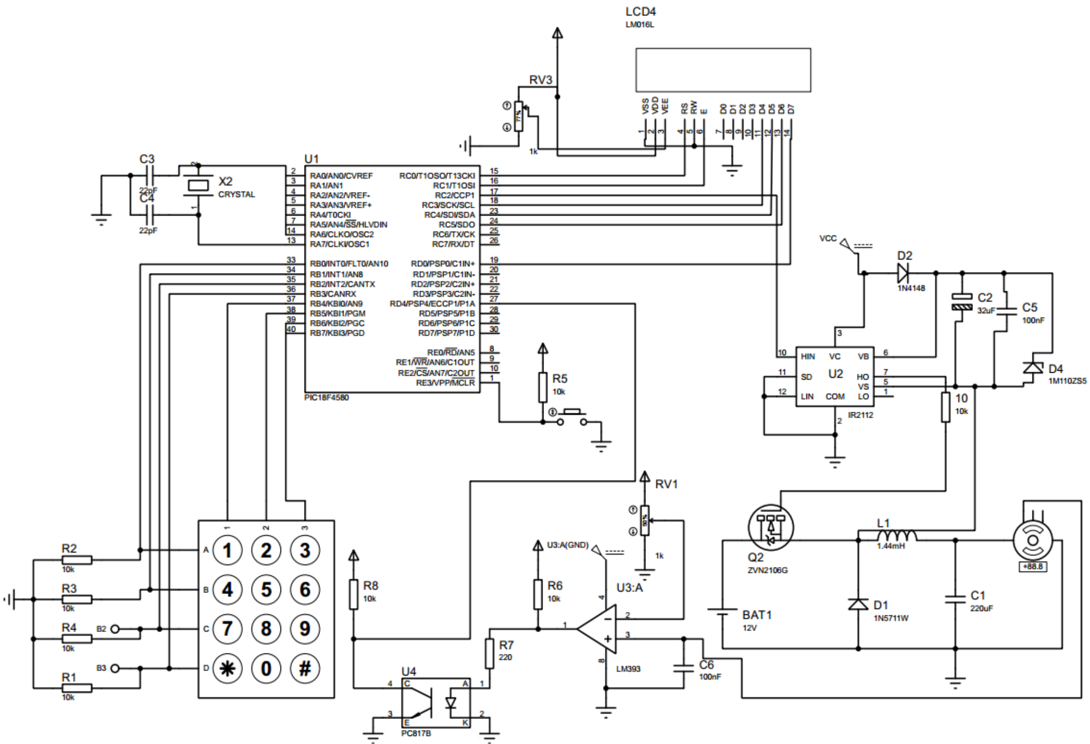

Figure 4.13 Final schematic diagram for the whole of the system.

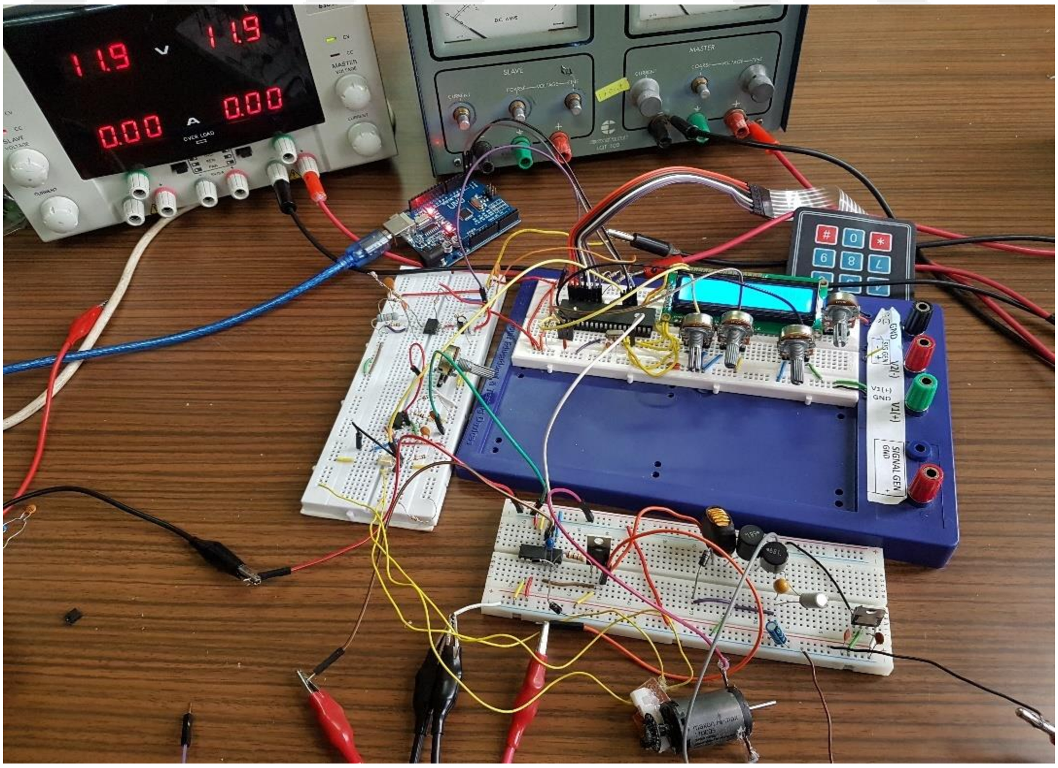

Figure 4.14 The experimental implementation in the laboratory for the whole of the system.

4.6 Buck Converter Output

The Pulse width Modulation signal within a specific frequency had been generated using PIC18F4580, that signal is boosted using the IR2110 (bootstrap circuit), then it was fed to step down converter. The main reason for using the DC-DC converter is to obtain a flat wave within a minimum amount of the ripple factor to resupplied the DC motor with the power. In this work, we selected two testing speed points one of them is the 1000 RPM, and the other one is 5000 RPM to cover the whole of the speed range. The duty cycle and the voltage have found in two different condition cases without the disturbance (as shown experimentally with the Figures 4.15, 4.16, 4.17 and 4.18), and within the disturbance (as shown in the Figures 4.19, 4.20, 4.21 and 4.22). It is clear that the duty cycle plays the pivotal role in controlling the DC motor speed by either increasing or decreasing. After the system has been exposed to the disturbance, the duty cycle has been growing as was expected from it to increase the voltage that entering the DC motor and hence compensating the decreasing in the speed. At the moment of dwindling the disturbance, everything will be returned to the normal situation until both of duty cycle and the voltage get the same previous values again as it was before the exposure to the disturbance.

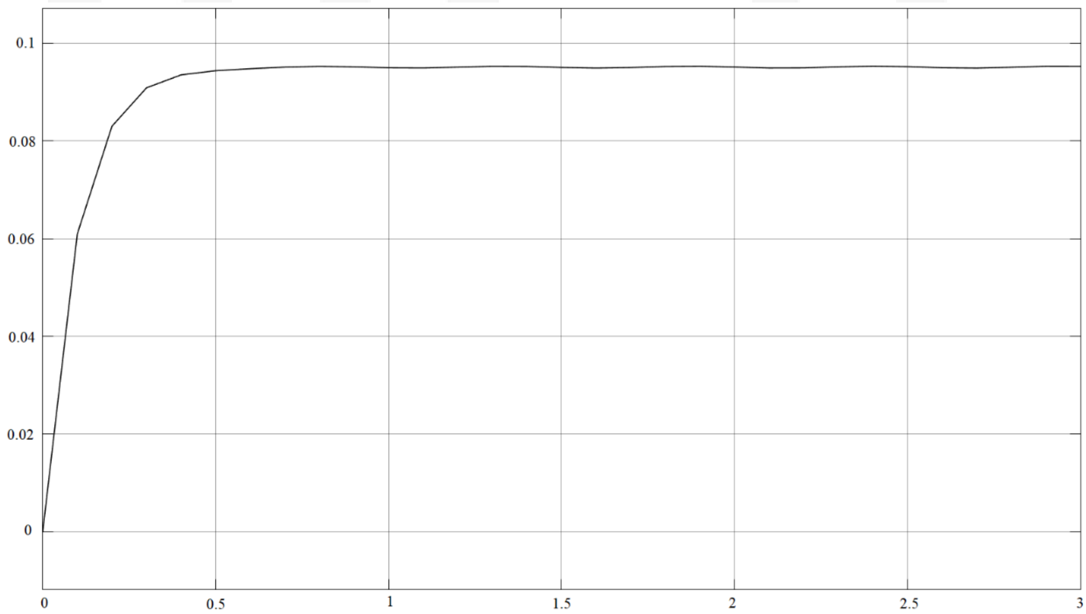

Figure 4.15 Empirical result for the duty cycle in 1000 rpm without disturbance.

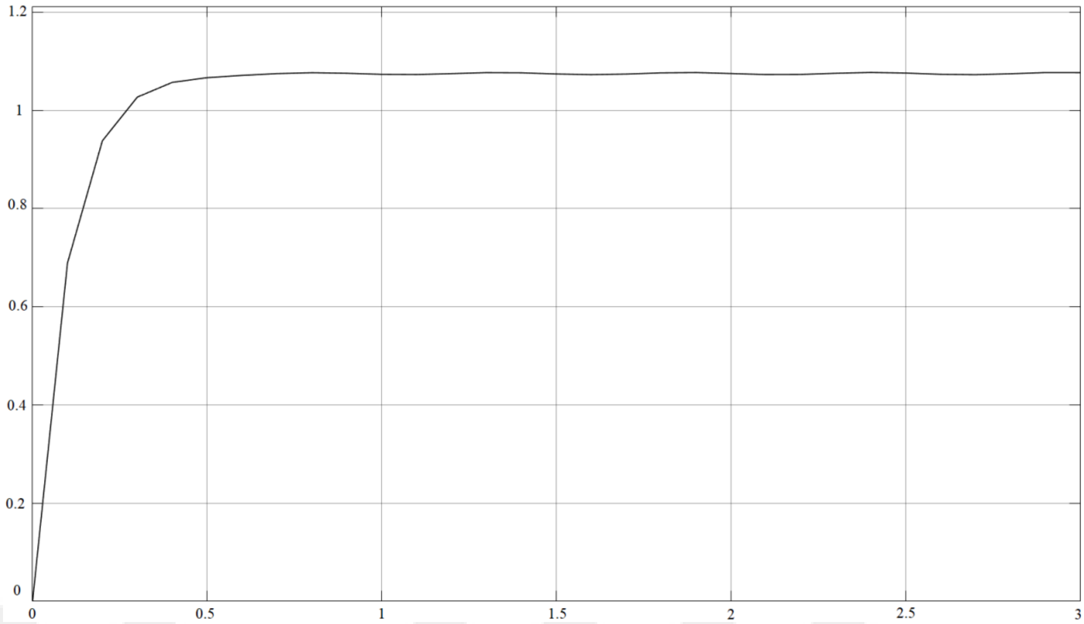

Figure 4.16 Empirical result for the buck converter output voltage in 1000 rpm without any disturbance.

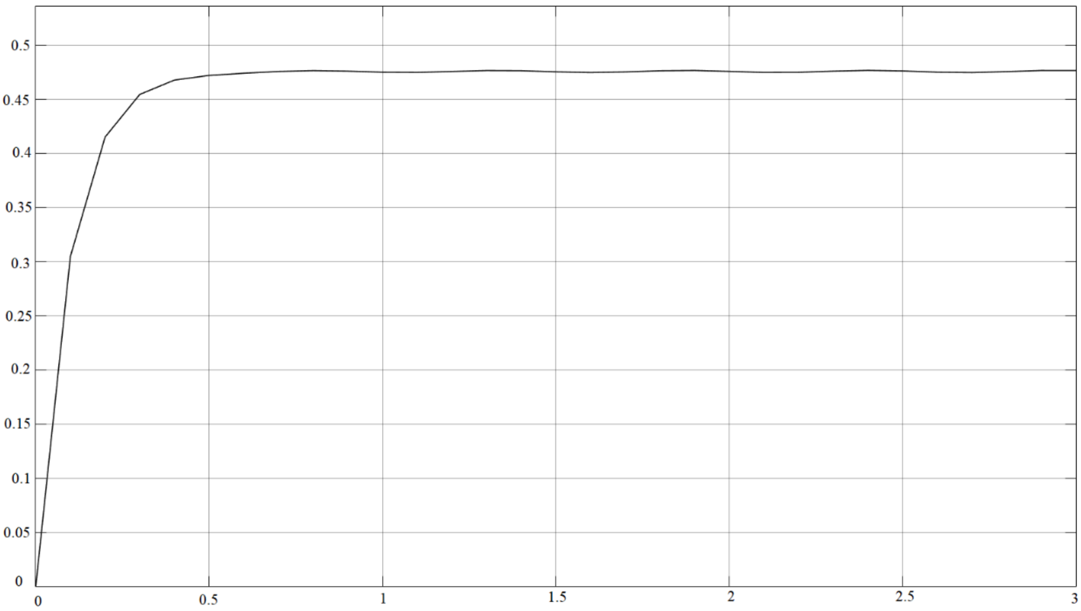

Figure 4.17 Empirical result for the duty cycle in 5000 rpm without disturbance.

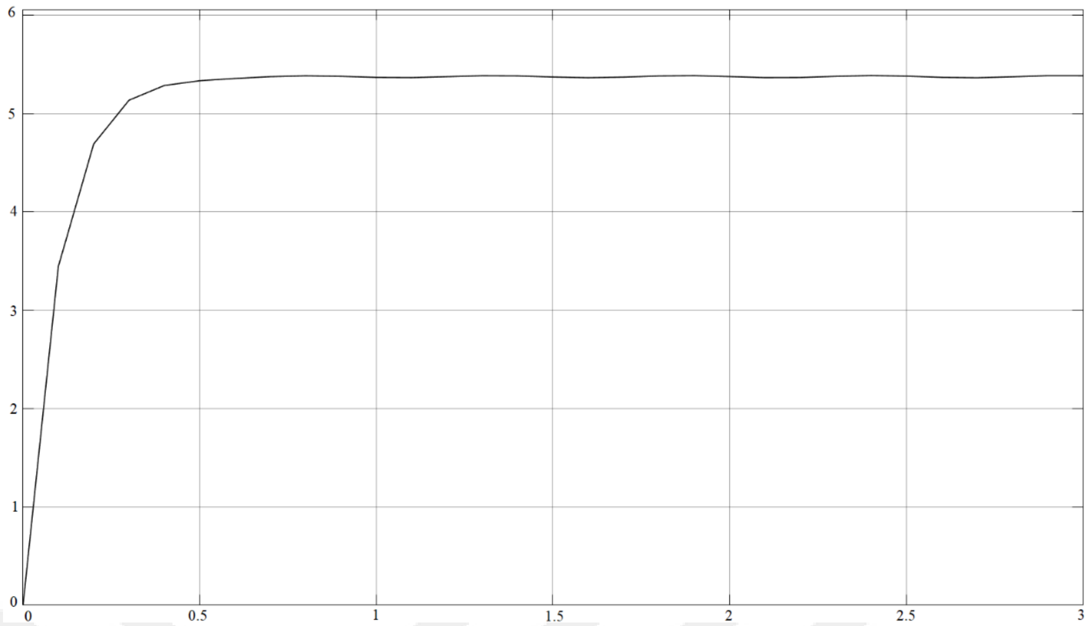

Figure 4.18 Empirical result for the buck converter output voltage in 5000 rpm without any disturbance.

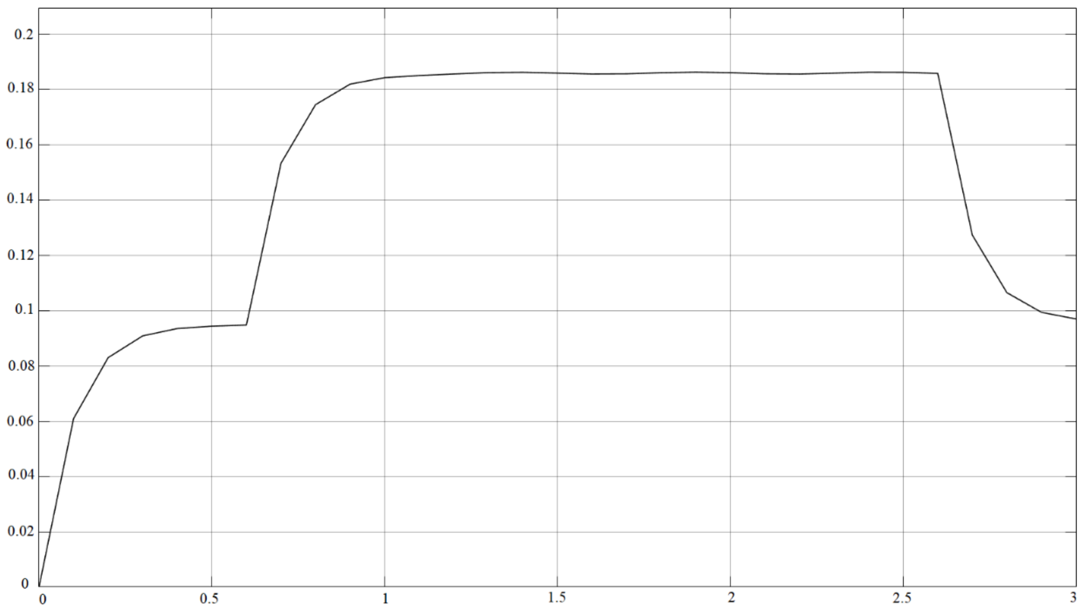

Figure 4.19 Empirical result for the duty cycle in 1000 rpm within a disturbance.

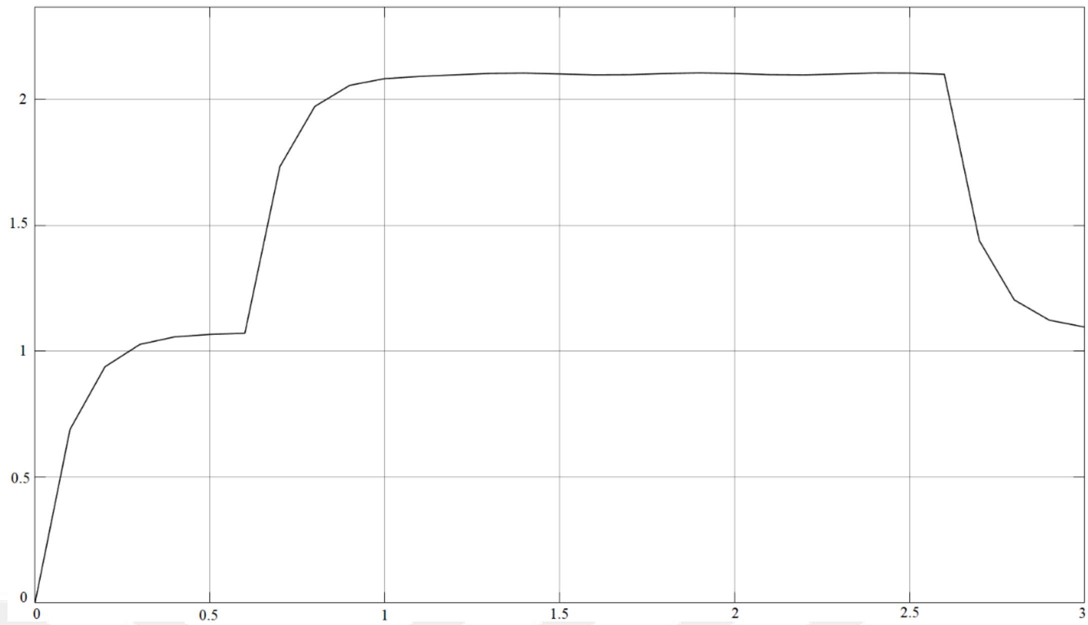

Figure 4.20 Empirical result for the buck converter output voltage in 1000 rpm within a disturbance.

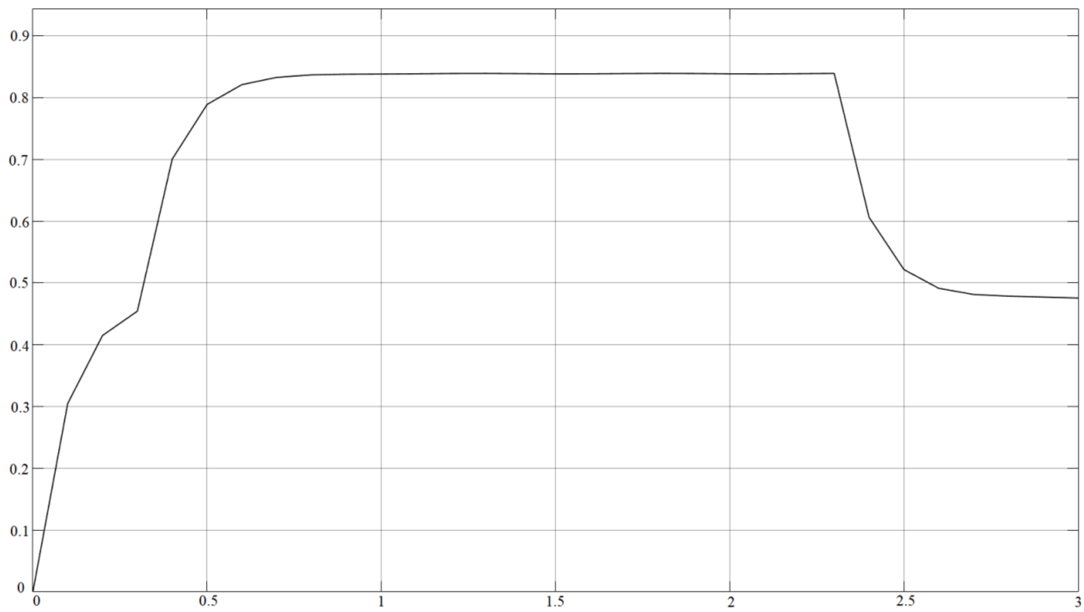

Figure 4.21 Empirical result for the duty cycle in 5000 rpm within a disturbance.

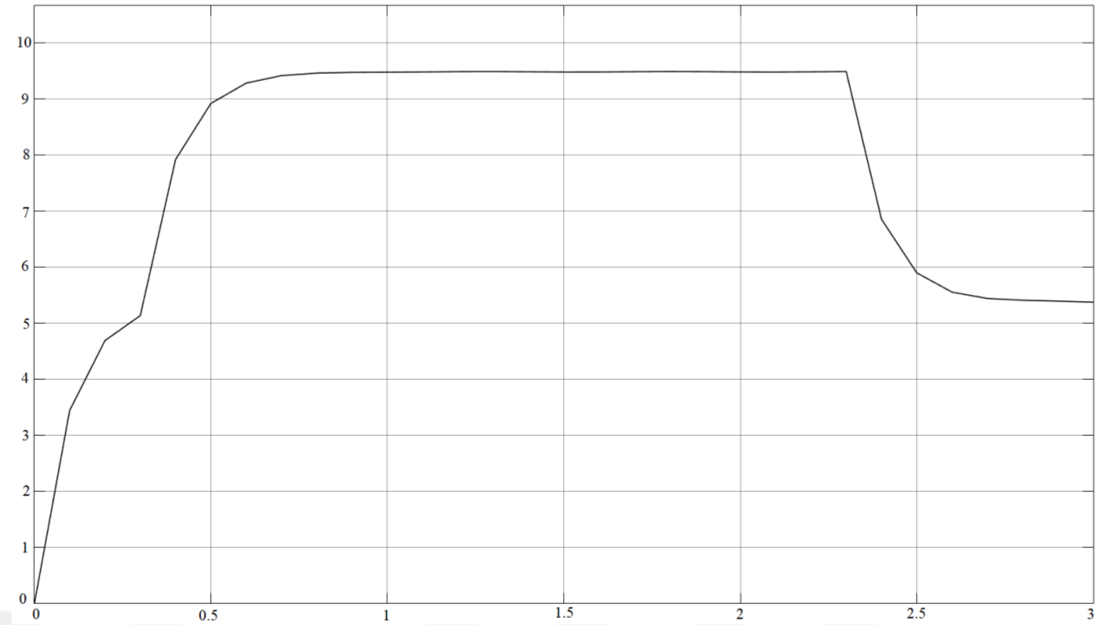

Figure 4.22 Empirical result for the buck converter output voltage in 5000 rpm within a disturbance.

For the Figures 4.19 and 4.20, it is clear that the system had exposure to an external disturbance at 0.6 seconds, so the duty cycle has been increased from 0.095 up to 0.2 for supplying a higher voltage (had elevating from 1.35V up to 2.3 V) to compensate the slump of the motor speed. For the Figures 4.21 and 4.22 at 0.3 seconds the disturbance occurred hence raising the duty cycle from 0.45 up to 0.85 and the buck converter voltage from 4.95 V up to 9.35V to compensate the descending in the speed.

It is important to mention that there is a non-palpable ripple (due to the scaling plot) within the previous figures will be discussed later.

From the above figures, we can realize that our system is so sensitive to any small changing in the duty cycle, for example, the slight change in the duty cycle (from 0.095 to 0.187) lifting the voltage from (1.04V to 2.05 V). Experimentally when we tested the DC motor in the open loop by applying 1.04V on its terminals, the speed measured as 763 RPM, and 1566 RPM in case of the 2.05 V.

4.7 DC Motor Output Speed

The experimental result in Figure 4.23 comes as an accentuation to the proportional relation between the DC motor speed and the applied voltage on its terminals which previously mentioned in equation 1.1, bearing in mind, the error which emerging from the fact that the brushed DC motors are inherently a non-linear system but for simplicity, we consider it as a linear.

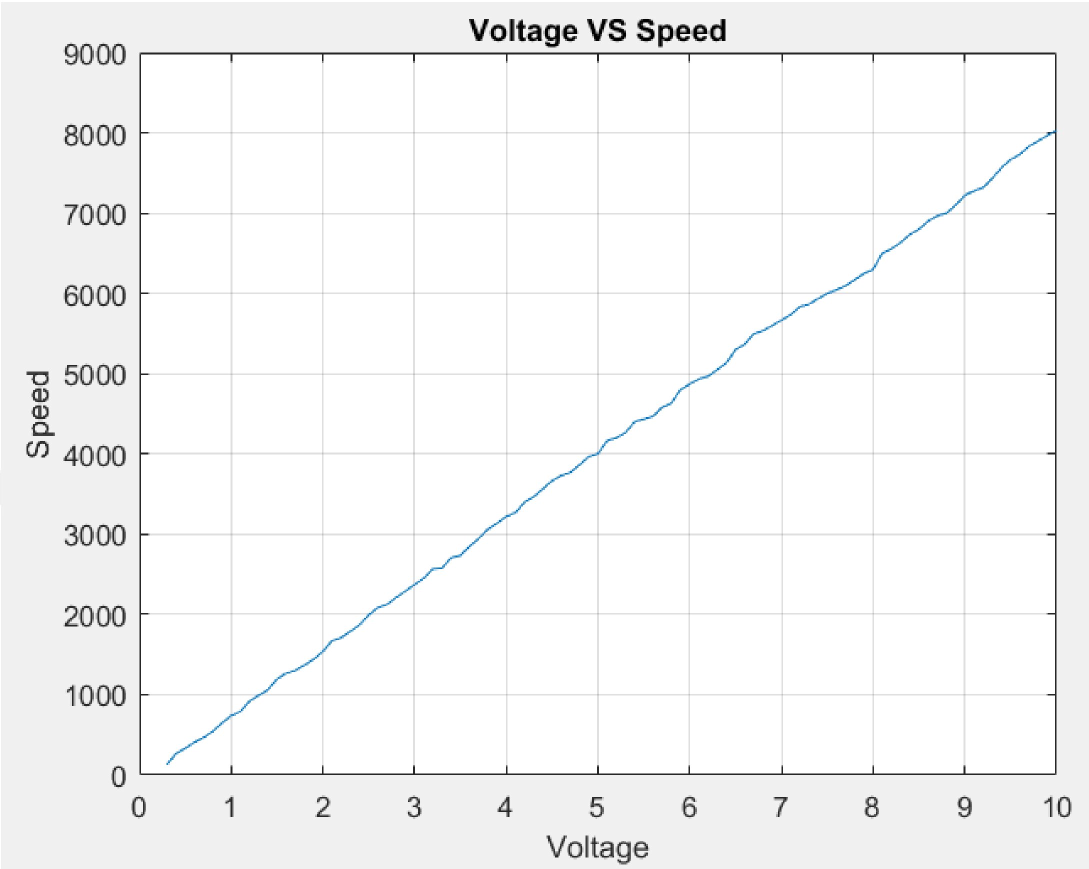

Figure 4.23 Empirical relation between the applied voltage on the DC motor and the actual speed.

Motivated from that direct relation, besides the fact which we previously mentioned it in the literature of the DC-DC converter (there is a proportional relation between both of the voltage and the duty cycle), we can deem the duty cycle are relating in a direct relationship with the speed of the permanent brushed DC motors.

In our system, the duty cycle engenders from the output value of the PI controller after doing the mapping procedure on it. This duty cycle is utilizing for driving the step-down converter, to convert the source voltage (12 V) to an upgrading voltage for acquiring the desired speed by either elevating or descending the duty cycle.

The simulation results for both of the duty cycle and the output speed have obvious shown in Figure 4.24 for 1000 RPM and Figure 4.25 with 5000 RPM there is 400m sec rising time in our system which is a brilliant result denoting an optimal PI-parameters tuning.

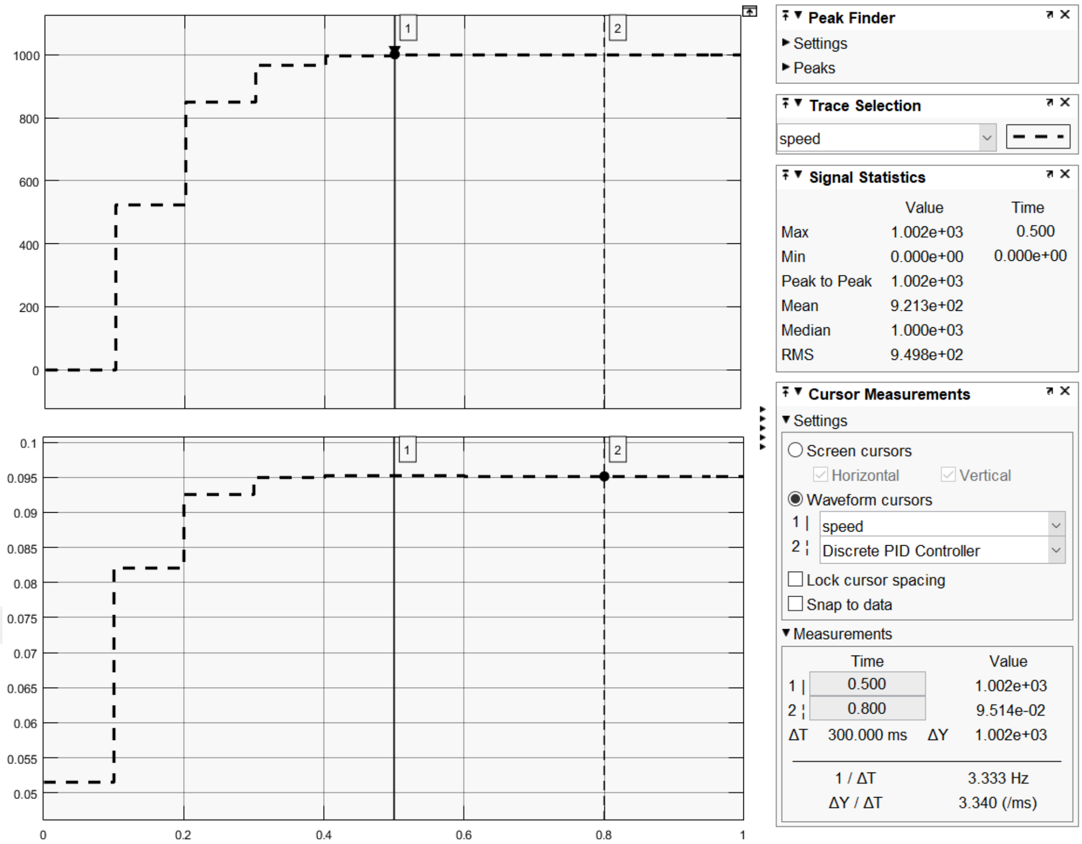

Figure 4.24 Simulation result for 1000 RPM and the duty cycle.

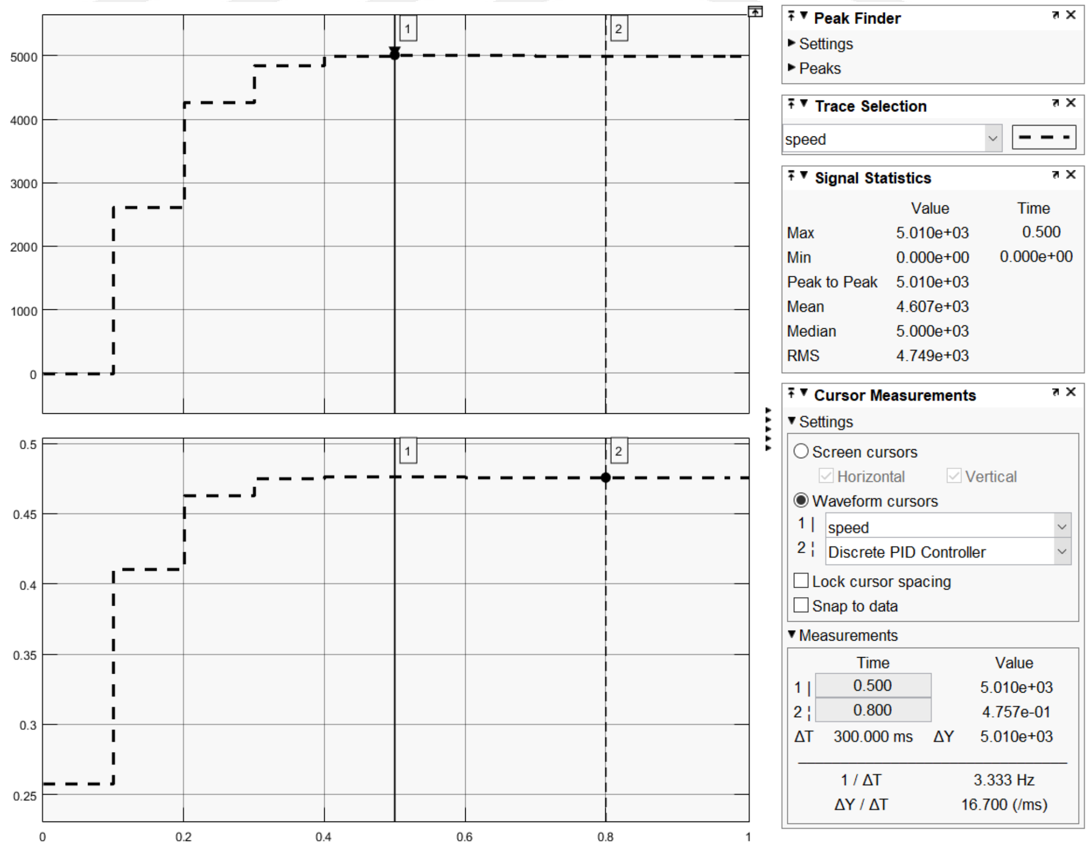

Figure 4.25 Simulation result for 5000RPM and the duty cycle.

The experimental results had obtained by sending the desired and the actual speeds with the error between them from a PIC18F4580 microcontroller via UART pin (after separating these values into two-bytes) to an Arduino UNO, which had used for combining these two-bytes and presenting them in an excel file via the PLX-DAQ software. After that, the final excel file was exporting to software program for drawing them. So, Figures 4.26, 4.27, 4.28, and 4.29 represent the actual speeds and the errors for the starting case of the DC motor without any disturbance, from those figures we can realize that the settling time was around 0.5 sec and there is a ripple in the output speed which engendered from the following reasons:

1-The natural frequency of the system (that inherently exists in every mechanical system).

2- The system was described and modeled as a linear system, while there is no such case in any real implementation for any system. That fact directly reflecting on the tuning of PI parameters, in addition to the uncertainties which was discarded from the modeling for simplicity purpose, such as the voltage drop in the MOSFET, Bootstrap circuit, Schottky diode and the internal capacitor resistance in addition to the fraction losses, iron loss wire connection losses, and etc. which omitted from the consideration.

3- The dealing with the discrete domain within 100m sec as a sampling time for including the whole of the speed range (100m sec allowing as to measure till 10 HZ so 33.33 RPM).

4- The obstacles associated with using the capture mode for measuring the frequency and hence the RPM. In spite of the speed advantages in using this way over of the regular one (using timer and counter) but also it involves some failures in the handling with the floating numbers engender from the failing of timer in counting the fraction parts of the counting. For example, with the 699 Hz input frequency, the duration will be 0.014306152 sec. Pursuant the circuit parameters, the time for each pulse to trigger the microcontroller for ticking is 0.5 μ sec. So, theoretically, timer1 must reach 2861.2303290415 in counting to get 699 reading on LCD, which is not true as it couldn't sensing the remainder part of the pulses. Meanwhile, the timer reads the value as 2861 and views 699 HZ or reads as 2862 and views 698 HZ on LCD. This rate of error will increase simultaneously with increasing the input frequency which has a remainder part (float number) in the count of the pulse period.

5- PWM resolution, from the PIC18F4580 data sheet, the PWM signal is generating via TIMER2 which is inherently 8 bits, so (0- 255) need to be scaling to a range from (0-100% including the fraction points) and so there is around 0.4 gap factor between every two adjacent numbers. In other meaning, there is 0.4 duty cycle gap which is not able to be sensed with the PIC18F4580. It is inevitably not a suitable thing to see it in a DC motor has a mechanical time constant equal to 24.3m sec and high specific characteristics lead to make it so sensitive with any small changing in the voltage.

For example, if the desired speed was 1000RPM, that is means from figure 4.23 there is 1.35 V must be applied on the terminals of the DC motor and hence 9.5% duty cycle. So, the microcontroller sends either 9.4% duty cycle and presenting 985 RPM or 9.8% duty cycle and presenting 1035 RPM. Both of these ripples 985 RPM and 1030RPM are adding to the natural frequency of the system besides the uncertainty in the transfer function and hence the PI parameters tuning, furthermore using the capture mode, all of these factors are combining causing to lift that ripple much more.

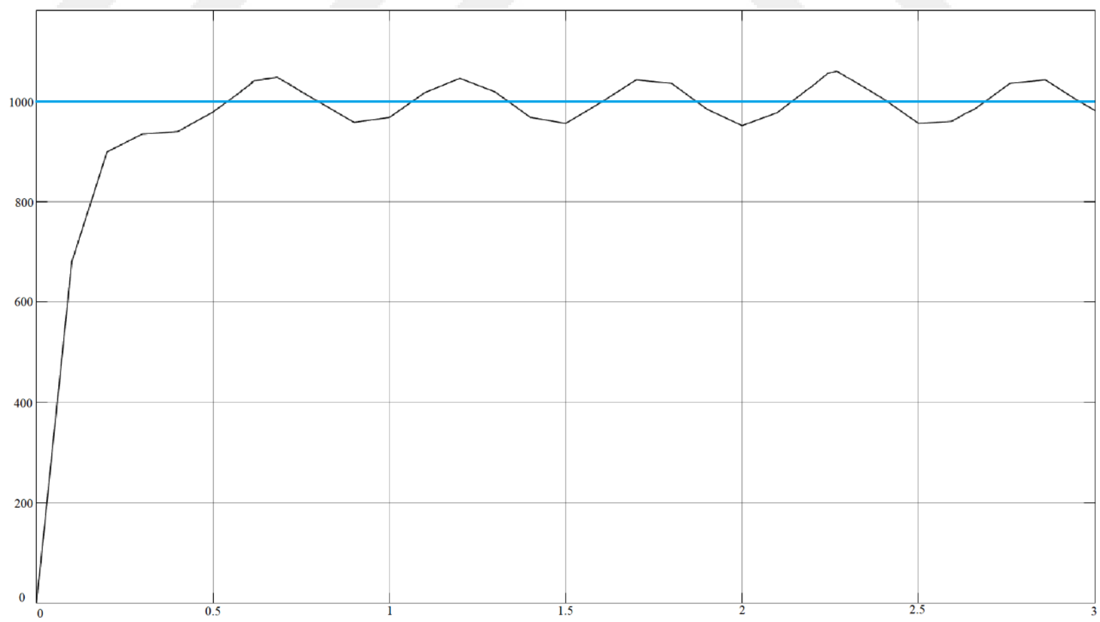

Figure 4.26 Experimental result for the actual speed in case of the 1000RPM desired speed.

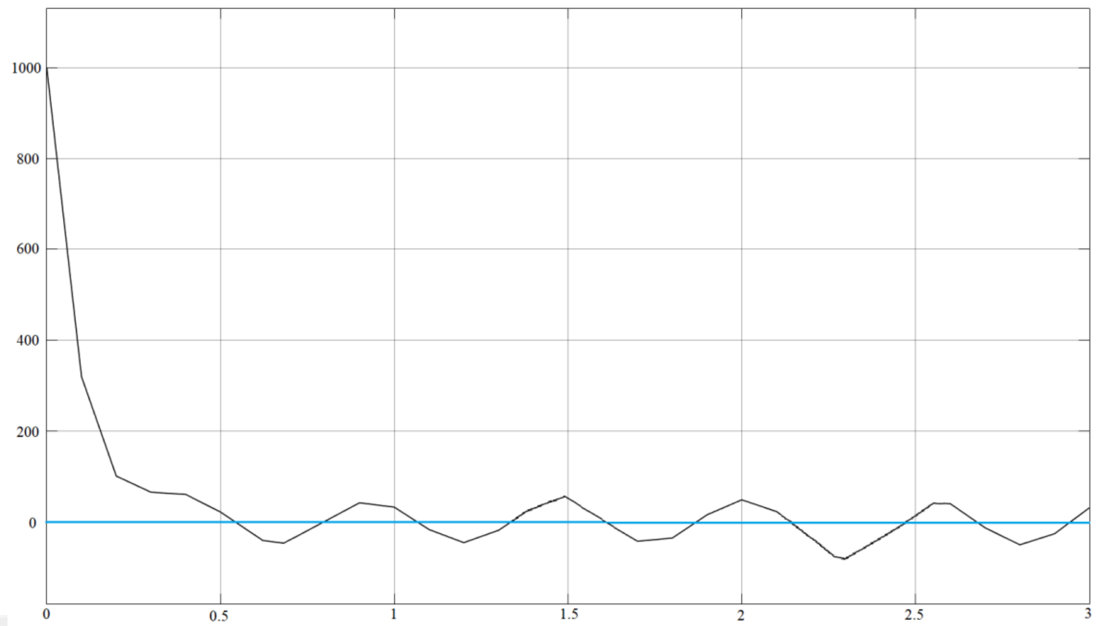

Figure 4.27 Experimental result for the error in case of the 1000RPM desired speed.

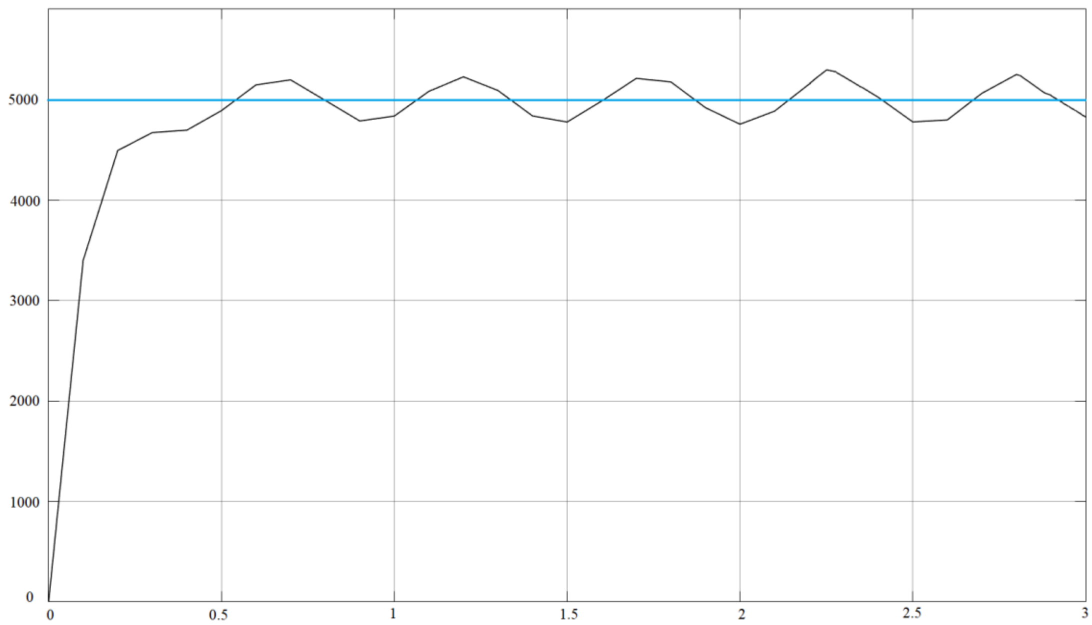

Figure 4.28 Experimental result for the actual speed in case of the 5000RPM desired speed.

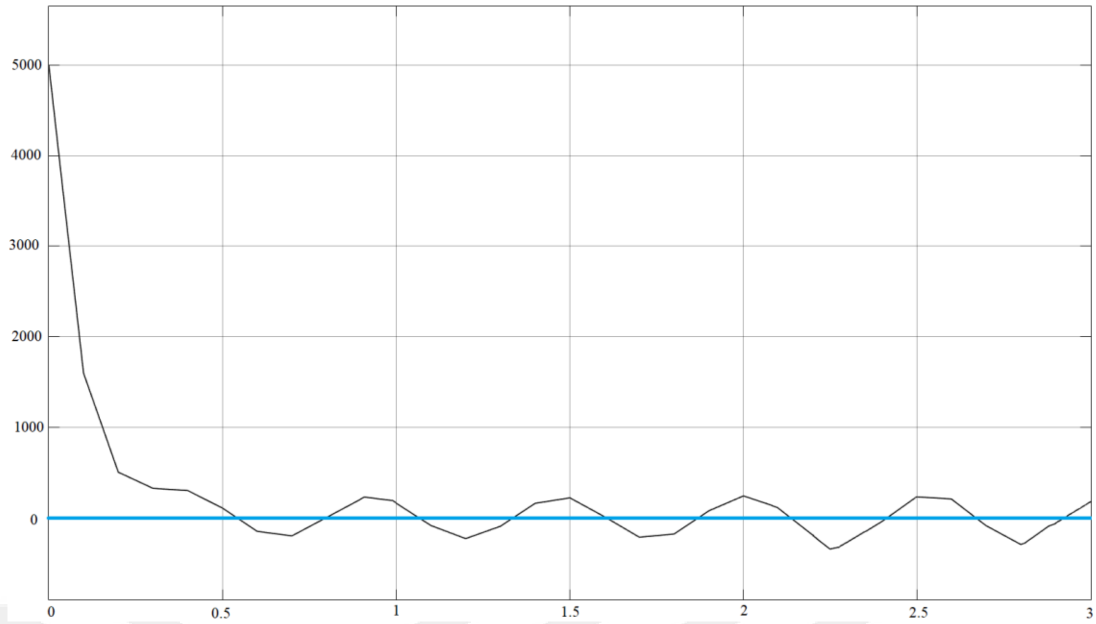

Figure 4.29 Experimental result for the error in case of the 5000RPM desired speed.

Figures 4.30, 4.31, 4.32 and 4.33 represent the actual speeds and the errors for the DC motor at the disturbance exposure.

At the moment when an external disturbance had been applying on the shaft of the DC motor, a dwindling in the speed occurred associated with the amount of that disturbance. At this moment the PI algorithm appears itself by increasing the duty cycle and hence the voltage that applied on the motor causing lifts in the speed again until it reaches the desired value.

At the moment of disturbance disposal, the speed is mounting suddenly due to the previously high voltage (which was applying to compensate the previous speed dwindling), so the PI algorithm works again in the opposite manner by reducing the duty cycle and hence the applied voltage until the DC motor speed is re-stabilizing to the desired value.

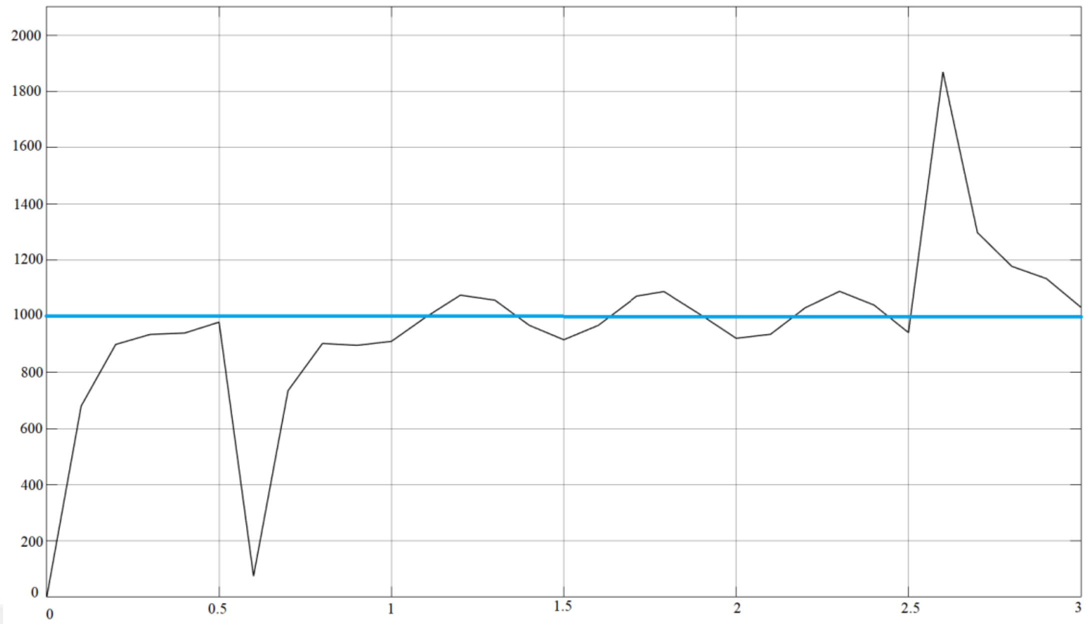

Figure 4.30 Experimental result for the speed in case of 1000RPM desired speed with applying an external disturbance.

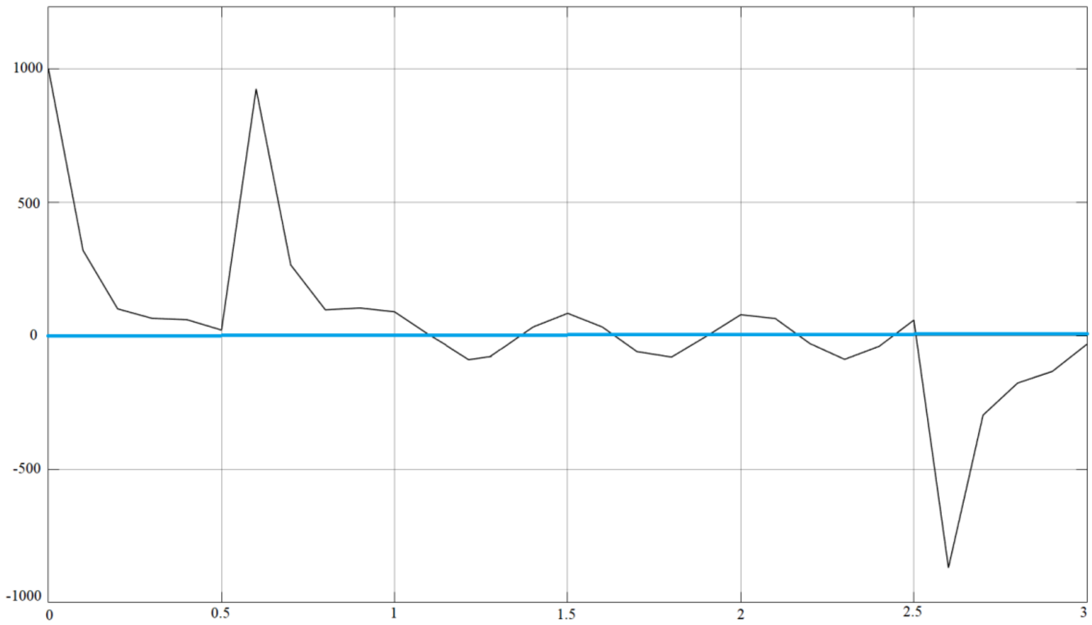

Figure 4.31 Experimental result for the error in case of 1000RPM desired speed with applying an external disturbance.

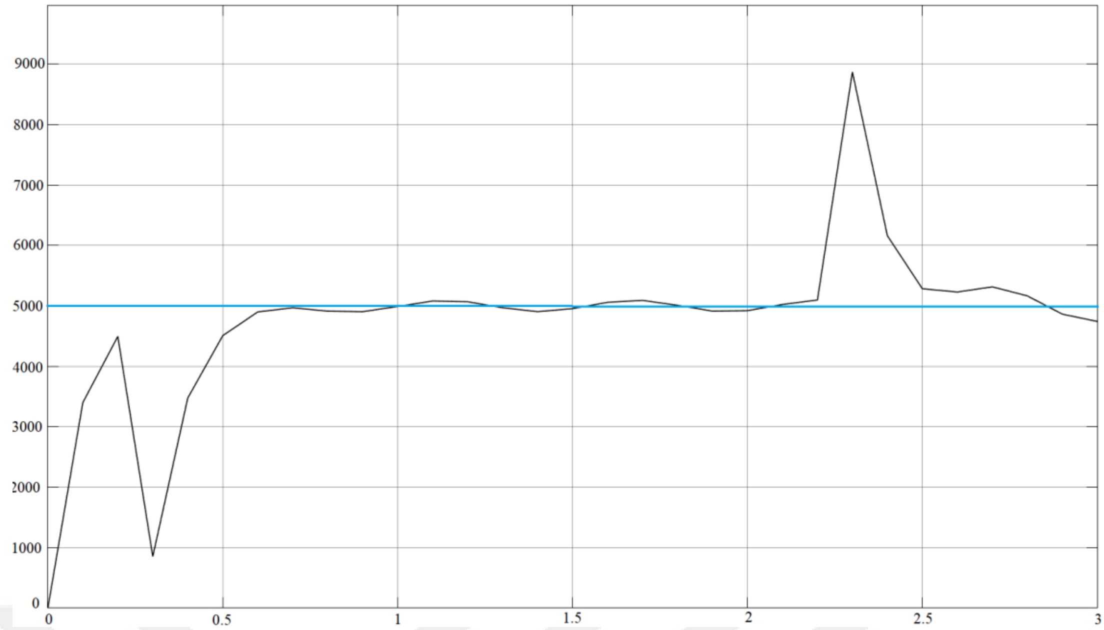

Figure 4.32 Experimental result for the speed in case of 5000RPM desired speed with applying an external disturbance.

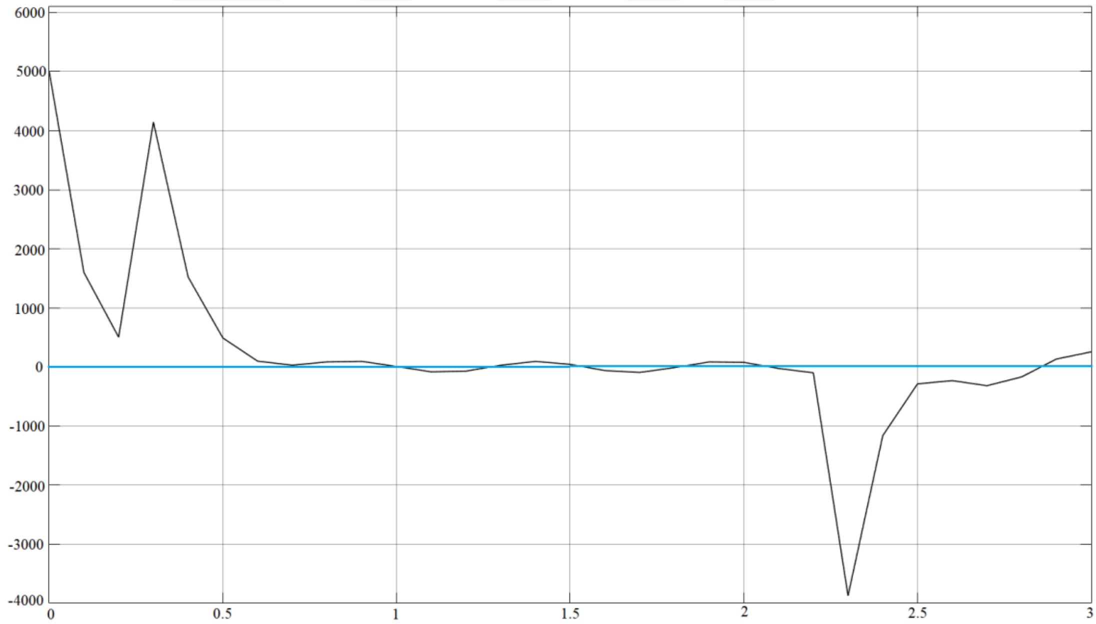

Figure 4.33 Experimental result for the error in case of 5000RPM desired speed with applying an external disturbance.

CHAPTER 5

CONCLUSION AND SUGGESTIONS

In this work (speed tracking system), the modeling and the transfer function that describes the system was extracted and used as the base for the PI parameters tuning part. After that, the stability of the system before and after utilizing the PI algorithm was checked using the Bode plot. Right of the bat, the stability of the system had been proved by the positive signs for both of the gain and phase margins.

The simulation results were brilliant with a perfect rising and settling time and with a minimum overshoot value in the whole of the tracking range. With the empirical results, the proportional relation between the applied voltage and the DC motor speed had been proved. Empirically the system presents a smooth trajectory for the starting period. In addition to that, the system had a perfect tracking response with some ripple due to the reasons mentioned before.

Experimentally the Schmitt trigger lm393 IC was brilliant in converting a shapeless signal to a square wave that can be sensed by the microcontroller.

As a recommendation for any future works in this field, try to use some advanced ways of system identifications like using data acquisition with LabVIEW software to approach the perfect description for the system to get access to the optimum PI parameters. Moreover, try to use the microcontrollers that have so high PWM resolution with a quartz crystal that has a high frequency to decrease the sampling time for performing every instruction command or using that data acquisition instrument itself that has been designing for that purpose. Furthermore, it is very crucial to elevate the sensor resolution by using smaller sampling time and more accurate sensors by increasing the number of slots as possible.

For the buck converter, it is pivotal to use inductor that has the minimum internal resistance value and using a capacitor that already has minimum ESR, besides, using

MOSFET and the bootstrap circuit as a low side MOSFET driver instead of the Schottky diode for reducing the voltage drop.

The last recommendation for anyone interested in this field is being away from converting the digital output signal from the speed sensor to an analog using LM331 IC because it has a high ripple factor that led to a wrong reading, besides having a sluggish response time because it inherently had designed for the conversion from analog to frequency. In spite of, they mentioned in LM331 datasheet that, it could be using for that purpose without any mentioning to its time response but my advice yes it could be used but not with the applications that need so high response time because the primary job of that IC is converting the voltage to the frequency and the reverse is a secondary role.

REFERENCES

[1] Antritter, F., Maurer, P. Reger, J. (2006). Flatness based control of a buck-converter driven DC motor, *International Federation of Accountants (IFAC)*, **39(16)**, 36-41.

[2] Boldea, I., Nasar, S. (2016). *Electric drives*. CRC Press: Boca Raton, Florida.

[3] Linares-Flores, J., Sira-Ramirez, H. (2004). DC motor velocity control through a DC-to-DC power converter, *In 2004 43rd IEEE Conference on Decision and Control (CDC)*, 5297-5302.

[4] Linares-Flores, J., Sira-Ramirez, H. (2004). A smooth starter for a DC machine: A Flatness Based Approach (ICEEE), *1st International Conference on Electrical and Electronics Engineering*, 589-594.

[5] Ogata, K. (2016). *Modern control engineering*. Prentice Hall: Delhi.

[6] Fadali, M. S., Visioli, A. (2012). *Digital control engineering analysis and design*. Academic Press: Waltham, Massachusetts.

[7] Bansal, U. K., Narvey, R. (2013). Speed control of DC motor using fuzzy PID controller, *Advance in Electronic and Electric Engineering*, **3(9)**, 1209-1220.

[8] Schröder, D. (2009). *Elektrische Antriebe-Regelung von Antriebssystemen*. Springer: New York.

[9] Mukherjee, A., Ray, S., Das, A. (2014). Development of Microcontroller Based Speed Control Scheme of BLDC Motor Using Proteus VSM Software, *International Journal of Electronics and Electrical Engineering*, **2**, 1-7.

[10] Mazidi, M. A., McKinlay, R. D., Causey, D. (2008). *PIC microcontroller and embedded systems: using Assembly and C for PIC18*. Prentice Hall: New Jersey.

[11] Doppelbauer, M. 1822. The invention of the electric motor 1800-1854. Philosophical Magazine. Available at: https://www.eti.kit.edu/english/1376.php. Accessed 01.01.2019.

[12] Lee, E. C. 2003. Review of variable speed drive technology. In Wire World Internet. Available at: http://www.enginuitysystems.com/files/avsde4%20(Variable %20speed%20drives).pdf. Accessed 01.01.2019.

[13] Chinnaiyan, V. K., Jerome, J., Karpagam, J., Mohammed, S. S. (2006). Design and implementation of high power DC-DC converter and speed control of DC motor using TMS320F240 DSP, *IICPE India International Conference*, 388-392.

[14] Ylitolva, K. (2011). Ward Leonard Control System, Msc thesis, Electrical Engineering Dept., Central Ostrobothnia University of Applied Sciences.

[15] Vodovozov, V. M., Vinnikov, D. (2008). *Electronic Systems of Motor Drive*. TUT Press: Tallinn, Estonia.

[16] Yano, M., Abe, S., Ohno, E. (2004). History of power electronics for motor drives in Japan, *IEEE Conference on the History of Electronics*, 1-11.

[17] Vodovozov, V., Jansikene, R. (2006). *Power electronic converters*. TUT Press: Tallinn, Estonia.

[18] Antsaklis, P. J. (1999). Intelligent control, *Wiley Encyclopedia of Electrical and Electronics Engineering*, **10**, 493-503.

[19] Lyshevski, S. E. (1999). *Electromechanical Systems, Electric Machines, and Applied Mechatronics*. CRC Press: Boca Raton, Florida.

[20] Linares-Flores, J., Sira-Ramírez, H. (2004). Sliding mode-delta modulation GPI control of a DC motor through a buck converter, *International Federation of Accountants (IFAC)*, **37(21)**, 405-410.

[21] Ortega, R., Perez, J. A. L., Nicklasson, P. J., Sira-Ramirez, H. (1998). *Passivity-based Control of Euler-Lagrange Systems: Mechanical, Electrical and Electromechanical Applications.* Springer Science and Business Media: London, UK.

[22] Linares-Flores, J. (2006). Control suave de velocidad de motores de CD mediante convertidores de potencia CD/CD.Doctoral dissertation, Ph.D. dissertation, Sección de Mecatrónica del Departamento de Ingenierıa Eléctrica del CINVESTAVIPN.

[23] Linares-Flores, J., Antonio-García, A., Orantes-Molina, A. (2011). Arranque suave para un motor de CD a través de un convertidor reductor CD-CD, *Ingeniería, investigación y tecnología*, **12(2)**, 137-148.

[24] El Fadil, H., Giri, F. (2006). Accounting of DC-DC power converter dynamics in DC motor velocity adaptive control, *IEEE International Conference on Control Applications*, 3157-3162.

[25] Ahmad, M. A., Ismail, R. R., Ramli, M. S. (2010). Control strategy of buck converter driven DC motor: A comparative assessment. *Australian Journal of Basic and Applied Sciences*, **4(10)**, 4893-4903.

[26] Sureshkumar, R., Ganeshkumar, S. (2011). Comparative study of proportional integral and backstepping controller for buck converter, *IEEE congress of Emerging Trends in Electrical and Computer Technology (ICETECT)*, 375-379.

[27] Bingol, O., Pacaci, S. (2012). A virtual laboratory for neural network controlled DC motors based on a DC-DC buck converter, *International Journal of Engineering Education*, **28(3)**, 713-723.

[28] Tumari, M. M., Saealal, M. S., Ghazali, M. R., Wahab, Y. A. (2012). H-infinity with pole placement constraint in LMI region for a buck-converter driven DC motor, *IEEE International Conference Power and Energy (PECon)*, 530-535. IEEE.

[29] Sira-Ramirez, H., Oliver-Salazar, M. A. (2013). On the robust control of buck-converter DC-motor combinations, *IEEE Transactions on Power Electronics*, **28(8)**, 3912-3922.

[30] Silva-Ortigoza, R., García-Sánchez, J. R., Alba-Martínez, J. M., Hernández-Guzmán, V. M., Marcelino-Aranda, M., Taud, H., Bautista-Quintero, R. (2013). Two-Stage Control Design of a Buck Converter/DC Motor System

without Velocity Measurements via a-Modulator, *Mathematical Problems in Engineering*, 1-11.

[31] Nagarajan, D. R., Sathishkumar, S., Balasubramani, K., Boobalan, C., Naveen, S., Sridhar, N. (2016). Chopper fed speed control of DC motor using PI controller, *IOSR-Journal of Electrical and Electronics Engineering (IOSR-JEEE)*, **11(3)**, 65-69.

[32] Silva-Ortigoza, R., Hernández-Guzmán, V. M., Antonio-Cruz, M., Munoz-Carrillo, D. (2015). DC/DC Buck power converter as a smooth starter for a DC motor based on a hierarchical control, *IEEE Transactions on Power Electronics*, **30(2)**, 1076-1084.

[33] Linares-Flores, J., Reger, J., Sira-Ramírez, H. (2010). Load torque estimation and passivity-based control of a boost-converter/DC-motor combination, *IEEE Transactions on Control Systems Technology*, **18(6)**, 1398-1405.

[34] Linares-Flores, J., Sira-Ramirez, H., Reger, J., Silva-Ortigoza, R. (2006). An exact tracking error dynamics passive output feedback controller for a Buck-Boost-converter driven DC motor, *In 2006 IEEE International Power Electronics Congress*, 1-5.

[35] Sönmez, Y., Dursun, M., Güvenç, U., Yilmaz, C. (2009). Start Up Current Control of Buck-Boost Convertor-Fed Serial DC Motor, *Pamukkale University Journal of Engineering Sciences*, **15(2)**, 278-283.

[36] Linares-Flores, J., Barahona-Avalos, J. L., Sira-Ramirez, H., Contreras-Ordaz, M. A. (2012). Robust passivity-based control of a Buck-Boost-converter/DC-motor system: An active disturbance rejection approach, *IEEE Transactions on Industry Applications*, **48(6)**, 2362-2371.

[37] Jiménez-Toribio, E. E., Labour-Castro, A. A., Muniz-Rodriguez, F., Perez-Hernandez, H. R., Ortiz-Rivera, E. I. (2009). Sensorless control of SEPIC and Ćuk converters for DC motors using solar panels, *In 2009 IEEE Electric Machines and Drives Conference*, 1503-1510.

[38] Linares-Flores, J., Sira-Ramirez, H., Cuevas-Lopez, E. F., Contreras-Ordaz, M. A. (2011). Sensorless passivity based control of a DC motor via a solar

powered Sepic converter-full bridge combination, *Journal of Power Electronics*, **11(5)**, 743-750.

[39] Linares-Flores, J., Reger, J., Sira-Ramírez, H. (2006, December). Speed-sensorless tracking control of a DC-motor via a double Buck-converter, *In Proceedings of the 45th IEEE Conference on Decision and Control*, 6229-6234.

[40] Divelbiss, A. W., Wen, J. T. (1997). Trajectory tracking control of a car-trailer system, *IEEE Transactions on Control systems technology*, **5(3)**, 269-278.

[41] Silva-Ortigoza, R., Silva-Ortigoza, G., Hernández-Guzmán, V. M., Barrientos-Sotelo, V. R., Albarran-Jimenez, J. M., Silva-Garcia, V. M. (2008). Trajectory tracking in a mobile robot without using velocity measurements for control of wheels, *IEEE Latin America Transactions*, **6(7)**, 598-607.

[42] Luo, M., Wang, D., Pham, M., Low, C. B., Zhang, J. B., Zhang, D. H., Zhao, Y. Z. (2005, November). Model-based fault diagnosis/prognosis for wheeled mobile robots: a review, *31st Annual Industrial Electronics Society Conference of IEEE* ,1-6.

[43] Silva-Ortigoza, R., Márquez-Sánchez, C., Marcelino-Aranda, M., Marciano-Melchor, M., Silva-Ortigoza, G., Bautista-Quintero, R., Muñoz-Carrillo, D. (2013). Construction of a WMR for trajectory tracking control: Experimental results, *The Scientific World Journal*,1-17.

[44] Silva-Ortigoza, R., Hernández-Guzmán, V. M., Antonio-Cruz, M., Munoz-Carrillo, D. (2015). DC/DC Buck power converter as a smooth starter for a DC motor based on a hierarchical control, *IEEE Transactions on Power Electronics*, **30(2)**, 1076-1084.

[45] Chen, Z., Gao, W., Hu, J., Ye, X. (2011). Closed-loop analysis and cascade control of a nonminimum phase boost converter, *IEEE Transactions on power electronics*, **26(4)**, 1237-1252.

[46] Chen, Z., Gao, W., Ye, X. (2010). Frequency domain closed-loop analysis and sliding mode control of a nonminimum phase buck-boost converter, *Control and Intelligent Systems*, **38(4)**, 245.

[47] Chen, Z., Hu, J., Gao, W. (2010). Closed-loop analysis and control of a non-inverting buck–boost converter, *International Journal of Control*, **83(11)**, 2294-2307.

[48] Chen, Z. (2012). PI and sliding mode control of a Cuk converter, *IEEE Transactions on Power Electronics,* **27(8)**, 3695-3703.

[49] Hamed, B., Al-Mobaied, M. (2011). Fuzzy PID controllers using FPGA technique for real time DC motor speed control, *Intelligent Control and Automation*, **2(3)**, 233-240.

[50] Skvarenina, T. L. (2001). The power electronics handbook, CRC press: Indiana.

[51] ICs, H. F. M. G. D. (2007). Application note an-978 Rev D. El Segundo, California, USA: Available at http://application-notes.digchip.com/014/14-15295.pdf.

[52] Kim, M. K., Jang, K. Y., Choo, B. H., Lee, J. B., Suh, B. S., Kim, T. H. (2002). A novel IGBT inverter module for low-power drive applications, *33rd Annual IEEE Conference on Power Electronics Specialists*, **2**, 642-647.

[53] Ang, K. H., Chong, G., Li, Y. (2005). PID control system analysis, design, and technology, *IEEE transactions on control systems technology*, **13(4)**, 559-576.

[54] Wu, W. (2012). DC motor parameter identification using speed step responses, *Modelling and Simulation in Engineering*, 1-5.

[55] Rashid, M. H. (2017). *Power electronics handbook.* Academic Press: Florida.